Surfactant-Polymer Chemical EOR and Subsequent Oil Bank Behaviour

Mohamed Sealiti

TU Delft Delft University of Technology

Surfactant-polymer chemical EOR and subsequent oil bank behaviour

By

Mohamed Sealiti

in partial fulfilment of the requirements for the degree of

Master of Science

in Applied Earth Physics

Petroleum Engineering Track

at the Delft University of Technology,

to be defended publicly on Wednesday November 28, 2018 at 10:00 AM.

Supervisor:	Prof. ir. C.P.W.J. van Kruijsdijk	
Thesis committee:	Dr. K.H.A.A Wolf,	TU Delft
	Dr. P.J. (Phil) Vardon	TU Delft
	Prof.dr. J. Bruining	TU Delft

Contents

Abstract

This thesis report, in all its ambiguities, is an attempt at describing the behaviour of an oil bank during a surfactant-polymer chemical flood. Core flood experiments are performed using three 7.5cm Fontainebleau cores of varying permeability, a 60cm low permeability Fontainebleau core, a 60cm composite high permeability Fontainebleau core and a high permeability 1m Bentheimer core. In general, all experiment performed had the same procedure of oil filling, waterflooding and chemical flooding. Some experiments are performed under a CT-scanner to obtain more insight in oil bank behaviour.

In this study, these oil banks are studied in core flood experiments using the Fontainebleau sandstone cores of varying lengths and one 1m Bentheimer Sandstone core. In these core floods the effects of certain parameters on the oil bank behaviour are examined. The parameters range from rock properties such as permeability and core length, to fluid properties such as optimality of the surfactant to viscosity of the surfactant-polymer and polymer.

After a waterflood the oil saturation is (close to) the irreducible oil saturation, wherein oil in a porous medium is dispersed over the pore network in unconnected droplets due to snap off. In a chemical flood, the surfactant reduces oil-water interfacial tension and liberates the trapped oil droplets. These mobilised droplets coalesce into a greater body of oil, the oil bank. The surfactant-polymer and polymer slugs, with relatively high viscosity, act as displacing agents with piston-like displacement in an ideal scenario.

Core flood experiments performed on 7.5 cm cores give some insight into the relevance of permeability, or rather pore geometry and optimal surfactant versus suboptimal surfactant. The comparison between experiments performed on the same 7.5cm high permeability core with different initial saturations show that a lower residual oil yields a smaller oil bank. A smaller volume of pure oil production was observed during the chemical flood at lower initial saturations. Comparison between 7.5cm cores of varying permeability give some insight into the effect on pore geometry on incremental oil recovery. Results show a lower recovery factor in both the waterflood and chemical flood at lower permeabilities, and again a smaller volume of oil during chemical flood at lower permeability. In the comparison between experiments using optimal and suboptimal surfactant, the suboptimal surfactant experiment yielded a lower recovery factor and less microemulsions produced.

The first experiment using a solid 60 cm core shows some differences with respects to the 7.5 cm core experiments. The permeability test shows that there is some heterogeneity within the core, with a factor 2 difference between the sections with lowest and greatest measured average permeability. This heterogeneity and low average permeability over the core are a possible reason for the generally low waterflood recovery factor, when compared to the 7.5cm core experiments. While production data shows a chemical flood incremental recovery factor of 40.5%, which is in line with 7.5 cm core experiments, the CT-scans show fingering and unstable displacement taking place. The composite 60cm core showed a greater heterogeneity in the permeability test, with average sectional permeabilities ranging from 45mD to 382md. The average core permeability of 72 mD however, is greater than that of the solid 60 cm core and may be the cause of the greater waterflood recovery factor. The chemical flood with an incremental recovery factor of 28% is much less efficient than in the solid 60cm core. This lower recovery factor becomes apparent in the CT-scans, where there is a great deal of fingering and unstable displacement. CT-scans show that the boundary between the stacked cores, acts as a heterogenous capillary boundary with strongly contrasting permeabilities, playing a relevant role in the unstable displacement.

A second experiment using the composite core, but this time surfactant-polymer and polymer solutions with greater viscosity shows a drastically improved sweep efficiency, with an increased incremental recovery factor of 58%. CT-scans show that there is almost piston-like displacement of the oil bank by the SP-slug up until the heterogenous boundary between the stacked cores. The oil bank travels through a thief zone but remerges further on. After the SP-slug flows through the thief zone, fingering and unstable displacement occurs. The polymer does sweep the core sections that were bypassed by the SP-slug. Saturation data from the CT-scans highlights the emergence and progression of the oil bank by showing an increased oil saturation in core sections as time progresses.

Permeability tests on the 1m Bentheimer core also show that there is heterogeneity within the core. There is a clear divide showing that the first half has an average permeability of about a factor 2 greater than the last section. With an average permeability of 1.4 Darcy over the entire core, there is much greater permeability than in any of the Fontainebleau cores. With a waterflood recovery factor of 54% in the 1m Bentheimer core, the relevance of pore geometry is again highlighted. The CT-scans of the 1m Bentheimer core experiments show very efficient piston-like displacement where the SP-slug sweeps the entire cross-sectional area of the core. The scans show the emergence and progression of the oil bank, where it increases in length as the flood progresses with highest saturation just past the SP-slug. Halfway through the core there is again a thief zone that acts as a preferred path for the oil. The oil bank passes through the thief zone but comes together again towards the core's outlet. The SP-slug however, is led into a fingering path after it passes through the thief zone.

Combined Buckley-Leverett and JBN relative permeability data give an insight as to how certain parameters affect oil mobility. The comparison between the 7.5cm low permeability and the solid 60cm cores, which have similar permeability, show that the core's length has a positive influence on the oil mobility. The greater core length gives more time and space for coalescence of the oil droplets into the oil bank.

Acknowledgements

As is normal with any project with a great deal of experimental work, this research project involved more than a few setbacks and unexpected turn of events. Even outside this thesis project several personal issues arose to complicate an already challenging endeavour. With all these challenges and obstacles standing in the way of progress and graduation, overcoming them would not have been possible without the support and involvement of several individuals. This report would be amiss if credit would not be given where credit is due.

First and foremost, I would like to extend my deepest gratitude to Faisal Al Saadi, who acted as a daily supervisor throughout this project. Without his help in explaining puzzling results and confusing data, this thesis report would not be what it is today. Even when burdened with the challenge of a PhD dissertation, he always found time for a sit-down and always offered motivating and supportive feedback. Being the pessimist that I am, you provided me with exactly what I needed from a supervisor.

Secondly, I would like to thank my main supervisor, Cor van Kruijsdijk, who's much required sanity checks and guidance always steered us in the right direction. It provided comfort knowing that such a knowledgeable person overlooked the entire process and set clear boundaries without just giving the answer to a research question. He has taught me a lot one the research subject, but also in the greater scheme of things about how to deal with setbacks and learn from them.

I also owe a great debt of gratitude to Karl-Heinz Wolf, who provided much needed support during the lab work. Not only his huge efforts in taking care of the logistics and accommodations behind performing a proper experiment, but also his vast knowledge of petrophysics had been nothing short of vital. His sense of humour and the many talks we had were a welcome change of pace to alleviate stressful times. More than a supervisor, he had been a friend during this project.

Inside the lab several lab technicians and fellow researchers played a vital role during the experiments. I thank Michiel Slob for his relentless support in setting up experiments and in keeping the set-up up and running. I thank Ellen Meijvogel-de Koning for her always cheerful support in the CT-room and beyond. I thank Jens van den Berg for surprising me with a freshly drilled or milled core on multiple occasions, Jolanda van Haagen-Donker for providing the many chemicals needed to perform the experiments, Karel Heller for sorting out the troublesome software issues that arose and Joost van Meel, Wim Verwaal, Mark Friebel, Swej Shah, Jiakun Gong and Martijn Janssen for jumping in to take CT-scans when no one else was available.

Outside of the project, immediate family and close friends provided a great deal of support and encouragement. Even though many of them are dealt a bad hand themselves, they never failed to help put things into perspective. My mother, brothers and sister I thank for their continuous and unconditional support throughout my time at this university. My close friends I thank for their crude and ruthless, yet hilarious and motivating comments in times of low morale. And lastly but certainly not least, I would like to extend my sincerest gratitude to my significant other, Hana Hasanbegovic, who always had nothing less than kind, supporting and endearing words to offer in trying times.

List of Figures

List of tables

List of Symbols

Symbol	Units	Description
OOIP	mL	Oil initially in place
RF	% of OOIP	Recovery factor
Nc	[-]	Capillary number
μ	Pa.s	(Apparent) dynamic viscosity
Q	m^3/s	Flow rate
γ	N/m	Surface Tension
M	[-]	Mobility ratio
λ	[-]	Mobility
k_r	[-]	Relative permeability
n	[-]	Corey exponent
f	[fraction of production rate]	Fractional flow of a certain phase
N_p	[# pore volumes]	Volume of oil produced
W_{id}	[# pore volumes]	Volume of water injected
S	fraction of pore space]	Saturation
ρ	Kg/m^3	Density
K	mD (10^{15} m^2)	Absolute permeability
A	m^2	Cross-sectional area
ΔP	[Pa]	Pressure difference
φ	fraction of bulk volume]	Porosity
N_{pe}	[-]	Peclet number
HU	[-]	Linearized attenuation coefficient
E	[J]	Energy

List of abbreviations

EOR	Enhanced Oil Recovery
SP	Surfactant-Polumer
HPAM	Hydrolysed Polyacrylamide
IFT	Interfacial tension
Subscript w	Pertaining to the aqueous phase
Subscript o	Pertaining to the oil phase
Subscript i	Pertaining to the initial conditions
Subscript e	Pertaining to the final conditions

Introduction

Enhanced Oil Recovery (EOR) is a term to refer to a collective of oil recovery methods beyond primary and secondary recovery methods, such as waterflooding. With primary natural gas drive mechanism which yields recovery factors of up to 20% of OIIP (Sandrea, 2007) and waterflooding which recovers 35% of OIIP globally on average (Muggeridge A, 2014), there remains a significant amount of oil unproduced. This unproduced oil remains trapped inside a reservoirs pore network and is held there by capillary forces or because it is bypassed the water flood.

With such a great portion of the world's oil reserves unexploited and an ever-increasing global demand for crude oil (International Energy Agency, 2017), EOR methods can potentially fill this imminent gap between supply and demand. The problem remains however, that still much is unknown about some physical processes that dominate EOR efficiency. This study aims to address one of these unknowns; namely, that of the emergence, displacement and production of an oil bank during a surfactant-polymer chemical flood.

1. Relevant theory

This chapter shows the pieces of theory relevant for the analysis of experimental data.

1.1 Capillary number and forces and trapping mechanism

The mobilisation of oil through a porous medium boils down to the balance of viscous forces versus capillary forces, a meeting that is described by the capillary number N_c. The capillary number is the ratio between the viscous forces that drive the flow and the capillary forces which resist the flow. It is a function of fluid viscosity dynamic viscosity μ [Pa.s], flow rate Q [m^3/s], porosity φ [fraction] and interfacial tension γ [N/m] and is described in equation 1.1.

$$N_c\,[-] = \frac{\mu * Q}{\varphi * \gamma} \qquad 1.1$$

The viscosity and porosity are fluid and rock properties, respectively, and remain unchanged. The parameters affecting the oil recovery are the flow rate and interfacial tension. Increasing the flow rate would result in an increase in viscous forces, which would increasingly outweigh the capillary forces, resulting in more oil being mobilised. The interfacial tension is the parameter that resists oil mobilisation. Lower interfacial tension would also result in a lower resistance to mobilisation and thus more oil being mobilised, which is exactly the task performed by the surfactant. Figure 1.1. shows the residual oil at different capillary numbers from experimental data: three capillary numbers pertaining to waterfloods at three different flow rates (0.12, 1 and 2 mL/h) and a capillary number corresponding to the surfactant-polymer injection with a lowered interfacial tension. The shows the reduction of the capillary number during the waterflood with increasing injection rate. It shows that even though the injection rate is increased with a factor 8 and then 16, no great amounts of increased oil production are achieved. The datapoints pertaining to the chemical flood show a significant reduction in oil saturation compared to the waterflood. The injection rate during the waterflood is increased greatly, increasing the capillary number by the same factor, but it is minor compared to the decrease in interfacial tension from 52 mN/m to 3 μN/m, a decrease of a factor 17333. These observations indicate that a surfactant is much more capable of giving viscous forces the upper hand over capillary forces than an increased waterflood injection rate.

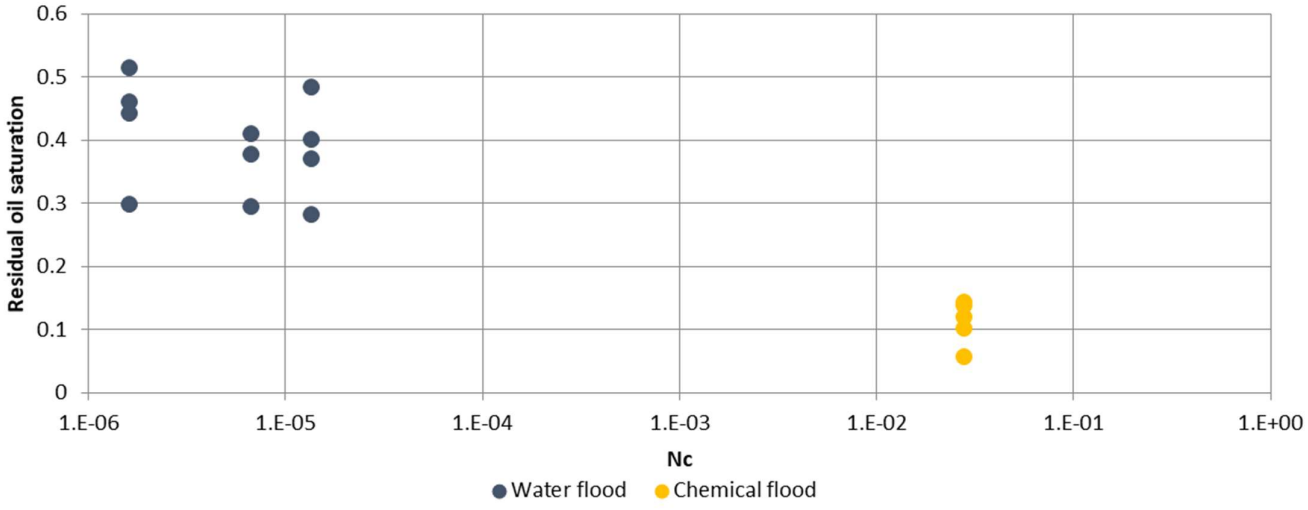

Figure 1.1: Capillary number and residual oil after water flood and chemical flood

Figure 1.2 shows a schematic capillary desaturation curve from (Lake, 1989). Again, it this illustrates the relation between capillary number and the residual oil saturation. What can be concluded is that a lower residual oil, and thus a more efficient sweep, comes with greater a capillary number.

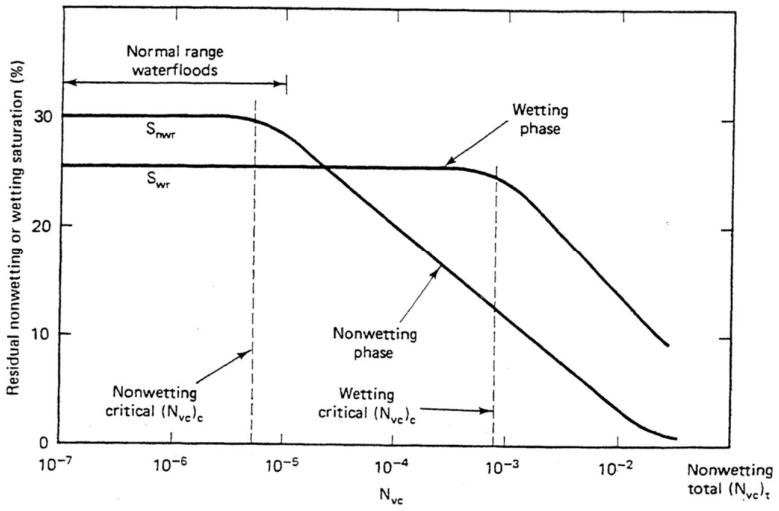

Figure 1.2: Schematic capillary desaturation curve

The trapping of the oil droplets after a waterflood happens through the snap-off concept, schematically illustrated in Figure 1.3. Here, a continuous body of oil flows through the pore network of a water-wet rock. It flows through the broader pore necks after which it encounters a narrower pore throat where oil droplets, or ganglia, are disconnected from the body of oil and remain trapped. In a surfactant flood the objective is to mobilise these oil ganglia and in an ideal case have them coalesce again into a continuous body of oil, or an oil bank.

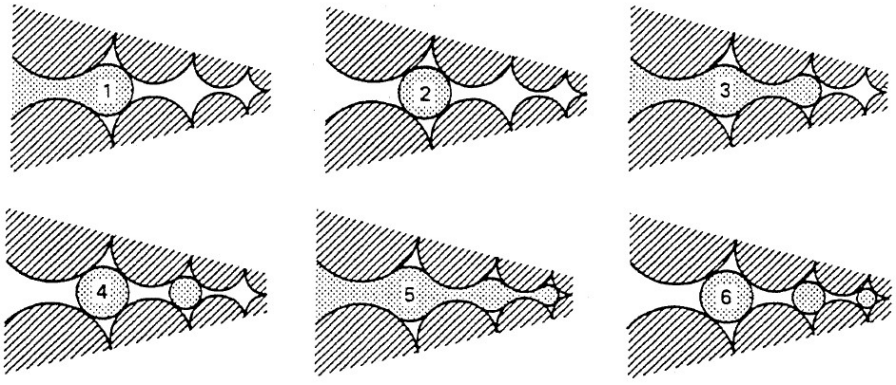

Figure 1.3: Schematic illustration of the snap-off process (Lake, 1989)

1.2 Mobility ratio and favourable displacement in oil-water systems

The mobility ratio M $[-]$ is a parameter that indicates the efficiency of a sweep of a displaced fluid by a displacing fluid. It is a function of relative permeability and viscosity of both the wetting phase and oil non-wetting phase, as shown in equation 1.1

$$M = \frac{\lambda_w}{\lambda_o} = \frac{k_{r,w} * \mu_o}{k_{r,o} * \mu_w} \qquad \text{Eq.1.2}$$

Parameters with the subscript "o" belong to the oil phase, the displaced fluid, and the subscript "w" indicates a parameter belonging to water, de displacing fluid, with λ $[-]$, k_r $[-]$ and μ $[Pa.s]$ denoting the mobility, relative permeability and viscosity respectively.

Favourable conditions are achieved when there is $M < 1$, so when viscosity of the displaced fluid is lower that the viscosity of the displacing fluid. These favourable conditions can lead to greater shock saturations, later breakthrough and subsequently a more efficient sweep. In the unfavourable conditions, or when $M > 1$, there is unstable displacement which can lead to fingering, smaller shock front saturation and early breakthrough leading to a less efficient sweep. A phenomenon depicted in Figure 1.4.

To obtain a favourable mobility ratio in the experiments performed in this thesis project, fluids must be injected in order of increasing viscosity. The chemical flood is started by a surfactant slug, viscosified using polymer, followed by a polymer-solution with polymer concentration such that the solution's viscosity is higher than that of the surfactant slug.

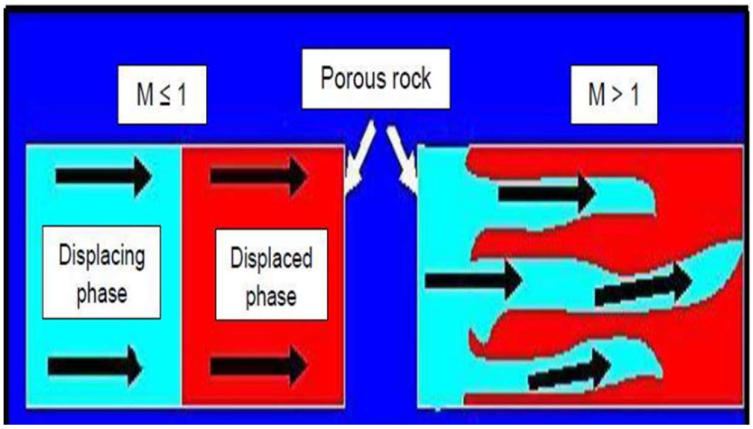

Figure 1.4: Displacement at favourable and unfavourable mobility ratio (Seright, 2005)

1.3 Surfactant

In a way, a waterflood for oil displacement in a porous medium is a battle between the capillary forces trapping the oil and the viscous forces displacing the oil. The recovery factor of a waterflood can only be so high since at some point residual oil is reached or further displacement of oil will require unrealistically high injection rates. A surfactant will allow an incremental recovery, additional produced oil after residual oil is reached in a waterflood, by lowering the interfacial tension (IFT) to ultra-low values. Capillary forces depend on interfacial tension of the present phases, so by lowering the interfacial tension the trapping effect of the capillary forces is mitigated.

The reduction in interfacial tension by the surfactant is a result of the properties of the surfactant at a molecular level. The typical surfactant molecule has a polar hydrophile head that is drawn to water and a nonpolar hydrophobic tail that is repelled by water; as is depicted in Figure 1.5.

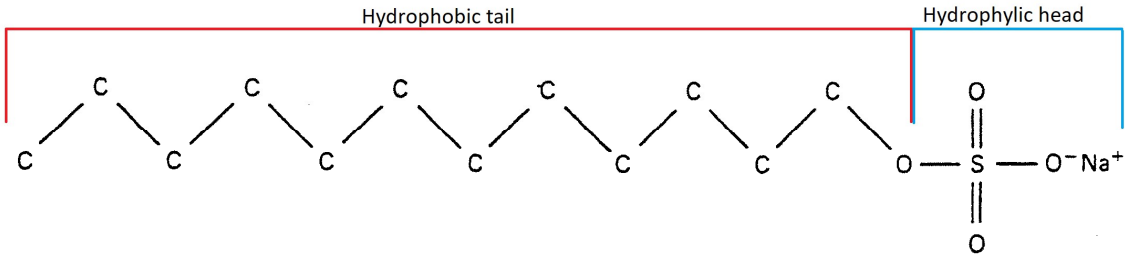

Figure 1.5: Sodium dodecyl sulphate, an example of a surfactant molecule

These two parts of the molecule with opposite affinity to water, enable the molecule to sit at the interface of a water and oil phase, effectively lowering the surface tension. One way to classify surfactants is based on the polarity of the polar head. In a cationic surfactant the polar head has a positive charge, in an anionic surfactant the head has a negative charge, in an amphoteric surfactant both negative and positive charges are present in the polar head and in a non-ionic surfactant the hydrophilic head is not polar at all but bonds to water through hydrogen bonding. At the critical micelle concentration, when the interface between aqueous and oil phase has no more room to accommodate surfactant molecules, micelles will form in one of these phases.

The behaviour of a surfactant mixture depends on several parameters, most important of which in this study, being salinity of the mixture. Depending on the salinity one observes one of three distinct Winsor surfactant-brine-oil systems (Winsor, 1968).

The Winsor type II(-) system is observed at suboptimal salinity, which is deemed nonoptimal within the framework of reduction of interfacial tension. Here, the surfactant is very soluble in an aqueous phase and poorly soluble in the oil phase. At equilibrium there will be a clear oil phase and an aqueous phase that contains swollen micelles. These micelles are basically oil droplets, covered in surfactant monomers that allow the oil droplets' solubilization in the aqueous phase.

The type II(+) system occurs at over-optimal salinity. This case is quite similar to the type II(-) in the sense that there is one clear phase and a phase containing micelles in the surfactant-brine-oil system, with major difference being the fact that the micelles are drawn into the oil phase.

Finally, there is the type III system. The number three refers to the fact that in this case, which occurs at optimal salinity, there are three distinct phases present: a clear aqueous phase, a clear oil phase and a microemulsion middle phase. This microemulsion middle phase is in direct contact with the brine and oil, resulting in two IFT's: one between the microemulsions and brine and one between the microemulsions and oil. The type III system is the preferred in EOR since its dramatic decrease in IFT dwarfs than of the type II(-) and II(+) systems.

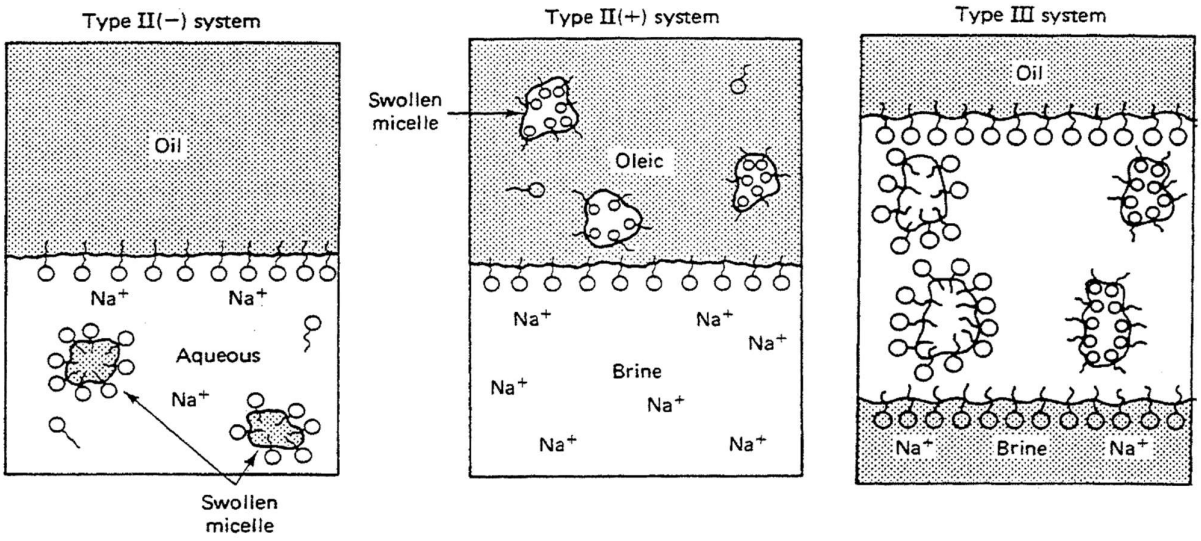

Figure 1.6: The three Winsor types of surfactant-brine-oil systems (Lake, 1989)

One way two find the optimal salinity is with a phase behaviour analysis. Here, surfactant-brine-oil mixtures are composed with ranging salinities. The objective here is finding a salinity where there is a clear oil and a clear brine with microemulsions in between; this would indicate that optimal salinity is reached. One would observe at suboptimal salinity a translucent brine and clear oil and at over-optimal salinity a clear brine and translucent oil. The results of the phase behaviour analysis performed in this study is discussed in Section 3.1.

1.4 Polymer

In this report, the term polymer is used to indicate a synthetic viscosifying soluble agent. As stated in Section 1.2, to obtain an efficient as possible sweep fluids are to be injected in a core flood experiment with at a favourable mobility ratio. The mobility ratio is best controlled through the viscosity of the injected fluids and favourable conditions are achieved by injected fluids at increasing viscosity. The hydrolysed polyacrylamide (HPAM) is in this project the polymer that is used to obtain desired viscosity in both the surfactant-polymer and polymer slug.

The viscosity of polymer solutions depends on several parameters, most important of these are temperature, polymer concentration, salinity and shear rate. The temperature in experiments is not expected to show significant fluctuations, so temperature effects on polymer solutions are neglected. Since HPAM-solutions are shear thinning nonnewtonian fluids, the viscosity also depends on the shear rate (Odell, 1988). Since viscosity depends on the shear, apparent viscosity measurements are performed at a shear rate typical for a sandstone of $6s^{-1}$ (Berg, 2017). Salinity is a pre-set parameter that is kept at a constant value. In Chapter 2, where the experimental setup is explains, it shows that the setup contains conductivity meters. To be able to clearly discern the polymer from other phases and solutions in the effluent, the choice is made for a low salinity polymer. This low salinity polymer should be clearly visible in effluent data due its low conductivity. The polymer concentration is chosen as key factor in obtaining a required viscosity.

An important note to keep in mind: in this report the term viscosity is used liberally, but since HPAM-solutions are dependent on shear rate, what is measured is apparent viscosity. Seeing as all viscosities are measured at the same shear rate and for the sake of simplicity, apparent viscosity is referred to as just viscosity.

1.5 Buckley-Leverett fractional flow theory

To get a better insight into the mobility of the displacing and displaced fluids in a core flood experiment, relative permeability estimations must be made. One tool to model fluid mechanics is the Buckley-Leverett (BL) equation (Leverett, 1942) combined with the Brooks-Corey (BC) equation (Corey, 1964). This tool is applied through history matching, wherein fitting parameters are chosen such that the estimated oil production from BL-theory matches experimental data. Major side note in this approach is de neglection of capillary and gravitational forces.

First step in applying BL-theory is defining a range of water saturations from the initial water saturation S_{wi} to the water saturation at residual oil conditions $S_w = 1 - S_{or}$. To obtain relative permeability for water and oil phase an initial estimate must be made for Corey exponents and endpoint relative permeability for both water and oil, n_w, n_o, $k_{rw,e}$ and $k_{ro,e}$ respectively. These parameters are used in calculating relative permeability of water and oil as a function of water saturation, as seen in equation set 1.

$$k_{rw} = k_{rw,e} * \left(\frac{S_w - S_{wi}}{1 - S_{or} - S_{wi}}\right)^{n_w} \qquad k_{ro} = k_{ro,e} * \left(\frac{1 - S_w - S_{wi}}{1 - S_{or} - S_{wi}}\right)^{n_o} \qquad \text{Eq.1.3}$$

With relative permeability at specific saturations and with viscosity of injected fluids known, using the BL-equation the mobility ratio can be determined and with the fractional flow of water and oil, M, f_w and f_o respectively.

$$f_w = 1 - f_o = \frac{\lambda_w}{\lambda_w + \lambda_o} = \frac{1}{1 + \frac{1}{M}};\ \text{with } M = \frac{k_{rw} * \mu_o}{k_{ro} * \mu_w} \qquad \text{Eq.1.4}$$

The next step in the process is to determine the water saturation at which breakthrough occurs ($S_{w,BT}$). This value is found by plotting the derivative of water fractional flow with respects to water saturation and a plot of the delta function $\frac{\Delta f_w}{\Delta S_w} = \frac{f_w}{S_w - S_{wi}}$, a plot depicted in Figure 1.7. The saturation where these two plots intersect is the water saturation at which breakthrough occurs.

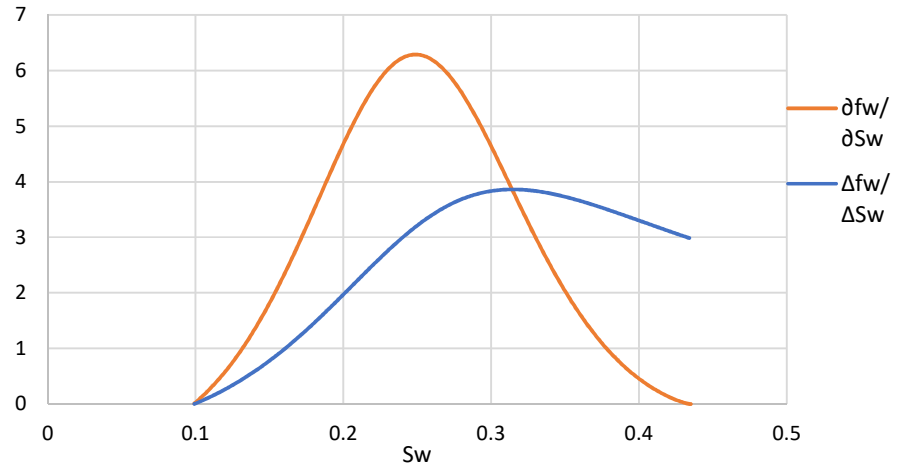

Figure 1.7: Derivative and delta function of water fractional flow

The water saturation at breakthrough is relevant in the Welge solution (Welge, 1952), wherein there is only production of oil before breakthrough of injected brine. So up to the point of breakthrough, volume of produced oil N_p is equal to the volume of injected brine W_{id}. After breakthrough the oil production in dimensionless porevolumes is determined using Equation 1.5.

$$N_p = S_w - S_{wi} + (1 - f_w) * W_{id} = S_w - S_{wi} + \frac{(1-f_w)}{\frac{\partial f_w}{\partial S_w}} \qquad \text{Eq.1.5}$$

The initial estimation of the Corey exponents and endpoint relative permeability may cause a mismatch between BL production data and experiment production data. The Corey exponents are iteratively re-estimated until a satisfactory match between production datasets is achieved. While determining proper Corey parameters the relative permeability data is also altered and reaches a solution that best describes the phase behaviour when production data is matched. In Sections 1.6 the JBN method, which provides another tool in generating relative permeability curves, is discussed.

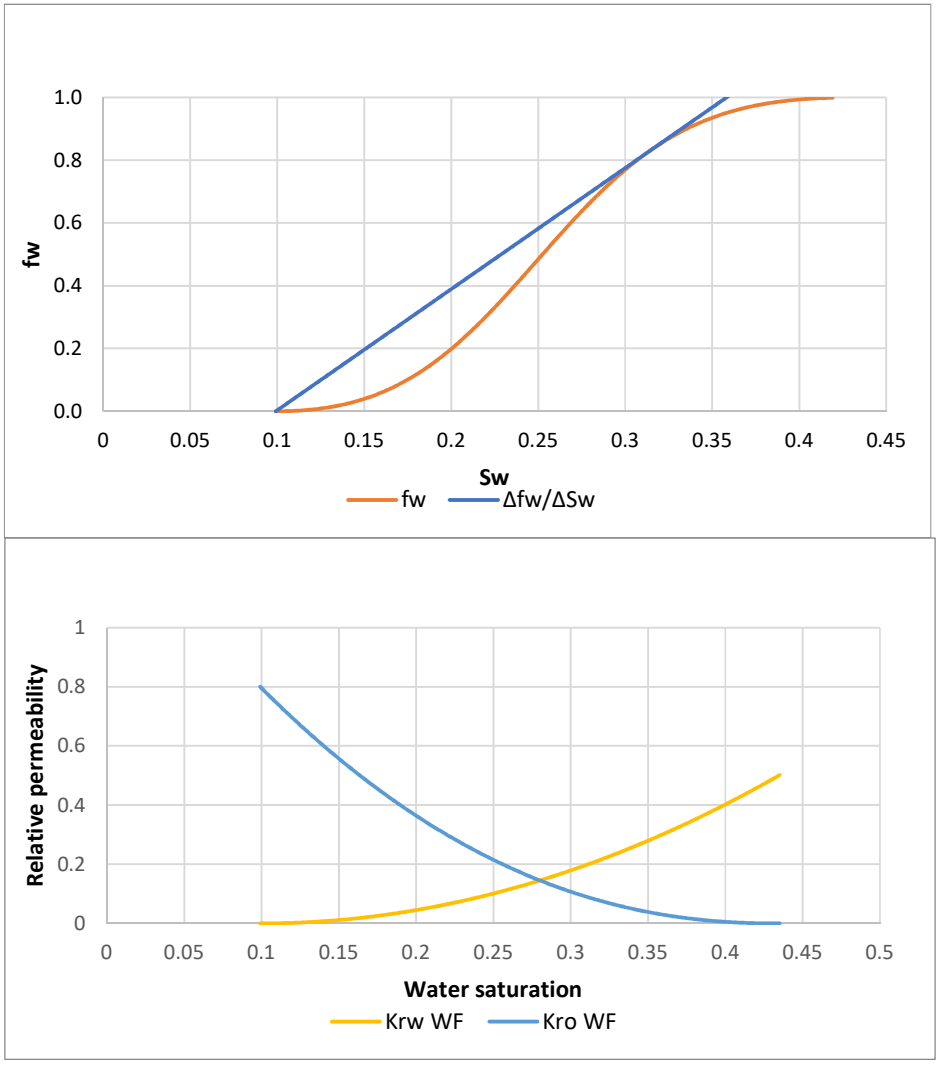

Figure 1.8: Typical relative permeability (bottom) and fractional flow (top) curves for a water flood

1.6 Johnson, Bossler and Naumann method for generating relative permeability curves

One method to evaluate phase behaviour through relative permeability curves is the Johnson, Bossler and Neumann (JBN) method (Johnson, 1959). It is a mathematical approach based on Darcy's law and Buckley-Leverett theory that utilizes production data from core flood experiments to calculate relative permeability. Most important input data required are pore volumes of injected water W_{id} [-], porevolume of produced oil N_p [-] and pressure difference over the entire core ΔP [Pa] along with other parameters like core dimensions and porosity.

First relevant parameter to define is the oil cut of the effluent f_o [-]. In this study the experimental setup contains a Coriolis meter at the outlet that measures the effluent density. This measured density ρ $\left[\frac{kg}{m^3}\right]$ and the known densities of oil and brine are used to calculate the oil cut, as seen in Equation 1.6.

$$f_o = \frac{\rho - \rho_{oil}}{\rho_{brine} - \rho_{oil}} \qquad \text{Eq.1.6}$$

Another definition for fractional flow of oil is described in Equation 1.7.

$$f_o = \frac{\lambda_o}{\lambda_w + \lambda_o} \text{ where } \lambda_o = \frac{K * k_{r,o}}{\mu_o} \qquad \text{Eq.1.7}$$

Darcy's equation for flow through porous media is also utilized in deriving an equation for relative permeability:

$$f_o * \frac{Q}{A} = \frac{K * k_{r,o}}{\mu_o} * \frac{dP}{L} \qquad \text{Eq.1.8}$$

Another relevant parameter is the relative injectivity I_r described in (Rapoport, 1953). This parameter is a function of injection rate (Q) and the initial and real-time pressure difference over the core, dP_i [Pa] and dP [Pa] respectively

$$I_r = \frac{dP_i}{dP * Q/A} \qquad \text{Eq.1.9}$$

Equations 1.7 and 1.9 are combined with Darcy's equation to obtain an equation for oil relative permeability, Equation 1.10

$$k_{r,o} = f_o * \frac{d\left(\frac{1}{W_{id}}\right)}{d\left(\frac{1}{W_{id} * I_r}\right)} \qquad \text{Eq.1.10}$$

Equation 1.10 is plugged into Equation 1.7 to obtain an equation for water relative permeability, Equation 1.11.

$$k_{r,w} = \frac{1 - f_o}{f_o} * \frac{\mu_w}{\mu_o} * k_{r,o} \qquad \text{Eq.1.11}$$

1.7 Permeability measurements to establish heterogeneity in pore geometry

An important tool in establishing permeability, and with it to some extent the heterogeneity in a core, are core flood permeability tests. In this stage where the core has not seen any oil yet, a single phase is injected into the core at different flow rates. While injecting pressure is measured at the inlet, at intermediate points along the core length and at the outlet to establish a pressure gradient over both the entire core, as well as smaller sections of the core. These measured pressure gradients and set injection rate are combined with 1 dimensional variant of Darcy's law to calculate average permeability over the entire core and over the smaller intervals. Darcy's law is seen in Equation 1.12.

$$\frac{Q}{A} = \frac{K}{\mu} * \frac{\Delta P}{\Delta x} \qquad \text{Eq.1.12}$$

The flow rate Q $\left[\frac{m^3}{s}\right]$ is set at the pump but is also measured using Coriolis meters to get more accurate values since pump flow rates can fluctuate. The cross-sectional area of the core A $[m^2]$, viscosity μ $[Pa.s]$ and length over which pressure gradient is calculated Δx $[m]$ are known from the setup design parameters or literature values. Rewriting the equation in filling in known and measured parameters yields permeability K $[m^2]$.

As stated before, a range of injection rates is implemented to get an as accurate as estimation for permeability. Injection is started at a relatively low injection rate of 0.5 mL/min, and ramped up to 3 mL/min in increments of 0.5. After the peak flow rate, the flow rate is decreased in the same but inverse fashion to the starting injection rate to ensure repeatability of results.

1.8 Tracer analysis to determine accessible pore volume

The tracer analysis is a tool to analyse the accessible pore volume of a core to obtain some insight into the residual oil saturation, the adsorption of polymer and/or surfactant and whether a core has returned to initial conditions after cleaning. In this method the experimental data is compared to model data, which depends on many parameters, most important of which being porosity and dispersion coefficient. (Coats, 1964)

For the experimental data the injected tracer has a potassium iodide concentration of approximately 100 ppm. It is injected at a consistent injection rate while the effluent is collected in 3 mL increments. The KI-concentration of the incremental effluent is measured. For a proper comparison with model data, the experimental data is expressed as KI-concentration of incremental effluent as a fraction of concentration of injected solution $\frac{C}{C_i}\ [-]$ vs injected pore volume $PV_i\ [-]$. Typically, plotting this data yields an S-shaped curve with concentration ratio starting at 0 and ending at 1.

The first step of the modelling tracer data is de calculation of the Peclet number N_{pe}, or the ratio of the advective transport over the diffusive transport:

$$N_{pe} = \frac{q*L}{\varphi*D} \qquad \text{Eq.1.13}$$

In this equation $q\ \left[\frac{m}{s}\right]$ denotes the superficial velocity, L $[m]$ the length of the core, φ the cores porosity and $D\ \left[\frac{m^2}{s}\right]$ the dispersion coefficient that reflects the heterogeneity of a core. The resulting Peclet number is used in Equation 1.14 to estimate effluent concentration.

$$\frac{C}{C_i} = 0.5 * \left(erfc\left(\sqrt{\frac{N_{pe}}{4*PV_i}} + 0.5 * (1 - PV_i)\right) + erfc\left(\sqrt{\frac{N_{pe}}{4*PV_i}} + 0.5 * (1 + PV_i)\right)\right) \qquad \text{Eq.1.14}$$

The model result is, like the experimental data, an S-shaped curve with concentration ratio starting at 0 and ending at 1. The goal then is to make the model data fit the experimental data, which is done by iteratively guessing porosity and dispersion coefficient. By changing porosity, the model curve is shifted left or right, while changing dispersion coefficient changes the S-shapes curvature. When experimental and model curves a best estimate of porosity is obtained, which, along with the core dimensions, can be used to establish accessible pore volume.

The results of a tracer analysis depend on several parameters, as stated above. Most relevant of these results is the estimation of pore volume, in order to know how much of a fluid to inject exactly when injected 0.5 PV of something, for example. Second most important result is evaluating whether the core has returned to its initial conditions after having been used in a core flood experiment. Improper cleaning of the core could allow some oil to remain inside its pore network, which has some consequences for following experiments.

The results of the tracer analysis and some relevant observations stemming from it are discussed in Appendix D.

1.9 Method for calculating oil saturation from CT-Scans

CT-scans provide a great insight in oil behaviour and possible oil bank behaviour. Many conclusions can be drawn with the naked eye by observing processed images of CT-scans. The processed images however often give a distorted view of reality. Images in grey scale often do not highlight saturation contrasts clearly enough to observe while images with synthetic colours give an exaggerated view of reality. To properly evaluate oil displacement, one should quantitively express these contrasts in oil saturation.

CT-scans provide data in Hounsfield units. Hounds Units HU $[-]$ are a linear expression of attenuation coefficient N $[m^{-1}]$ with the attenuation coefficients of water and air at ambient conditions as references (Feeman, 2010); Equation 1.15 shows the equation how HU is expressed.

$$HU = 1000 * \frac{N - N_{water}}{N_{water} - N_{air}} \quad \text{Eq.1.15}$$

So, the real parameter is measured in a CT-scan is attenuation coefficient of a material, which results from Lambert-Beer law. Here the attenuation coefficient is calculated from the initial energy E_0, final energy E $[J]$ and travelled distance of a photon, as seen in Equation 1.16.

$$E = E_0 * e^{N*d} \quad \text{Eq.1.16}$$

In general, a photon loses more energy when passing through a denser material, resulting in a higher attenuation coefficient and HU. This relation is the premise in the calculation of saturation wherein the CT's HU are treated as density in a porous medium. For a porous medium with both oil and water density is calculated using Equation 1.17.

$$\rho_{bulk} = \rho_{matrix} * (1 - \varphi) + \varphi * S_o * \rho_{oil} + \varphi * (1 - S_o) * \rho_{brine} \quad \text{Eq.1.17}$$

For a porous medium with only brine density is calculated using Equation 1.18. The same equation holds for a dry porous medium with only air in the pores by using density of air instead of density of brine.

$$\rho_{bulk} = \rho_{matrix} * (1 - \varphi) + \varphi * \rho_{brine} \quad \text{Eq.1.18}$$

By replacing the densities with HU for each material one can get an estimation for saturation. The following equations are obtained:

$$HU_{experiment} = HU_{matrix} * (1 - \varphi) + \varphi * S_o * HU_{oil} + \varphi * (1 - S_o) * HU_{brine} \quad \text{Eq.1.19}$$

$$HU_{core,S_w=1} = HU_{matrix} * (1 - \varphi) + \varphi * HU_{brine} \quad \text{Eq.1.20}$$

$$HU_{dry\ core} = HU_{matrix} * (1 - \varphi) + \varphi * HU_{air} \quad \text{Eq.1.21}$$

Equations 1.20 and 1.21 are subtracted from one another to obtain an estimation for porosity.

$$HU_{core,S_w=1} - HU_{dry\ core} = (1 - \varphi) * HU_{matrix} + \varphi * HU_{brine} - (1 - \varphi) * HU_{matrix} - \varphi * HU_{air} = \varphi * HU_{brine} - \varphi * HU_{air}$$

$$\varphi = \frac{HU_{core,S_w=1} - HU_{dry\ core}}{HU_{brine} - HU_{air}} \quad \text{Eq.1.22}$$

The CT measurement of the brine saturated porous medium is subtracted from the CT-measurement of the porous medium during a core flood experiment, the equation is rewritten to obtain an expression for saturation and the equation for porosity is plugged into it.

$$HU_{experiment} - HU_{core,S_w=1}$$

$$= HU_{matrix} * (1-\varphi) + \varphi * S_o * HU_{oil} + \varphi * (1-S_o) * HU_{brine} - (1-\varphi) * HU_{matrix} - \varphi * HU_{brine} \quad \text{Eq.1.23}$$

$$S_o = \frac{1}{\varphi} * \frac{HU_{experiment} - HU_{core,S_w=1}}{HU_{oil} - H_{brine}} = \frac{HU_{brine} - H_{air}}{HU_{core,S_w=1} - HU_{dry\ core}} * \frac{HU_{experiment} - H_{core,S_w=1}}{HU_{oil} - HU_{brine}} \quad \text{Eq.1.24}$$

Major footnote to consider here is that these calculations are an estimate only. A linear relation between density and attenuation coefficient is not an accurate one and some materials strongly deviate from this relation. Specifically, materials containing iodide, such as the iododododecane oil used in this study, have a high attenuation coefficient. Appendix C discusses these deviations and the accuracy of these calculations further.

1.10 Experimental objectives

As the title of this thesis report indicates, the major goal of this study is to evaluate the behaviour of an oil bank during surfactant-polymer chemical EOR. This study evaluates this behaviour through core flood experiment. However, chemical floods are generally too complex to attribute certain observations to a single specific fluid or rock property.

Within the framework of previously done work, most relevant influence on effect on the oil bank behaviour, is that of the core length. Previous studies ((Al Saadi, Ongoing) and (Wijsman, 2018) contain much data on the effects of experimental parameters on the oil bank behaviour. The greatest difference between those experiments and those performed in this study is the fact that in this study cores of greater length are used. In the long run, by combining results from this study, (Al Saadi, Ongoing) and (Wijsman, 2018), some elaborate conclusions about the effects of core length on the oil bank behaviour can be derived.

The length of a porous medium is not the only factor that affects the oil bank behaviour, and this study aims to address the effects of these other parameters as well. The effects of core permeability, heterogeneity, surfactant-polymer optimality and viscosity are also considered in studying the oil bank behaviour.

The oil bank behaviour will be attempted to be described, both qualitatively and quantitively, using direct production data from core flood experiments, relative permeability analysis of production data, CT-scan images and processed data of CT-scans.

2 Experimental setup

Core preparation

Before it is inserted into the setup, the drilled and cut core is to be covered in a sealing epoxy glue layer. The sole purpose of this glue is to ensure that there is no radial outward flow from the core, so that flow only occurs over the length. The core is initially covered in a thin layer of glue to ensure proper adhesion to the thicker glue layer where it is cast in later. Air bubbles may be trapped in the glue as it dries, it would therefore be wise to identify any potentially problematic bubbles via CT-scan

Leak test

The leak test is performed by closing the setup's outlet while flooding it with helium. When the system is saturated with helium and there is an overall consistent pressure, the helium supply is closed off. In a setup without leaks the pressure remains consistent over the entire setup; if a rapid pressure drop is observed, it is very likely that there is a leak somewhere. (Swej Shah, 2017).

Vacuuming and brine saturation

To ensure the core is fully saturated with brine and no air is trapped, a certain procedure must be adhered to. At no pumping conditions with no backpressure the setup is flooded with CO_2 to flush out the air, since CO_2 has better solubility in water than air. After a few minutes the CO_2 supply is shut off, the setup inlet is closed and the outlet is connected to a vacuum pump. The entire system is vacuumed until a consistent pressure is reached throughout the entire setup. While still vacuuming, degassed brine is pumped into the system until brine is observed at the outlet. Finally, the vacuum pump is disconnected and flow is directed in its normal path via backpressure regulator. Finally, the backpressure is increased in 5 bar increments while brine is pumped through the system.

Oil saturation

Some considerations have been made in the setup to maximise oil saturation. One of which is that oil is injected into the core from what would be the outlet during a water or chemical flood; this ensures that there is stable brine displacement with the help of buoyancy in the case of a vertically aligned core, since lighter oil would be injected from the top. Second consideration is the implementation of a semi-permeable plate at what would be the outlet during oil injection. This semi-permeable plated is extremely water-wet, so it easily allows brine pass through it while inhibiting the flow of oil. Figure 2.1 shows these flow paths.

In this study two types of oil are used, namely Dodecane and Iodododecane of which relevant properties are presented in Table 2.1. The Dodecane oil is the simplest type of oil with density lower and viscosity higher than that of water, much like a reservoir oil, and is used in most experiments. The Iodododecane oil is used only in experiments where CT-scans are performed, since it is denser than brine and contains an Iodide-group, which produced a stronger contrast in attenuation coefficient than any other material in the core.

Table 2.1: Types of oil used and their physical properties

Name	Chemical formula	Density (kg/m^3)	Viscosity (cP) at 6 s^{-1} shear rate
Dodecane	$C_{12}H_{26}$	750	2.2
Iodododecane	$CH_3(CH_2)_{11}I$	1190	3

Tracer injection

The goal of the tracer analysis is determining the accessible pore volume of the core. This gives some insight with respects to the oil saturation, adsorption of surfactant or polymer and the extent in which the core has returned to initial conditions after cleaning. The injected tracer has a potassium iodide concentration of approximately 100 ppm. It is injected at a consistent injection rate while the effluent is collected in 3 mL volumetric increments. The KI-concentration of the incremental effluent is measured and gradual increase in KI-concentration is analysed with a set of equations to establish accessible pore volume, as is discussed in Section 1.8.

Waterflood

The objective of a waterflood in this study is to bring the core's oil saturation as close to residual oil as possible. The waterflood is performed at an injection rate that, in this setup, coincides with the typical field rate of 1 foot/day. The injected brine must have a very specific salinity, namely the same as the SP-mixture. After the injection of 1 pore volume (PV) of brine, when no more oil is produced, the injection rate is increased. These bump floods occur at increasingly higher injection rates until no more oil is produced after increasing the injection rate.

Chemical flood

The chemical flood is performed in a specific manner, predetermined by previously done work (Wijsman, 2018) (Al Saadi, Ongoing). Initial step in the injection of 0.5 PV of SP cocktail, followed by 1 PV of polymer solution and finally 1 PV of brine. The specific composition of the SP and polymer mixtures are discussed in Section 3.1.

CT-scans

Some of the experiments performed in this study, are done under a CT-scan. The goal here is to obtain more insight into the behaviour of the injected and produced fluids. The CT-scanner discerns phases based on density, and to a lesser extent the chemical composition. The benefit of this is there is a clear difference between displacing and displaced fluids, which allows a visualization of certain physical phenomena, such as oil bank formation and the stability of the displacement.

Setup components

Data acquisition by the set-up is done using several components with each their relevance and accuracy. Figure XX shows a schematic overview of the set-up and where these components are situated.

First of these relevant components are two identical Bronkhorst M14 Mini Cori-Flow Coriolis mass flow meters. These Coriolis meters measure density $\left[\frac{kg}{m^3}\right]$ and mass flow rate $\left[\frac{g}{hr}\right]$ with both parameters having an uncertainty range of 0.2%. One mass flow meter is situated at the start of the flow path after the pumps and the second is situated at the very end just before the back-pressure regulator. The greatest benefit of using two Coriolis meters is that any mismatch between their measurements is a strong indicator that there is either a leak or that steady state has not been reached yet.

Second relevant measuring apparatuses are the conductivity meters. The benefit of the devices is that they are a very useful tool in discerning the different fluids used in the experiment from one another, since they have strongly contrasting electrical conductivities. The conductivity meter at the outlet helps confirm the type of fluid being produced, while the conductivity meter at the inlet gives an estimate of the conductivity of a certain fluid. The word “estimate” hints at the fact that these meters were found to be unacceptably inaccurate. After being linked together with brine flowing through them, the devices were found to show a difference of 9.7% in measured conductivities. This observation rendered any conductivity measurements not suited for further calculations but are still a very useful indicator of fluid types.

Pressure measurements are performed using a set of 12 Keller Series 11 Piezoresistive Pressure Transducer. With a measuring range of 0.01 to 100 bar, they are more than able to handle a core flood’s conditions. These specific pressure transducers have an uncertainty of 0.2%.

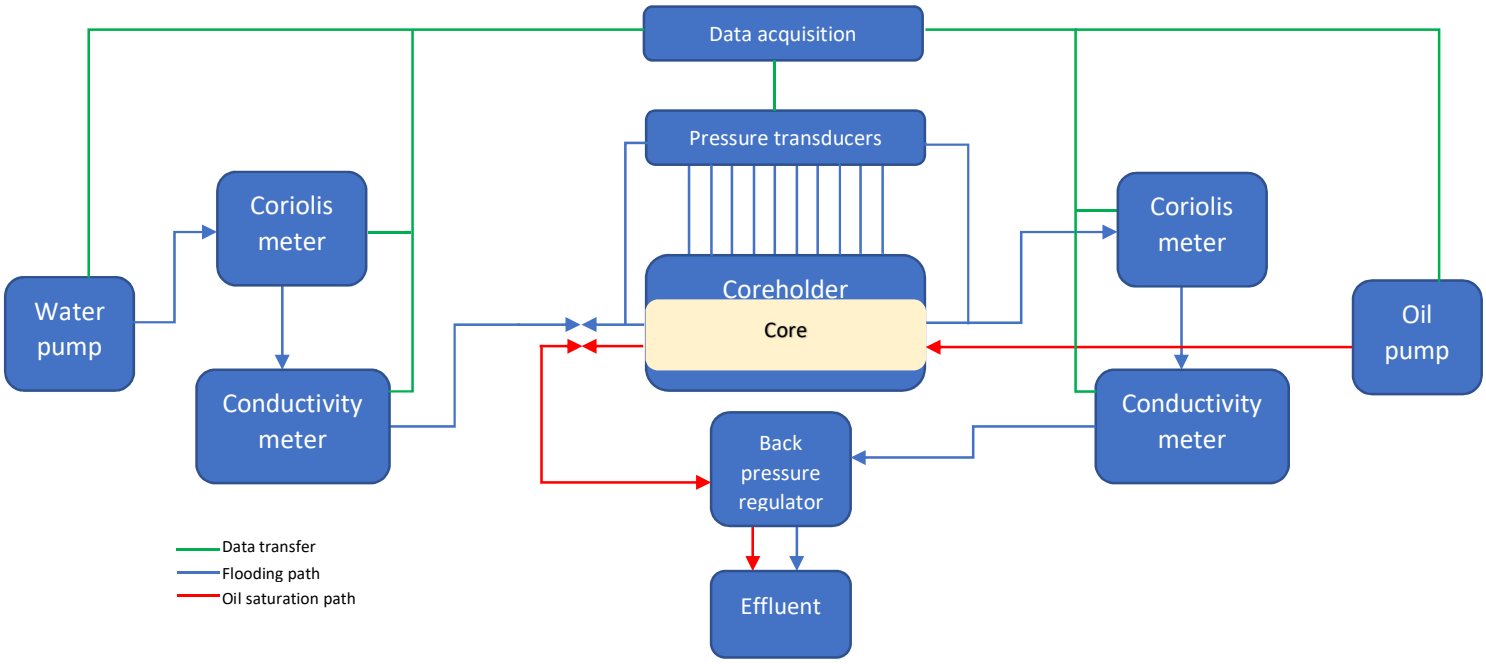

Figure 2.1: Schematic overview of the core flood setup

3 Results and conclusions

3.1 Phase behaviour analysis and establishing optimal conditions

As discussed in Section 1.3, the phase behaviour analysis was performed to determine the conditions wherein the optimal Type III system of phases is achieved. The basic principle is to vary salinity, but keep other parameters, concentrations of cosolvent and active surfactant component, constant. A range of mixtures was made with salinities ranging from 2.5% to 5% in 0.5% increments. What is noteworthy is that the dodecane oil is lighter than water, so lies on top. The result of the phase behaviour analysis for a Dodecane system is depicted in Figure 3.1.

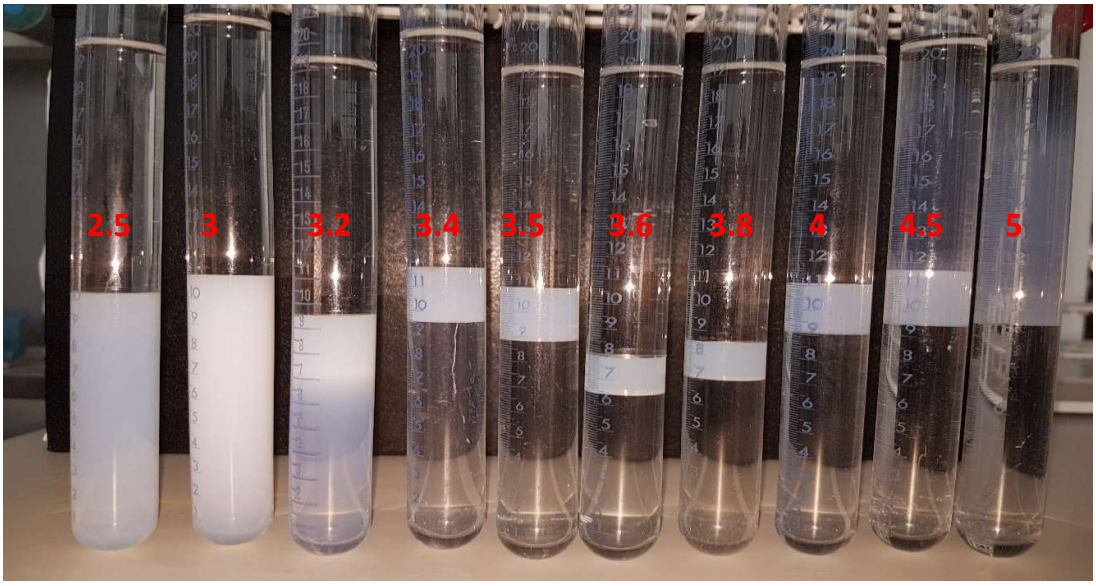

Figure 3.1: Results of the dodecane oil phase behaviour analysis (numbers indicate salinity in %wt NaCl)

At first glance, the results in Figure 3.1 seem to follow the Winsor types of surfactant-brine-oil systems depicted in Figure 1.6 in Section 1.3. It appears that at salinities up until 3.2%, the micelles are drawn into the water phase making it opaque, leading to the conclusion that at salinity of 3.2% or lower there is a Type II(-) suboptimal Winsor system. At a salinity of 4% or higher, it seems that the micelles are drawn into the oil phase, allowing the conclusion that at these salinities one is dealing with a overoptimal Type II(+) Winsor system.

At salinities between 3.2% and 4% there are seemingly clear brine and oil phases with a distinct microemulsion phase between them. These results alone give a wide range of salinity where the optimum may lie, since the naked eye alone cannot clearly discern where in this range exactly the optimum lies. The best estimate for an optimum salinity with these specific types of brine and oil follows from interfacial tension measurements in (Wijsman, 2018), the results of which are depicted in Figure 3.2.

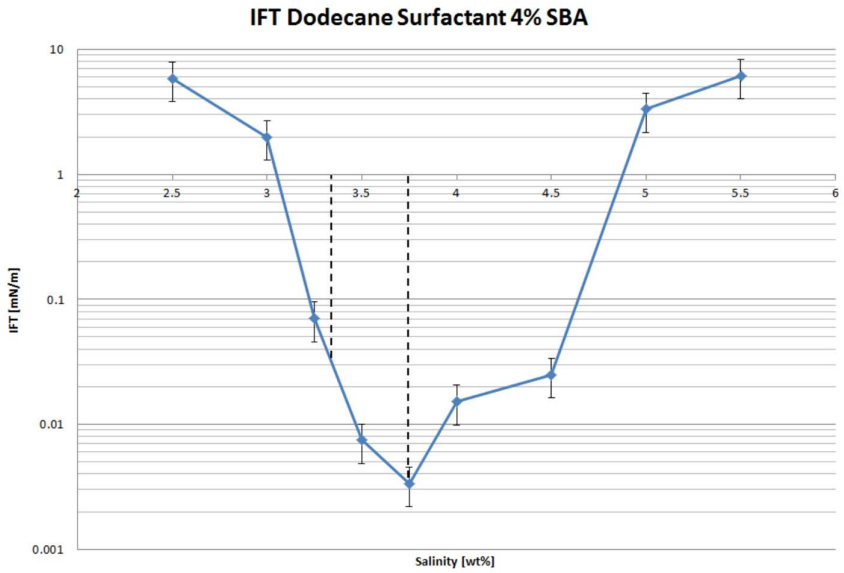

Figure 3.2: Interfacial tension measurements at varying salinity (Wijsman, 2018)

From the graph in Figure 3.2, it appears indeed that the optimum salinity lies between 3.2% and 4%. The greatest reduction in IFT is observed at a salinity of 3.75%, so from here on this salinity will be referred to as the optimal salinity for an experiment with dodecane oil. For iododododecane oil the optimum salinity was found at 4.5%.

Figure 3.3 shows the results of the phase behaviour analysis for the iododododecane oil. The iododododecane oil is denser than water so here it lies at the bottom. Up to 4% NaCl salinity microemulsions are drawn into the water phase, so up to 4% there is suboptimal surfactant. At 7% salinity there are overoptimal surfactant, since microemlusions are observed in the oil phase, leaving a range between 4% and 7% where the optimum may lie. IFT measurements in (Wijsman, 2018) show that the biggest reduction in IFT is measured at 4.5% NaCl salinity, which is hence chosen as the optimal salinity.

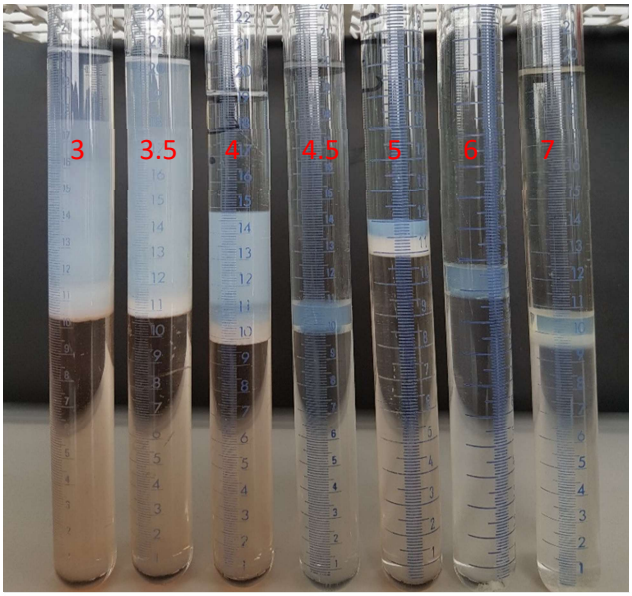

Figure 3.3: Results of iododododecane phase behaviour analysis (numbers indicate salinity in %wt NaCl

3.2 Results and discussion of 7.5cm core experiments

3.2.1 Typical 7.5 core flood experiment and production data analysis

Figure 3.4 shows a typical plot of the data gathered from a core-flood experiment containing both the data from the waterflood and chemical flood. The parameters describing this specific experiment are seen in Table 3.1.

Table 3.1: Relevant parameters of 7.5HP1 experiment 1					
Rock type	Core length	Core porosity	Core Permeability	SP-salinity	Initial S_o
Fontainebleau	7.5cm	0.16	120 mD	3.75% (optimal)	0.75

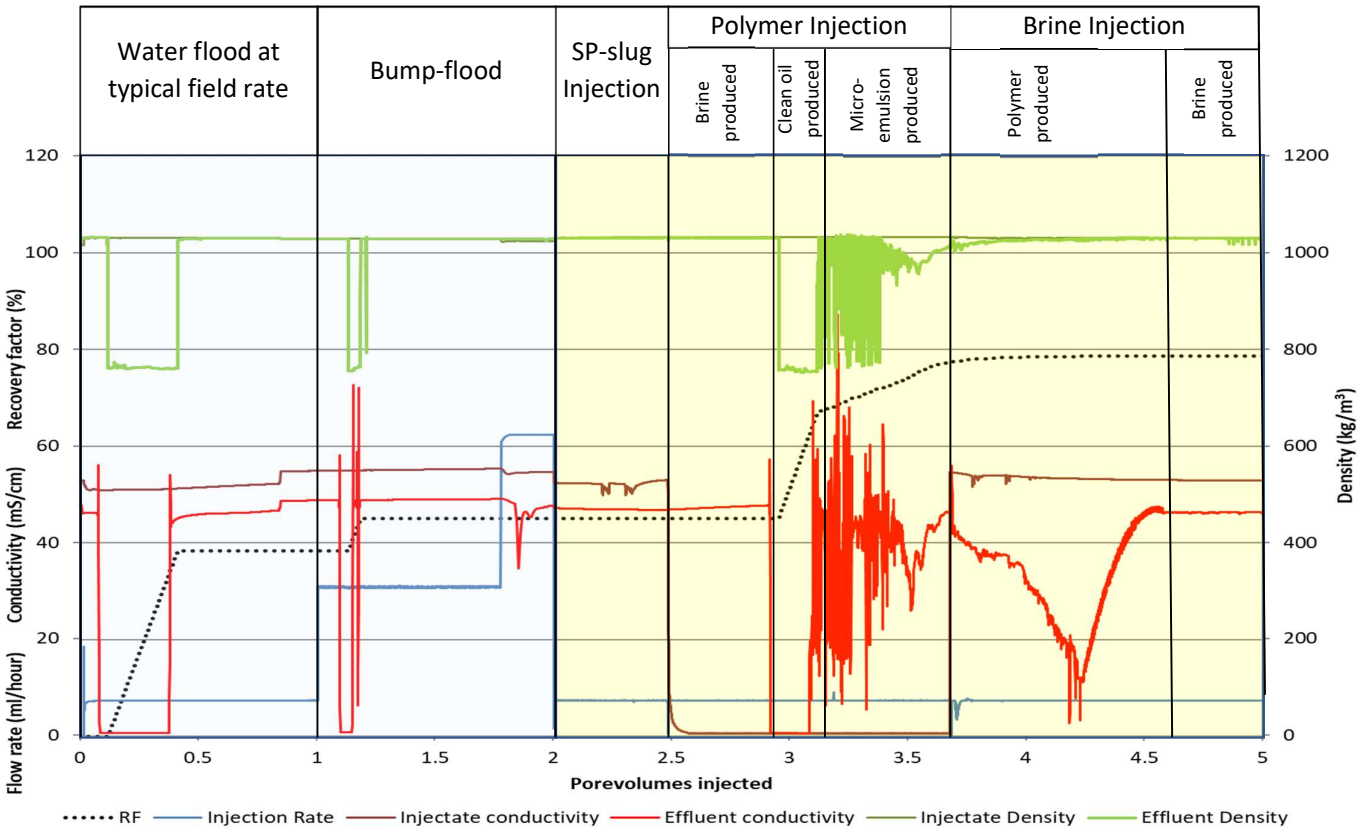

Figure 3.4: Production data with a 7.5cm core and optimal surfactant

The waterflood section of this graph contains several observations that are expected from a waterflood performed as described in Chapter 2. The injection rate shows, as discussed before, an initial injection rate of 6 ml/hour (or 0.12 mL/min), which corresponds to the typical field rate of 1 feet/day. Following this typical injection rate, after 1 PV injected, are the bump-floods at 30 mL/hour and 60 mL/hour, respectively. The conclusion to this bump-flood follows from the fact that after increasing the injection rate from 30 to 60 mL/hour there is no more oil production, rendering a further increase of injection rate futile.

The produced oil at the typical field rate, seen in the graph between 0 and 0.5 PV, is not only observed in the density data, where density is that of dodecane oil (750 kg/m^3), but is also confirmed by the effluent conductivity, which goes to values close to 0.7 mS/cm. The oil recovery of the waterflood is a total of 45% of the initial oil in place (OOIP), of which 39% is produced at the standard field rate and an additional 6% produced at the bump-floods.

The data of the chemical flood also shows several consistencies pertaining to the procedure discussed in Chapter 2. The chemical flood starts with the injection 0.5 PV of the SP-solution, seen in Figure 3.4; the injectant density does not show much difference between the SP and brine, while the injectant conductivity shows a slight drop from brine to SP, which is a result of the low conductive Butanol cosolvent.

The SP-slug is followed by 1 PV of polymer, which is observed between 2.5 and 3.5 PV injected in the low injectant conductivity, but not so much in the density. The polymer is followed by brine, which results in injectant conductivity and density identical to that before the SP is injected.

Up to approximately 3 PV injected, the effluent data shows that there is only brine produced. From 3 PV injected there is extremely low effluent conductivity and effluent density identical to that of dodecane oil. This “clean oil” section of the production data shows that there is an oil cut of practically 100%. This interval of pure oil production may have been the result of a vacant space inside the core holder. Brine and oil may have accumulated there, and buoyancy may have moved the oil further down the flow path.

Following this clean oil is a section of alternating oil and brine. The reason for these interchanging oil and water production are a result of the Coriolis meter, where fluids flow through tubes so small that separation of phases occurs. Following the production of the alternating oil and brine is the production of microemulsions, which is confirmed by the intermediate values, with respects to oil and SP values, for effluent density and conductivity. Following the microemulsions is the production of polymer which shows a significant drop in conductivity. The experiment is concluded with the injection and production of brine.

3.2.2 Repeat experiments using high permeability 7.5cm core

The experiment described in Section 3.2.1 above was repeated times under the same conditions, with dodecane oil and optimum surfactant, to ascertain the repeatability of results. Only difference between the two experiments is an initial oil saturation of 0.75 in experiment 2 and 0.73 in experiment 2.

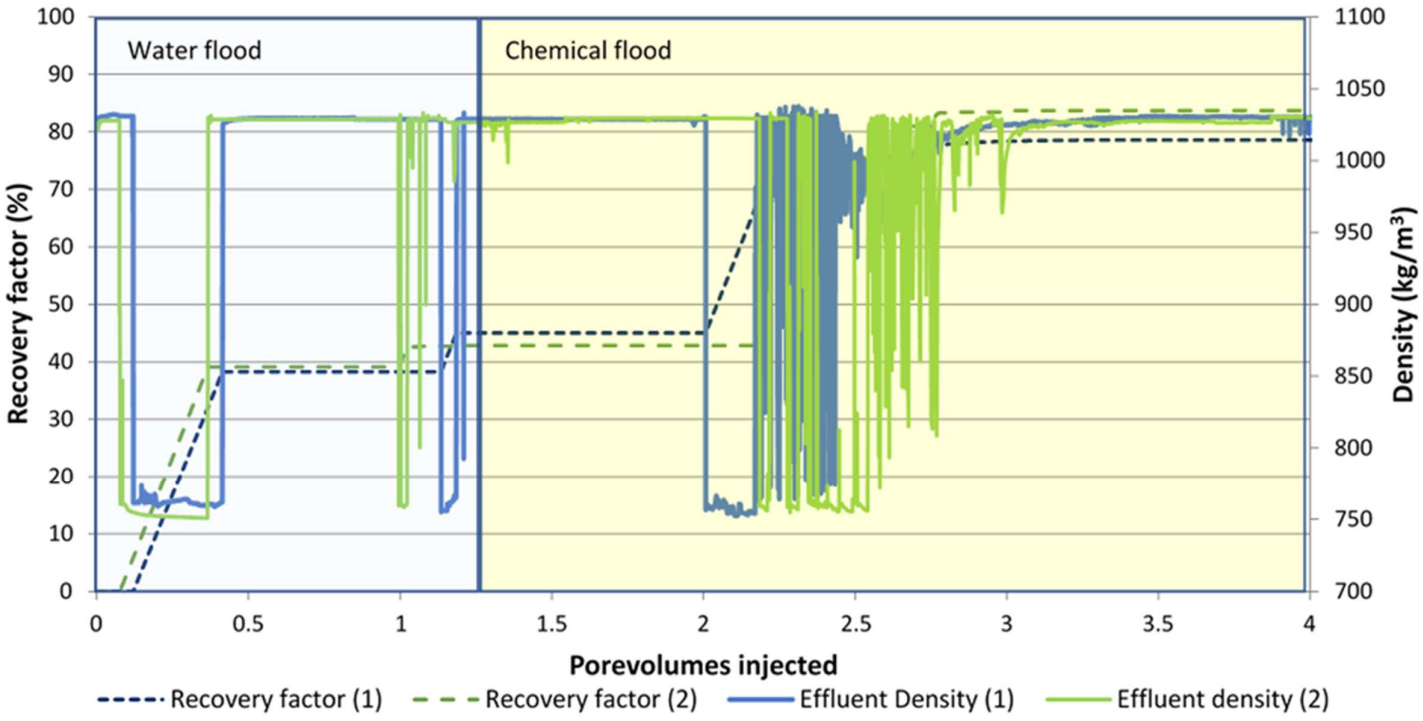

Figure 3.5: Comparison of experiment 1 and repeat experiment 2

The experiments show fairly consistent recovery factors for waterflood and total recovery of 45% and 79% and 43% and 84%, for experiments 1 and 2 respectively. At the standard injection rate of 0.12 mL/min recovery factors are 38% for experiment 1 and 39% for experiment 2, with bump-floods yielding an additional recovery of 5% to 6%. The oil production during the chemical flood does shows some significant results. Experiment 1 shows a greater interval of clean oil, whereas in experiment 2 more water is produced in this oil bank.

3.2.3 Effects of varying initial oil saturation on incremental oil recovery

During the oil filling in the experiments described in the previous section the aim was to obtain an as high as possible oil saturation. The experiments showed that at the maximum saturation within the limitations of this study, leaves a residual oil saturation after waterflood that is enough to obtain an oil bank during the SP flood. This begs the question what the effects would be of a lower residual oil after waterflood on the formation of an oil bank and the incremental recovery of the chemical flood. To obtain a lower residual saturation after waterflood, charging of the core was limited to lower oil saturations in experiments 3 and 4 than previously done. Initial saturations of experiments 3 and 4 are 0.48 and 0.54, respectively; both experiments were done on the same core as the one described in Table 3.1. Figure 3.6 shows the result of these experiments.

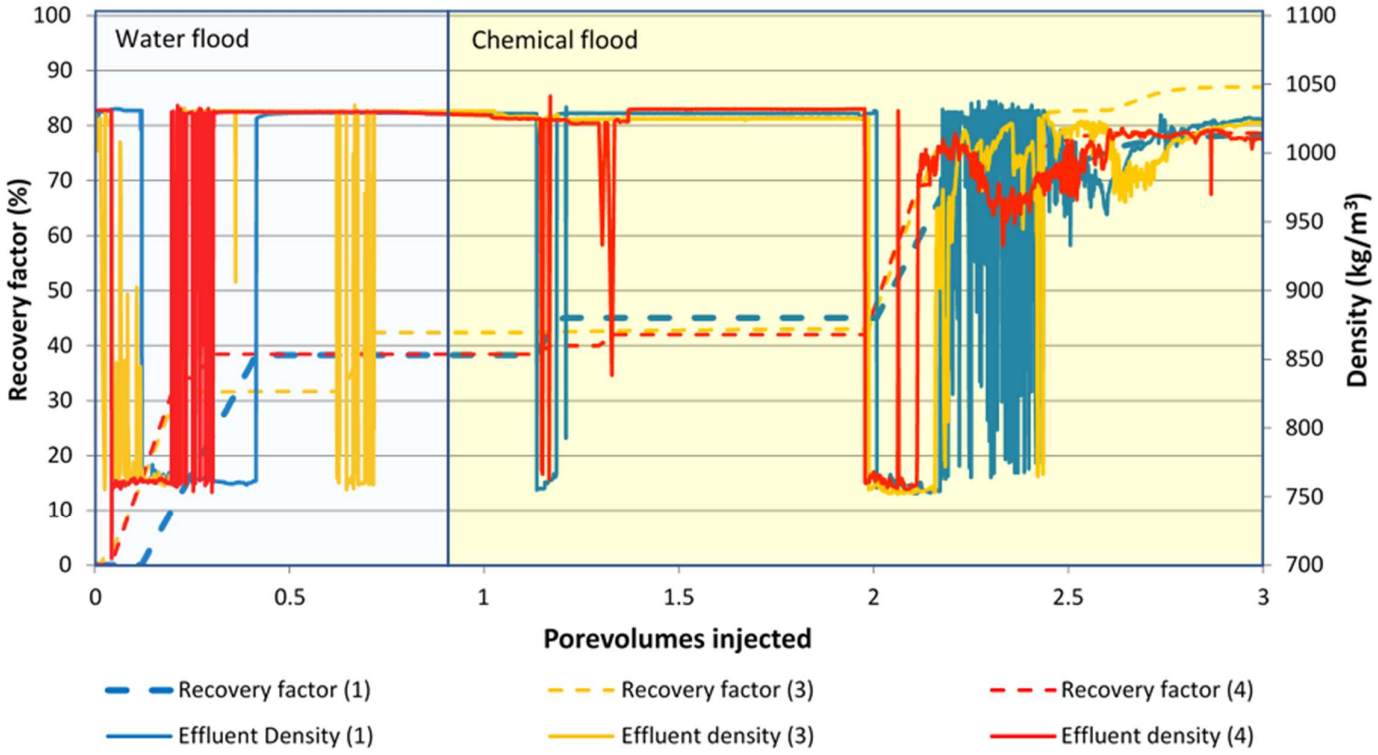

Figure 3.6: Comparison of experiments 1, 3 and 4 with ranging initial saturations

The production data depicted in Figure 3.6 shows that indeed, a different initial oil saturation has certain ramification for the incremental oil. All three experiments have similar waterflood recovery factors, from 42% to 45%, and since they have similar waterflood recoveries but different initial saturations, it is reasonable to assume that the chemical floods do indeed start from different residual oil saturations. Most striking difference is that size of the "clean oil" bank; it appears that experiment 4, with the lowest initial recovery has smallest amount of clean produced oil. Noteworthy is also the fact that in experiment 1, with the highest oil saturation, more microemulsions are produced than experiment 3 and even more so than experiment 4.

3.2.4 Effects of permeability and porosity on incremental oil recovery

Part of this study is the evaluation of the effects of rock properties on the incremental oil recovery. In service of this study goal, core flood experiments are performed on three cores of similar length but different porosity and permeability; rock properties of these cores are seen in Table 3.2.

Table 3.2: Rock properties of 7.5 cm core samples (RF's)

Sample	Permeability (mD)	Porosity	S_{oi}
7.5HP1	120	0.16	0.85
7.5LP1	34	0.13	0.90
7.5LP1	14	0.10	0.88

Figure 3.7 below, shows the result of these experiments with a focus on the production of the oil bank. The waterflood recovery factor of core 7.5LP1 and 7.5LP2, the low perm cores, lay closely together at 37%, while in the high perm 7.5HP1 core a recovery factor of 43% is achieved in the waterflood. The incremental oil recovery during the chemical flood is 42%, 41% and 35% of OIIP were achieved for cores 7.5HP1, 7.5LP1 and 7.5LP2, respectively.

Major difference between these results is observed when focussing on the clean oil, or rather the oil bank, produced during chemical EOR. The clean oil produced, relative to the core pore volume, seems to increase in size with increasing permeability and porosity. One explanation for this observation is the effect of pore geometry on capillary forces (Lake, 1989); at lower permeability there is a tighter pore network. The function of surfactant is lowering the interfacial tension, but at low permeability, IFT still remains higher than in a high permeability scenario.

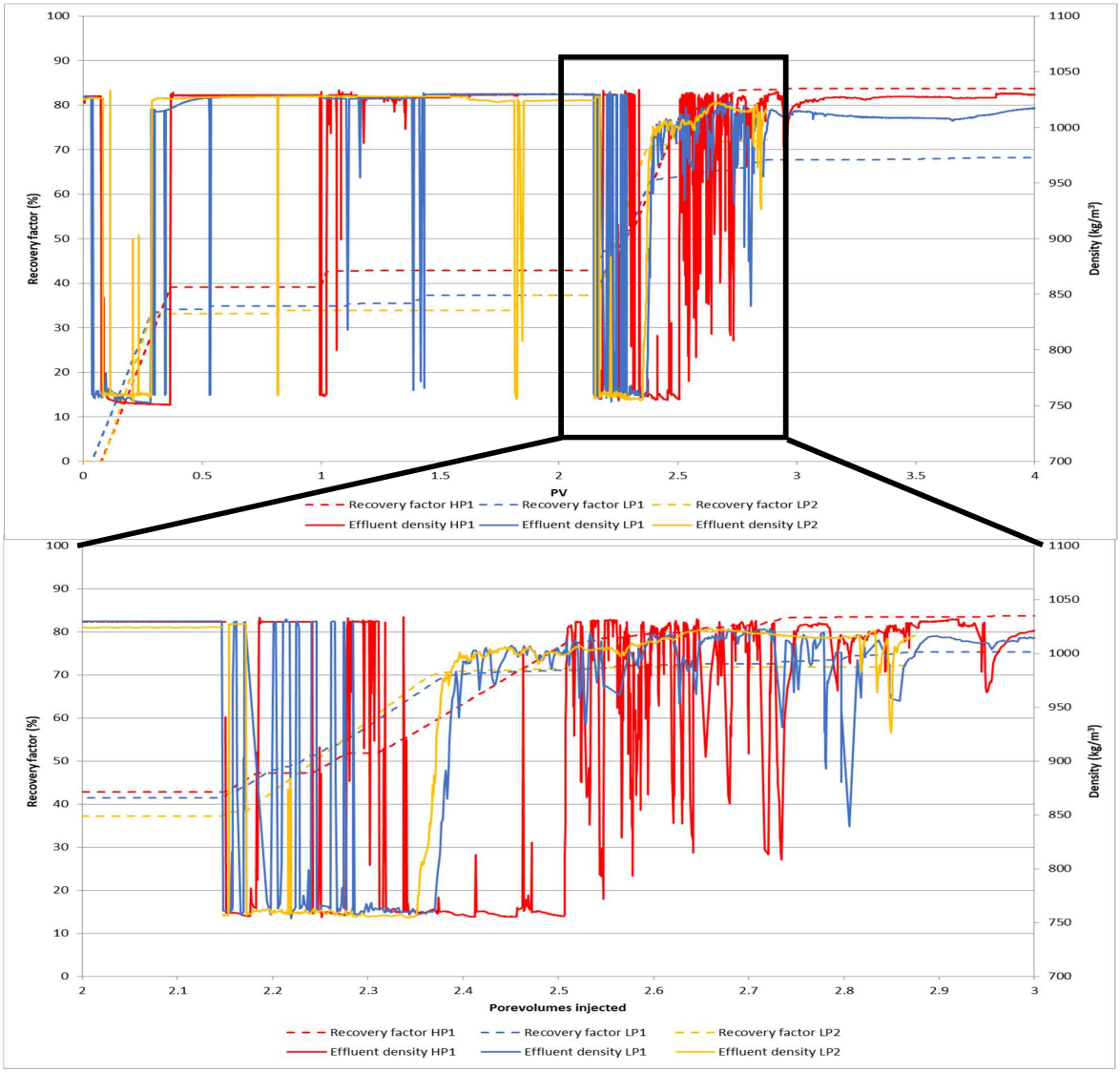

Figure 3.7: Comparison of production data of cores of varying permeability

3.2.5 Effects of optimal and suboptimal surfactant solution on incremental oil recovery

Part of this study was the evaluation of the effects of optimality of the SP-slug on the production data. To answer this research question, the experiment discussed in Section 3.2.1 was repeated using a suboptimal surfactant mixture with a NaCl concentration of 1%. The parameters of these experiments are depicted in Table 3.3 and the production in Figure 3.8.

Table 3.3: Relevant parameters of experiments with 7.5 cm core and optimal or suboptimal SP

Experiment	SP-salinity	Initial S_o	Waterflood recovery factor (% of OIIP)	Chemical flood incremental recovery factor (% of OIIP)
1	3.75% (optimal)	0.75	45%	34%
6	1% (suboptimal)	0.73	48%	21%

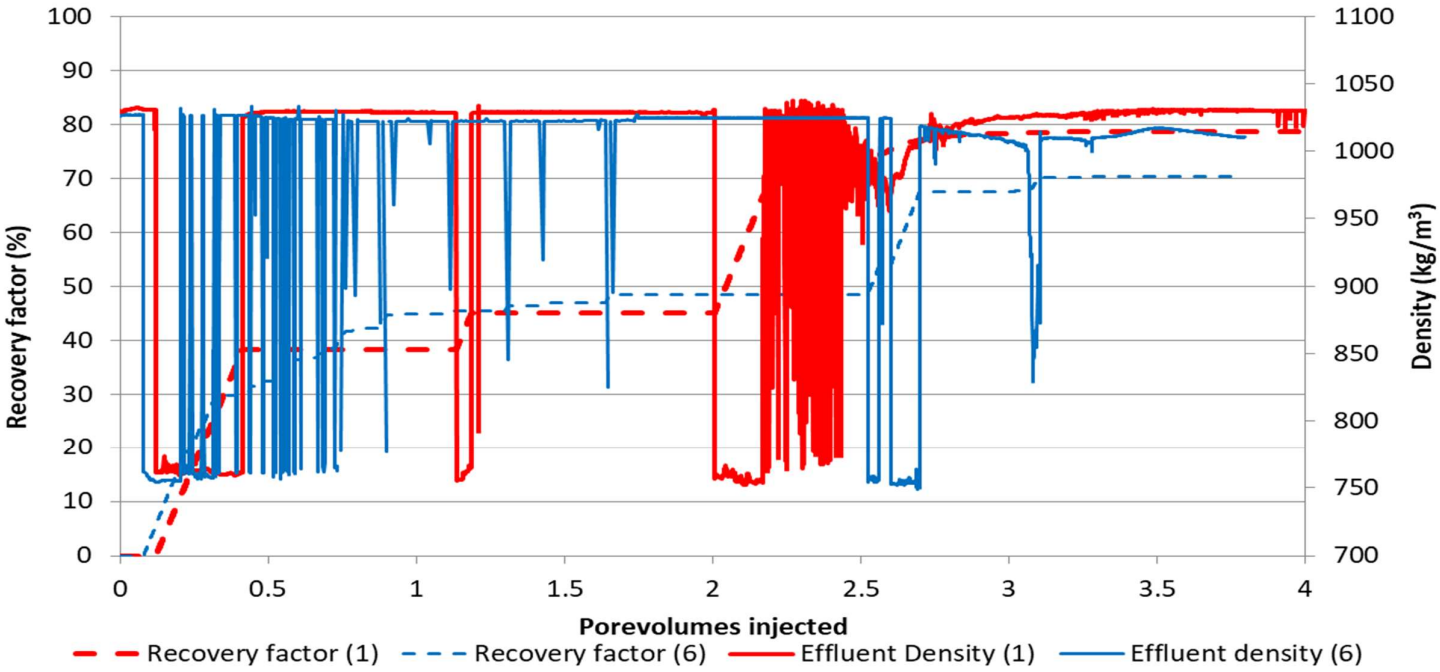

Figure 3.8: Comparison of results of experiments with optimal (1) and suboptimal surfactant (6)

The waterflood recovery factors are similar, while there is a substantial different in the recovery factors from the chemical flood, wherein the suboptimal yields less produced oil. Other observation stems from the effluent density in Figure 3.8. It appears that in experiment 6, with suboptimal surfactant, much less microemulsions are produced than in the experiment with optimal surfactant. This is to be expected since, as discussed in Sections 1.3 and 3.1 in a suboptimal surfactant the micelles are drawn into the water phase.

Table 3.4: Recovery factors for 7.5cm cores at varying permeabilities

Core sample	Waterflood recovery factor (% of OIIP)	Chemical flood incremental recovery factor (% of OIIP)
7.5HP1	43%	42%
7.5LP1	37%	41%
7.5LP2	37%	35%

3.3 Results and conclusion of solid 60 cm core experiments

In this section, the results of the core flood experiments using 60 cm cores will be presented and discussed. Unlike the 7.5 cm core flood experiments, some of the experiments using 60 cm cores were performed under a CT-scanner and using iododododecane oil. The iododecane has phase behaviour properties different from the dodecane oil, but it is much more visible in a CT-scan. The CT-scans give great insights into the displacement processes during oil production. Furthermore, previously done experiments with a 60cm core showed that the standard procedure, wherein 0.5PV of SP-solution is injected, is not suited to adequately evaluate the oil bank behaviour. Reason for this is the fact that breakthrough occurred by the time 0.5PV of SP is injected. Initial assumption was that this was caused by unstable displacement, which is confirmed by the CT-scans in Figure 3.12. This early breakthrough failed to capture the oil bank behaviour throughout the entire chemical flood, more specifically during polymer injection. Considering this, the choice was made to limit the SP volume to 0.25 PV.

3.3.1 Establishing heterogeneity through permeability measurements

With the procedure described in Section 1.7 (permeability test), permeability measurements were performed on the 60cm core before it had seen any oil. Unlike the 7.5 cm cores', in these experiments multiple pressure sensors were located along the core's length, rather than just at the outlet and inlet. This allowed for the measurement of pressure gradients over sections of the core, and permeability calculations over core sections using Darcy's equation. Figure 3.10 shows the results pertaining to these measurements, with section 2-3 for example, showing the data for the core section between pressure sensors 2 and 3

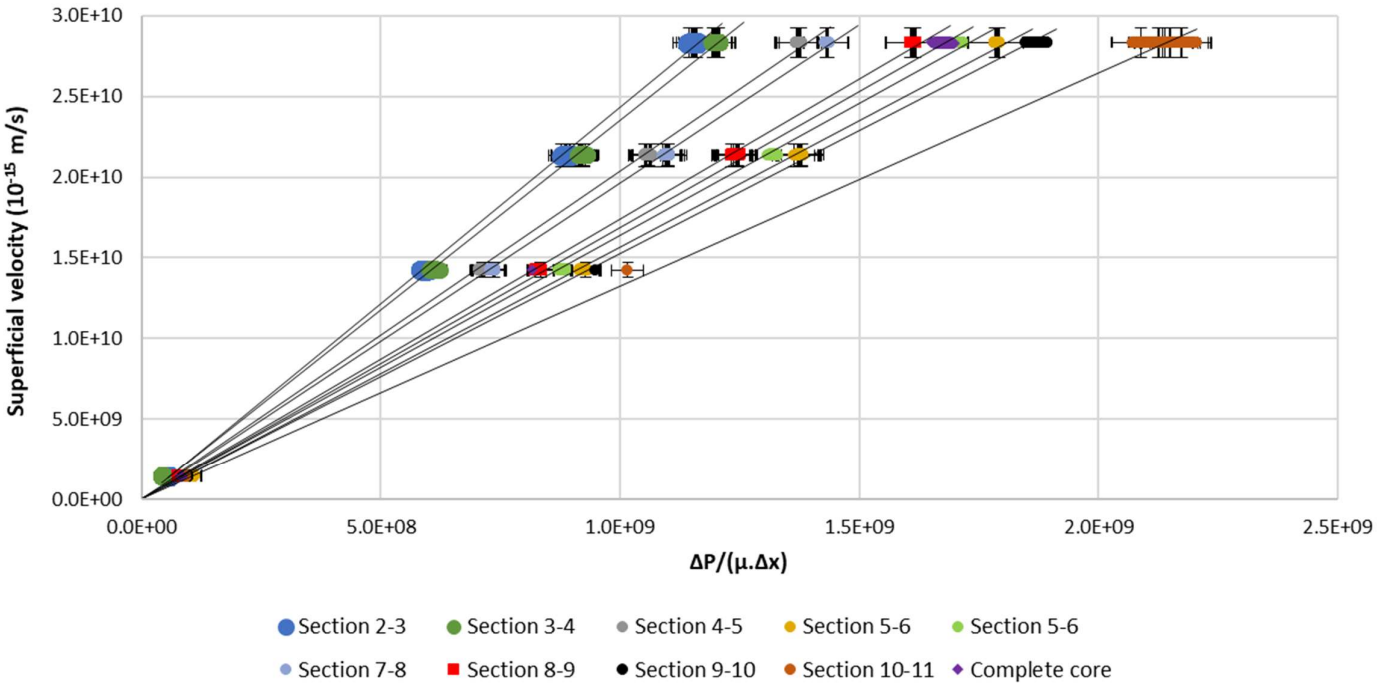

Figure 3.9: Permeability data for 60cm core (Section 2-3 for example, refers to the core section between sensors 2 and 3)

Sections 2-3 and 10-11 show the greatest spread in data, the former of which due to fluctuating pump pressure and the latter due to fluctuations in the backpressure regulator. This spread was found to be so great in sections 1-2 and 11-12 that data belonging to these sections has been omitted. In comparing the sections, it becomes clear that there is quite a difference in rock properties. It appears that towards the core outlet the slope in the datapoints, and thus also permeability, decreases.

Slopes of these linear trendlines, or averaged permeability, per section is seen in Table 3.5. In terms of permeability there is almost a factor 2 difference between the smallest and greatest measured values.

Table 3.5: Mean permeability per core section of 60cm core										
Section	2-3	3-4	4-5	5-6	6-7	7-8	8-9	9-10	10-11	Complete core
K_{mean} (mD)	24.3	23.4	20.4	15.6	16.4	19.6	17.4	15.2	13.2	17.8

3.3.2 Production data of solid 60cm core

Figure 3.11 shows the production data of 60 cm core flood experiment 3, the first 60 cm experiment which was deemed a succes. Table 3.6 shows the relevant parameters and results for this experiment.

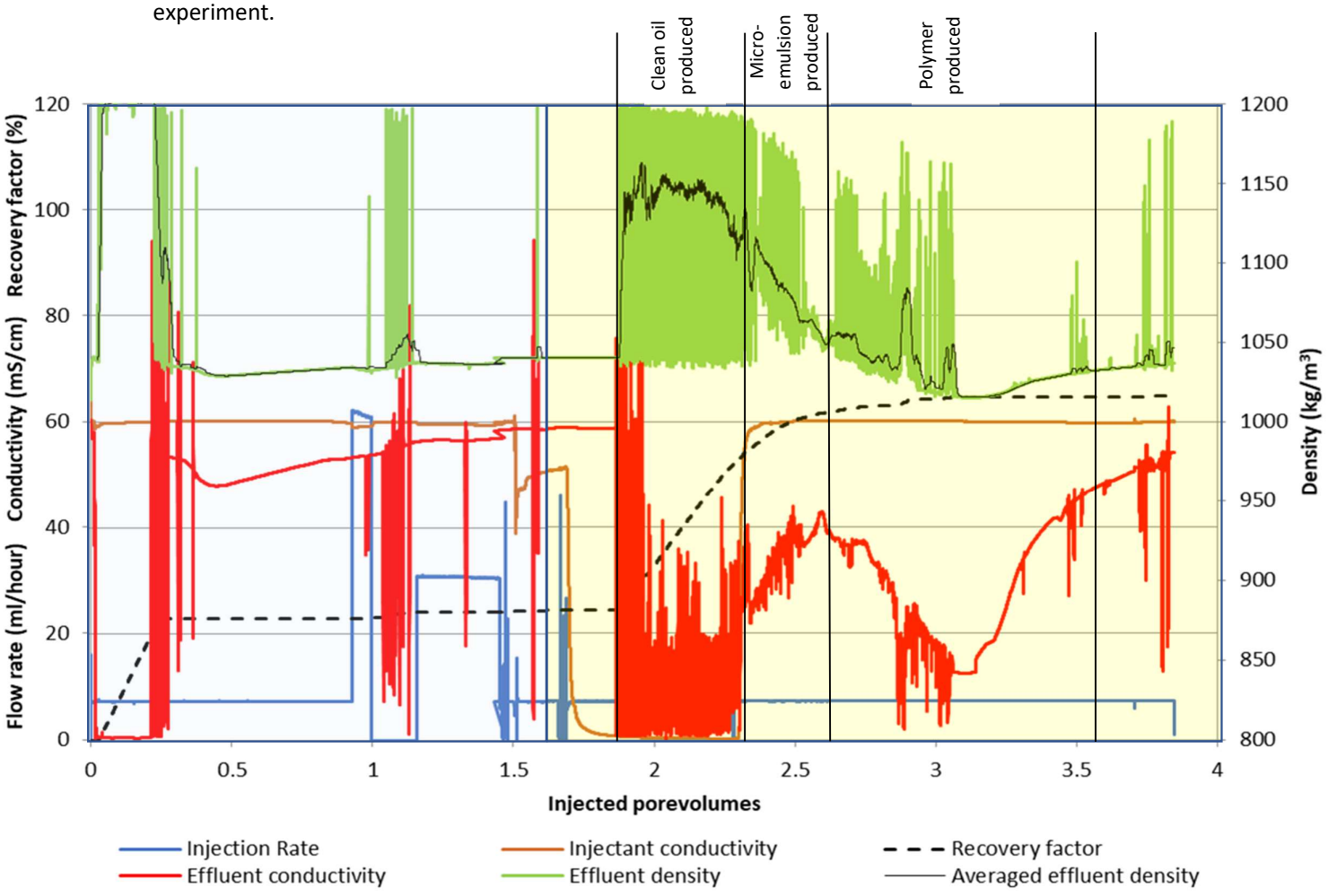

Figure 3.10: Production data of experiment 3 using 60 cm solid core (optimal surfactant)

Table 3.6: the relevant parameters and results for experiment 3 using a 60 cm solid core					
SP-salinity (%wt NaCl)	SP viscosity (cP)	Polymer viscosity (cP)	Oil viscosity (cP)	Waterflood recovery factor (% of OIIP)	Chemical flood incremental recovery factor (% of OIIP)
4.5 (optimal)	12	17	2 (iododododecane)	24.3	40.5

With respects to the waterflood, what stands out most is the relatively low recovery factor of 24.3% of OOIP. Compared to the 7.5 cm core experiments where waterflood recovery ranging between 37 and 48%, this is indeed quite low. The same effect was observed in the comparison of the high and low permeability 7.5cm cores in Section 3.2.4. Although the reduction in waterflood recovery is much greater in the 60cm cores, the permeability and porosity reduction is also greater. This result can again be attributed to a tighter pore network wherein capillary forces play a bigger resisting force in oil mobilisation.

Point of interest in the oil production during the chemical flood, is the shape of the oil bank. Where there was a clean oil bank with an oil cut of close to 1, in this 60cm experiment there is water production along with oil production. The effect of alternating water and oil is caused by the thin capillary tubes in the Coriolis meter (Tromp, 2006). What it boils down to, is when producing both water and oil ($0 < f_o < 1$), the water and oil phases are separated and travel along the tube as plugs, causing alternating registration of density of water and oil. The fluctuating effluent density in Figure 3.11 is somewhat chaotic and confusing, but averaged effluent density gives a clearer picture of the produced fluids. It appears that the peak oil production occurs around 2 PVi, after which it starts dropping until microemulsions are produced. At better picture is given by the oil cut based on average effluent density, depicted in Figure 3.12.

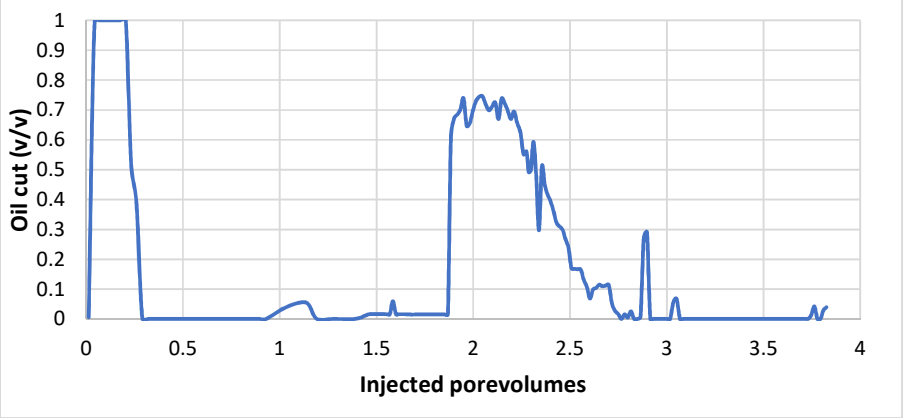

Figure 3.11: Averaged oil cut of experiment 3 using 60 cm solid core

It shows that at peak oil production there is an oil cut of up to 0.75. With the start of production of microemulsions the oil cut declines. Just before 3 pore volumes injected there is another increase in oil cut. This second spike can be attributed to the fact that at this point the polymer is close to the outlet and brings along any oil unswept by the SP-slug. One other possible explanation for this observation is that of the capillary end effect. The capillary end effect traps oil at the outflow face of the core causing a locally high oil saturation. The mobilisation of the oil trapped by the capillary end effect may cause this second spike in oil cut. The incremental recovery of 40.5% of OOIP is consistent compared to recovery factors in the 7.5cm cores.

3.3.3 CT-scans of 60cm solid core

Figure 3.12 below shows the CT-scans taken during the chemical flood described in the previous section. The first CT-scan shows that the experiment started out somewhat troublesome. It appears that at the beginning, in injected fluids flowed around the core and entered it through a pressure tab at around 2/3 of the core's length. This problem was tackled by increasing the confining pressure, which stopped further leakage.

The second scan shows the SP-slug entering the core and just beyond the slug the presence of an oil bank. The presence of the oil bank is identified by the increased radiodensity (or houndsfield units), causing the redder colour in the processing of the scans. The following scans show the oil bank being pushed forward, albeit not in a very efficient sweep. In an efficient sweep there would be piston like displacement with no oil being bypassed by the SP-slug. In this case however, the SP-slug fingers through the core and bypasses the outer sections of the core.

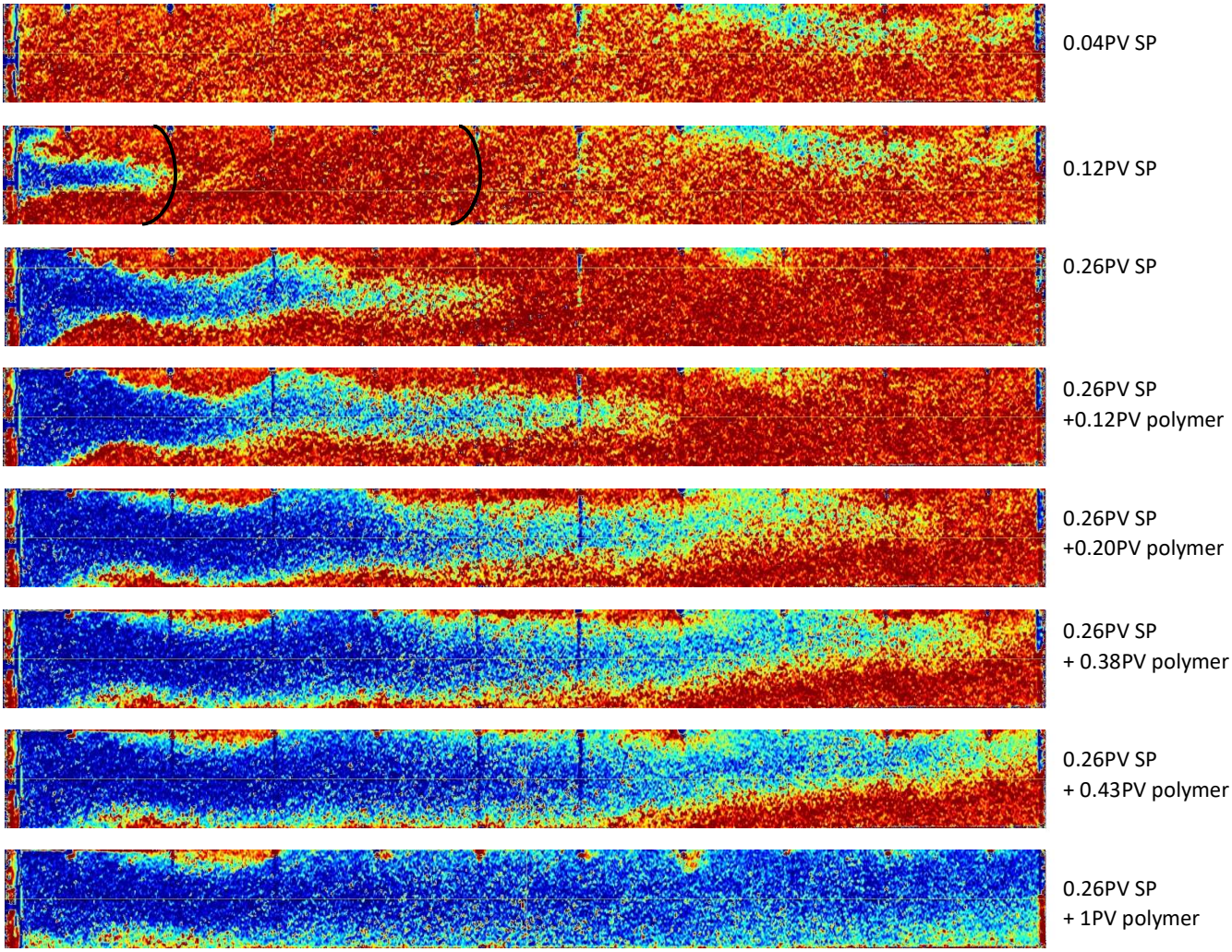

Figure 3.12: CT-scans of chemical flood of experiment 3 of 60cm solid core (vertical cross-section at the core centre). Chemicals are injected from the left. Blue and red colours signify low and high oil saturation, respectively. Annotations beside the scans indicate the injected volume at the time of the scan

In the fourth scan and onward, the higher viscosity polymer is injected, which does seem to improve sweep efficiency. Sections previously bypassed by the SP-slug are now swept by the polymer-slug. The last scan shows the core at the end of the chemical flood. It appears that some sections, especially close to the inlet, contain some bypassed oil.

3.3.4 Comparing iodododecane and dodecane oil experiments with a 60cm solid core

As stated before, the experiments performed under a CT-scanner were done using the iodododecane oil, which shows greater contrast than other phases. This begs the question, to what extent one can compare the experiment discussed in previous sections with experiments performed outside the CT-room using dodecane oil. Figure 3.13 shows the comparison of follow-up experiments 4 and 5 using dodecane oil. In both these experiments again, optimal surfactant was used with viscosities of 10 and 15 for the SP and polymer solutions, respectively.

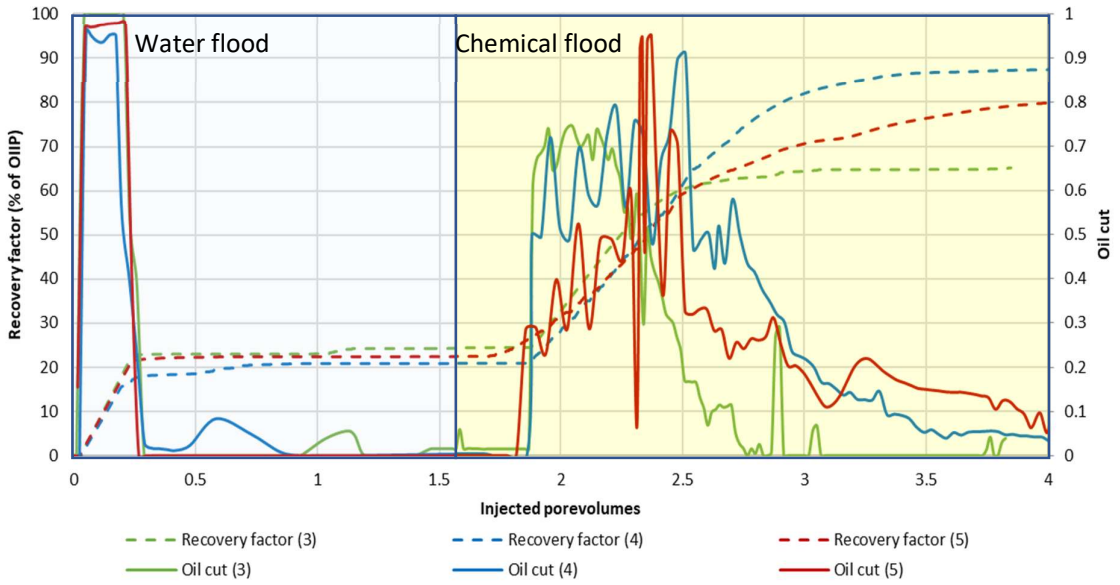

Figure 3.13: Recovery factors for iodododecane experiment 3, dodecane experiment 4 and dodecane repeat experiment 5

One conclusion that can be drawn from these results stems from the waterflood recovery factor. It appears that for both types of oil the recovery factor lies around 20% of OIIP. What this tells is that the relatively low recovery factor compared to the 7.5cm cores, is not a result of the oil used, but rather a consequence of the heterogeneity within the core.

Second conclusion corresponds to the oil recovery in the chemical flood. The dodecane oil experiments seem to have greater recovery factors and higher peak oil cuts for the chemical flood, as depicted in Table 3.7.

Table 3.7: Relevant parameters of iodododecane experiment 3 and dodecane experiments 4 and 5

	Experiment 3	Experiment 4	Experiment 5
Initial oil saturation	0.77	0.75	0.76
Waterflood recovery factor (% of OIIP)	24	21	22
Chemical flood incremental recovery factor (% of OIIP)	41	66	57

Since all three experiments were performed on the same core, this difference can only be attributed to the oil mobility. Even though the two oils have different viscosities, research by (Wardlaw, 1982) shows that viscosity has little to no effect on the capillary trapping of oil. The only major cause left for this phenomenon is the extent in which the surfactant lowers the interfacial tension. As stated in Section 3.1, measurements of interfacial tension were performed by (Wijsman, 2018) in dodecane systems, but not in iododecane systems. Considering the results in this study, one would expect the reduction of IFT in a iododododecane system to not be as great as that in a dodecane system, effectively lowering the oil mobilisation and recovery factor during chemical flood. As for the difference in peak oil cuts, it appears that these peaks occur in a later stage of the chemical flood in the dodecane experiments. This may be the result of a shorter oil bank in the dodecane experiments. When the oil bank is shorter and local oil saturation is higher in the oil bank, the oil bank itself and peak oil production come in later.

3.4 Results and conclusions of stacked 60 cm core experiments

The solid 60cm core described in the previous chapter, was found to have an average permeability which was relatively low in the range of permeabilities for the Fontainebleau sandstone. In pursuit of a core of equal length but higher permeability, two separate 30cm cores with higher permeability were stacked together (stacking procedure described in Appendix E).

3.4.1 Establishing heterogeneity through permeability measurements

Since the experiments discussed in this chapter were performed using a composite core, it is especially relevant here to quantify the heterogeneity within the core. Figure 3.14 shows the permeability measurements for each section between pressure transducers along the core. Please note, the boundary between the two cores that were stacked lie between sensors 5 and 7; in order not to damage the boundary no pressure transducer slot was drilled for sensor 6.

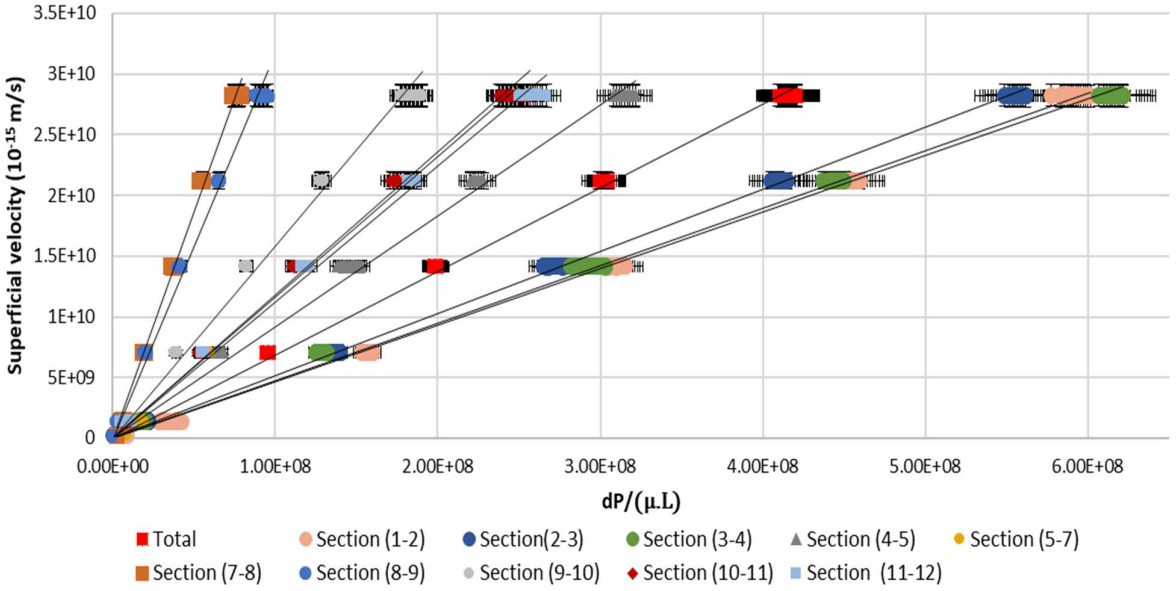

Figure 3.14: Permeability data for stacked 60cm core (Section 2-3 for example, refers to the core section between sensors 2 and 3)

The data shows quite a spread in permeability. Point of focus is section 5-7 where the boundary between the smaller cores lays. The mean permeability per section in Table 3.8 shows that the permeability across the interface is well above that of the mean over the complete core, but still realistic when compared to other sections. What stands out are the permeabilities across sections 7-8 and 8-9; these high values however are not to be taken seriously since sensor 8 was found to be malfunctioning in a later stage. Disregarding these sections, at appears that the second core (sections 9-10, 10-11 and 11-12), has higher permeability than the initial core (sections 1-2, 2-3, 3-4 and 4-5).

Table 3.8: Mean permeability per core section of stacked 60cm core

Section	Complete core	1-2	2-3	3-4	4-5	5-7	7-8	8-9	9-10	10-11	11-12
K_{mean} (mD)	72.2	45.2	58.1	58.5	102.7	107.2	329.7	381.7	180.3	131.7	125.7

3.4.2 Production data of experiment 1 using a composite 60cm core

The initial experiment performed using the composite 60cm core was done in the CT-room, so using iodododecane oil. The injectants in the chemical flood were like those from previous experiments, with optimal salinity surfactant and polymer viscosity of approximately 10cP and 15cP, respectively.

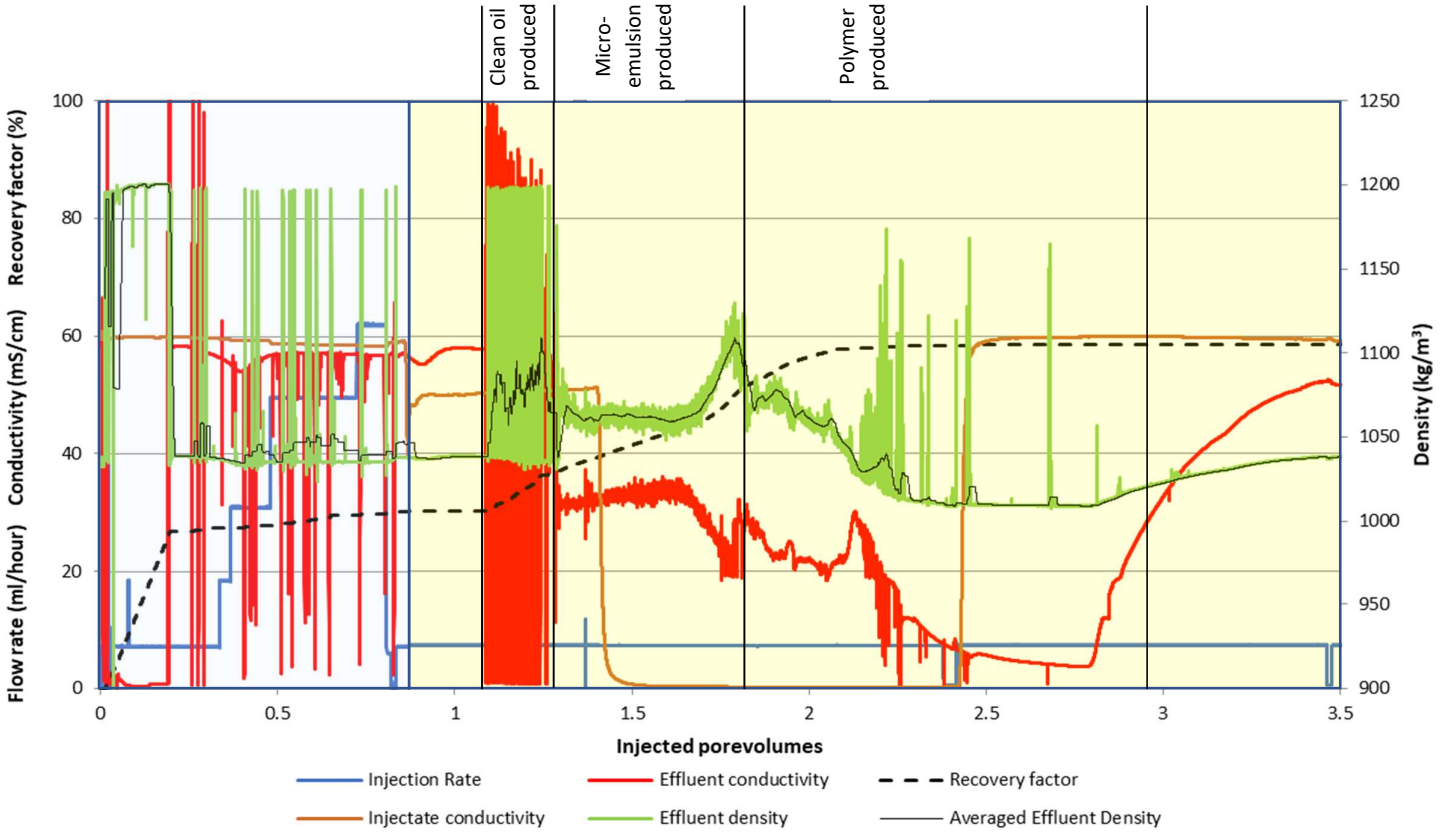

Figure 3.15: Production data of 60cm composite core experiment 1

Table 3.9: Relevant parameters of experiment 1 using composite 60cm core							
Initial oil saturation (% of PV)	SP-salinity (%wt NaCl)	SP viscosity (cP)	SP volume (PV)	Polymer viscosity (cP)	Polymer volume (PV)	Waterflood recovery factor (% of OIIP)	Chemical flood incremental recovery factor (% of OIIP)
67%	4.5 (optimal)	10	0.5	15	1	30.2	28.4

In this specific experiment, time restraints demanded that the experiment came to a swift conclusion. To speed up the process, the bump floods in the waterflood were initiated as soon as breakthrough had occurred, rather than wait for no oil production at the typical field rate. The waterflood recovery factor of 30.2% of OIIP, though higher than in any experiment with the 60cm low permeability solid core, does still not reach values encountered in the 7.5cm experiments. Possible explanation is that the higher permeability and subsequent lesser capillary forces allow a waterflood recovery higher than in the solid 60cm core, but heterogeneity still plays a limiting factor in sweep efficiency compared to the 7.5cm cores.

The chemical flood incremental recovery factor of 28% of OOIP is much lower than anything encountered in previous experiments. Probable reason for this would be an inefficient sweep due to heterogeneity, especially at the interface between the stacked cores. The CT-scans in Section 3.4.3 will shed more light on this reasoning. The effluent density shows that in the chemical flood, one still does not encounter the clean body of oil with oil cut 100%, as was seen in the 7.5cm core experiments. There is again alternating brine and oil production due to constraints in the experimental setup, as described in Section 3.3.4. The average effluent density shows a small oil bank of about 0.25PV being produced. Beside the volume, the oil bank is also of poor quality. Figure 3.16 showing the averaged oil cut, exhibits a relatively low oil cut during oil bank production. Where in the 60cm solid core there was an oil cut of up to 0.75, here it does no exceed 0.35. Later, during polymer injection there is another spike in oil cut. At this point the polymer production is imminent, and some oil unswept by the SP-slug is being produced. Density and conductivity of the effluent show an early breakthrough and microemulsion production, even before polymer injection is started. This low recovery factor, low oil cut and early breakthrough support the notion that sweep efficiency had been poor during this experiment.

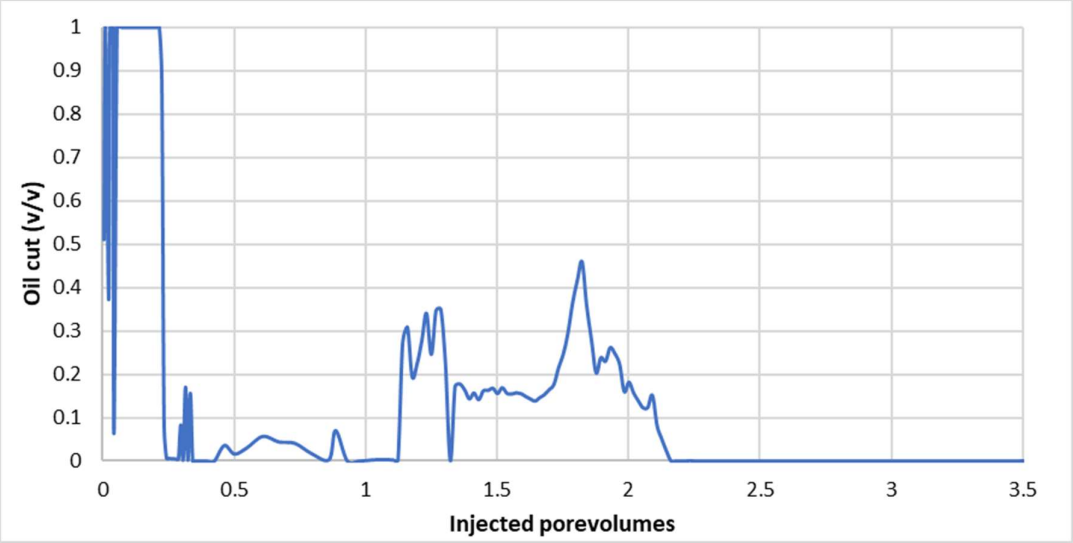

Figure 3.16: Averaged oil cut of experiment 1 with a 60cm composite core

3.4.3 CT-scans of experiment 1 using a composite 60cm core

Figure 3.17 below shows the CT scans taken during the chemical flood in experiment 1 with the stacked 60cm core. The images show some similarities with those taken using the solid 60cm core, discussed in Section 3.3.3. Figure 3.17(a), shows the result of the waterflood. Noteworthy is the fact that the core section closest to the inlet retains the highest oil saturation after the waterflood. In the permeability measurements it was established that this section had the lowest permeability and this CT-scan shows that indeed lower permeability and its implications for pore geometry are a limiting factor in mobilising oil. It appears that there is a great deal of fingering taking place during this flood. In this case however, it appears there is another factor causing the inefficient sweep, as seen in Figure 3.17(e). The boundary between the two cores composing the composite core forms a partial capillary boundary. The lower part of this boundary acts as a strong capillary boundary, and effectively allows the upper part to act as a preferential path for the SP-slug. Figures 3.17 (e) and 3.17(f) also show the oil bank being broken by the elongated SP-slug. The oil bank is not much of a bank at all, when compared to Figure 3.12, and is smeared along the SP-finger. Figure 3.17(e) confirms the observation from the production data wherein breakthrough occurred at 0.45 pore volumes injected, before polymer is injected. Figure 3.17(g) shows a completed chemical flood and the extent of the poor flood with unswept oil at the bottom of the core. Comparing Figures 3.17(f) and 3.17(g) shows the increase in sweep efficiency by the polymer. The polymer does displace some oil bypassed by the SP-slug but does itself bypass some sections at the core bottom. The polymer also appears to be affected by the heterogeneity at the boundary, but its higher viscosity mitigates this effect to some extent.

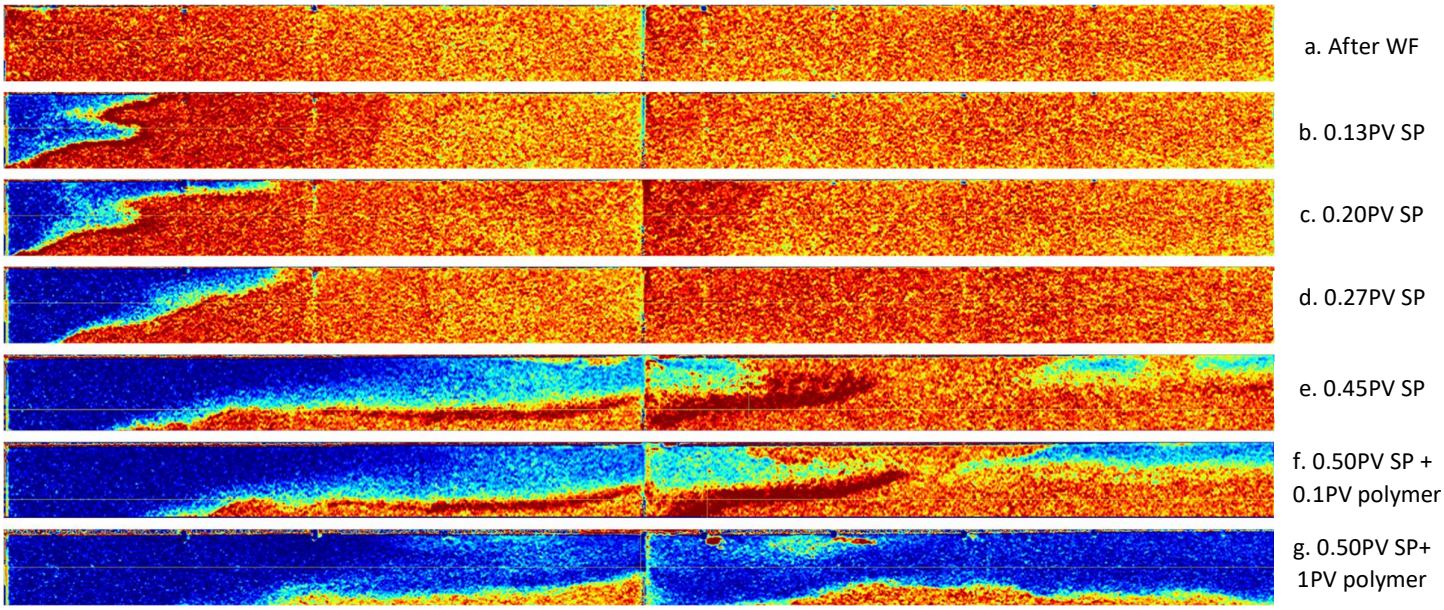

Figure 3.17: CT-scans of chemical flood of experiment 1 of 60cm composite core (vertical cross-section showing tip of finger). Fluids are injected from the left. Blue and red colours signify low and high oil saturation, respectively. Annotations beside the scans indicate the injected volume at the time of the scan

In attempting to obtain a core of higher permeability and less heterogeneity than the solid core discussed in Section 3.4.1, the opposite result was achieved. The boundary between the stacked cores increases heterogeneity and renders solid 60 cm core as the least heterogeneous one of these two. This composite core shows the sensitivity of the chemical flood to core heterogeneity. Even though the solid 60 cm core had relatively less surfactant injected into it and had lower permeability, the incremental oil recovery after chemical flood was still 12.1% greater than that in the composite core.

The waterflood recovery factor however, is 6.8% greater in the composite core, as one would expect in a higher permeability core. The greater heterogeneity in the composite core plays not so big a role that waterflood recovery is lower than in the solid core. The trade-off between greater heterogeneity and better permeability was such that there is a positive nett change in water flood efficiency.

3.4.4 Oil saturation from CT-scans in experiment 1 using a composite core

As discussed in Section 1.9, data from CT-scans can be used to estimate oil saturation along the core. Figure 3.18 shows the results of such an analysis performed using the CT-scans from the previous section.

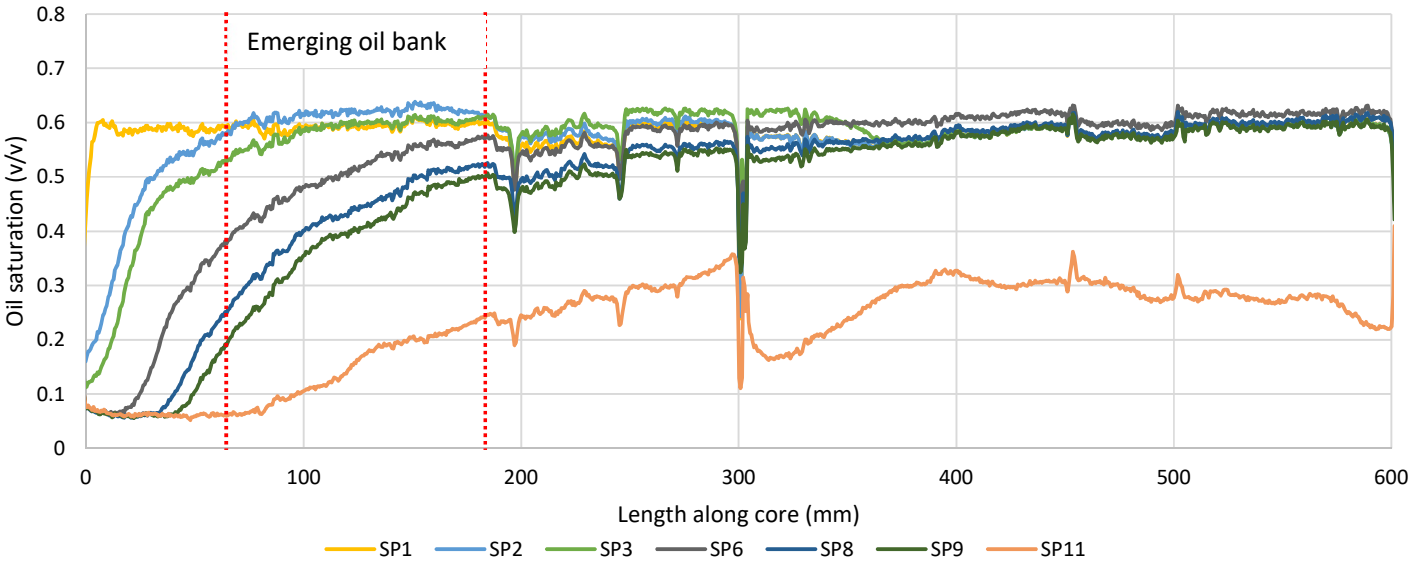

Figure 3.18: Saturation profiles per CT-scan in experiment 1 using composite core

Ideally, when observing an oil bank in a saturation profile such as Figure 3.18, one would observe a with time laterally migrating interval with oil saturation greater than in any previously taken CT-scan; the greater this increased oil saturation, the greater the oil bank and sweep efficiency. In this case however, it appears that there is not much of an oil bank to be observed. When comparing saturation data from CT-scans SP1 and SP2, one sees an oil bank emerging. This oil bank however, is no longer clearly observed further on, supporting the notion that there is no clear oil bank visible in the CT-scans.

3.4.5 Production data of repeat experiment 2 using a composite 60cm core and high viscosity chemical flood

Experiments discussed in previous section and Section 3.3.3 show that the standard procedure with 10cp and 15cP viscosity for surfactant-polymer and polymer respectively, generally yield an inefficient sweep where fingering and oil bypass occur. Since the chemical flood was designed such that there are favourable mobility ratios, one would not expect such unfavourable displacement, least of all in the solid 60cm core. This observation resulted in the notion that perhaps the microemulsions formed during a Type(III) surfactant-oil system play a role in flood front instability. Viscosity measurements of the microemulsions at optimal conditions (Al Saadi, Ongoing) showed that this was indeed the case. The microemulsions were found to have a viscosity of 40cP. In service of obtaining a stable displacement, repeat experiment 2 was performed using surfactant-polymer and polymer mixtures with viscosities of 45cP and 50cP, respectively

Table 3.10: Relevant parameters of experiment 2 using composite core

Initial oil saturation (% of PV)	SP-salinity (%wt NaCl)	SP viscosity (cP)	SP volume (PV)	Polymer viscosity (cP)	Polymer volume (PV)	Waterflood recovery factor (% of OIIP)	Chemical flood incremental recovery factor (% of OIIP)
71%	4.5 (optimal)	45	0.5	50	1	32.4	58.4

Figure 3.19 shows the production data belonging to this experiment. The data shows a waterflood recovery factor if 32.4% of OIIP, which is very similar to the 30.2% observed in experiment 1. The chemical flood shows a great increase in incremental recovery factor compared to experiment 1. Contrary to experiment 1, breakthrough does not occur here during SP-injection. These two observations support the conclusion that the chemical flood sweep is more efficient this time around.

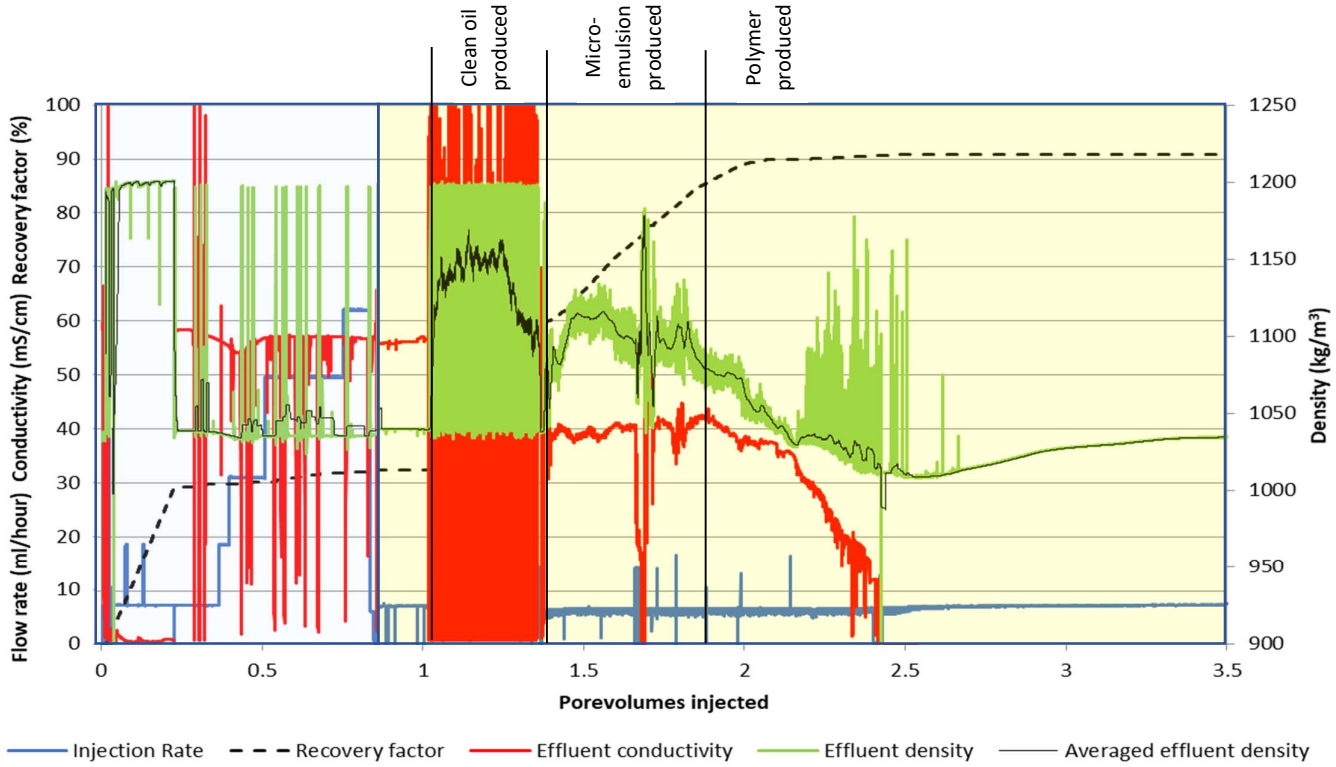

Figure 3.19: Production data of composite core experiment 2 (partially missing effluent conductivity)

The oil cut of the effluent is another tool to support the increased quality of the oil bank. Where the oil cut was around 0.35 in experiment 1, here oil cut reaches 0.78 during oil bank production. The oil cut increases again when the polymer slug sweeps some bypassed oil and reaches 0.91 at its peak. These results show that increasing the viscosity of the chemical flood injectants beyond that of the microemulsions drastically increases sweep efficiency and oil recovery. Other relevant observation from this Figure is that oil production starts much sooner in experiment 2 than in experiment 1.

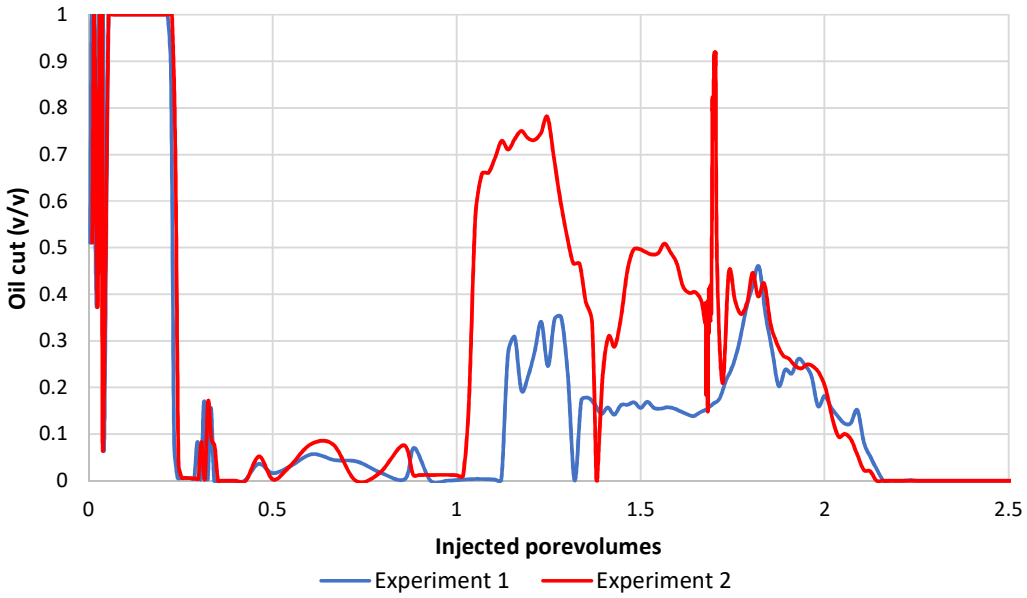

Figure 3.20: Averaged oil cut of experiment 2 using 60cm composite core (with experiment 1 for comparison)

3.4.6 CT-scans of experiment 2 using a composite 60cm core

CT-scans taken during experiment 2 confirm the conclusion that sweep efficiency had indeed been better than in experiment 1, as seen in Figure 3.21. Figures 3.21(b, c, d, and e) show the progression of the SP-slug. Unlike the previous experiment, there is barely any fingering and the slug sweeps almost the entire cross-sectional area of the core. Comparing the scan after the waterflood with the following scans, there is a clear increase in oil saturation in the core section in front of the SP-slug, showing the formation and displacement of an oil bank. The CT-scan in Figure 3.21(D) was taken moments after oil production had started and it shows the oil bank close to its maximum length. In Figure 3.21(f) and onward the SP-slug is pushed forward by the polymer and passes through the heterogeneous boundary. Because it is “squeezed” through the permeable section of the boundary, fingering seems to occur. The capillary boundary allows flow through a core section so small that it causes a sharp fingering of the SP-slug. Figure 3.21(g) shows the moment of breakthrough, which causes the drop in oil cut in Figure 3.20 just before 1.5 pore volumes injected. After breakthrough the SP-slug finger seems to thicken just after the boundary and sweep efficiency is again increases, effectively increasing the oil cut as seen in Figure 3.20.

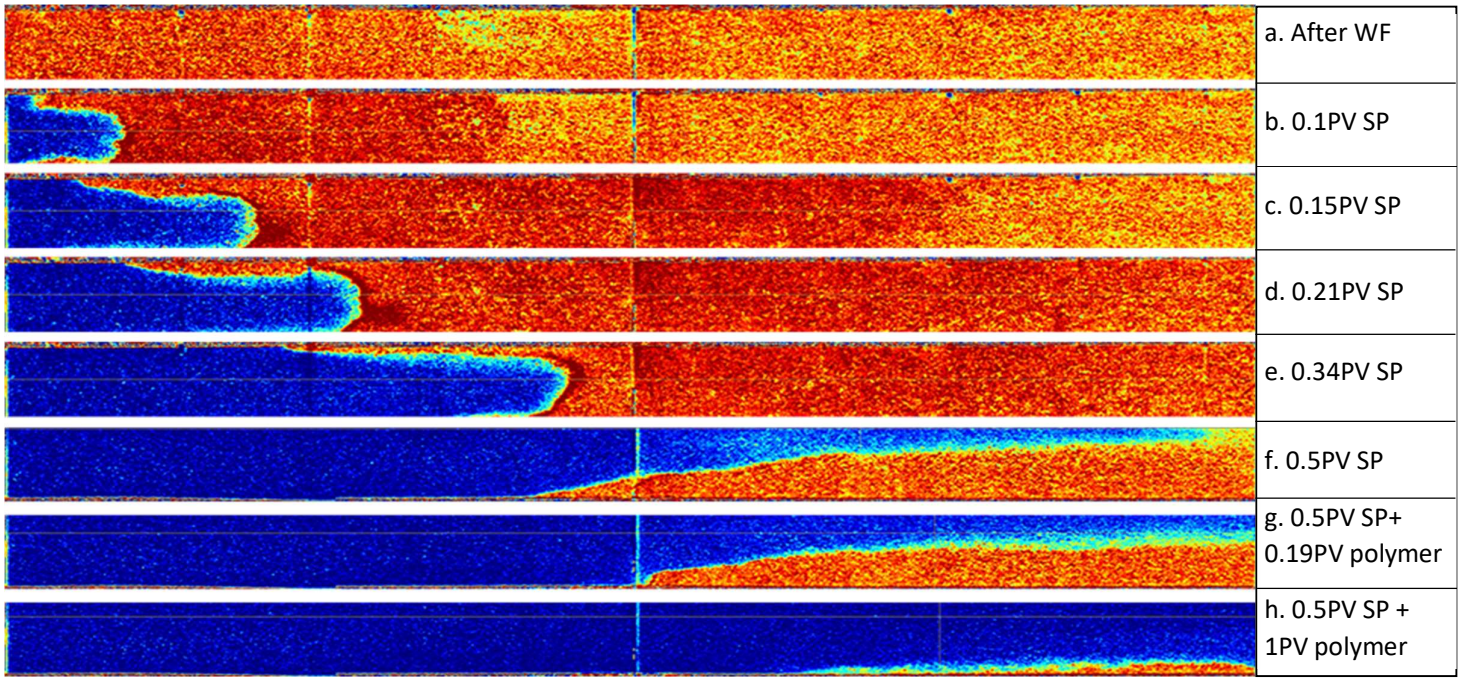

Figure 3.21: CT-scans of chemical flood of experiment 2 of 60cm composite core (vertical cross-section of core centre). Fluids are injected from the left. Blue and red colours signify low and high oil saturation, respectively. Annotations beside the scans indicate the injected volume at the time of the scan

3.4.7 Oil saturation from CT-scans in experiment 2 using a composite core

The CT-scans taken in experiment 2 were also used in calculating oil saturation in the core; the result is seen in Figure 3.22. Comparing the profiles from scans SP1 and SP2 immediately shows the emerging oil bank; there is an increased oil saturation between the dotted lines. Comparing scans SP1 and SP3 shows how the oil bank has progressed; there is an increased oil saturation between about 120mm from the inlet all the way to the outlet. Scan SP6 shows the presence of the oil bank even after it has passed through the heterogeneous boundary. Scans SP8 and SP9, taken while the SP-slug travels through the boundary, show that during this period no clear oil bank is formed. In scan SP11, when the polymer in being injected, an increased oil saturation is observed at the outlet. The polymer sweeps some bypassed oil which accumulates at the end as a re-emerging oil bank. Scan SP14 shows the result of the chemical flood. Just before and just after the heterogeneous boundary, where a great deal of oil was bypassed in the previous experiment, a better sweep has passed in this case.

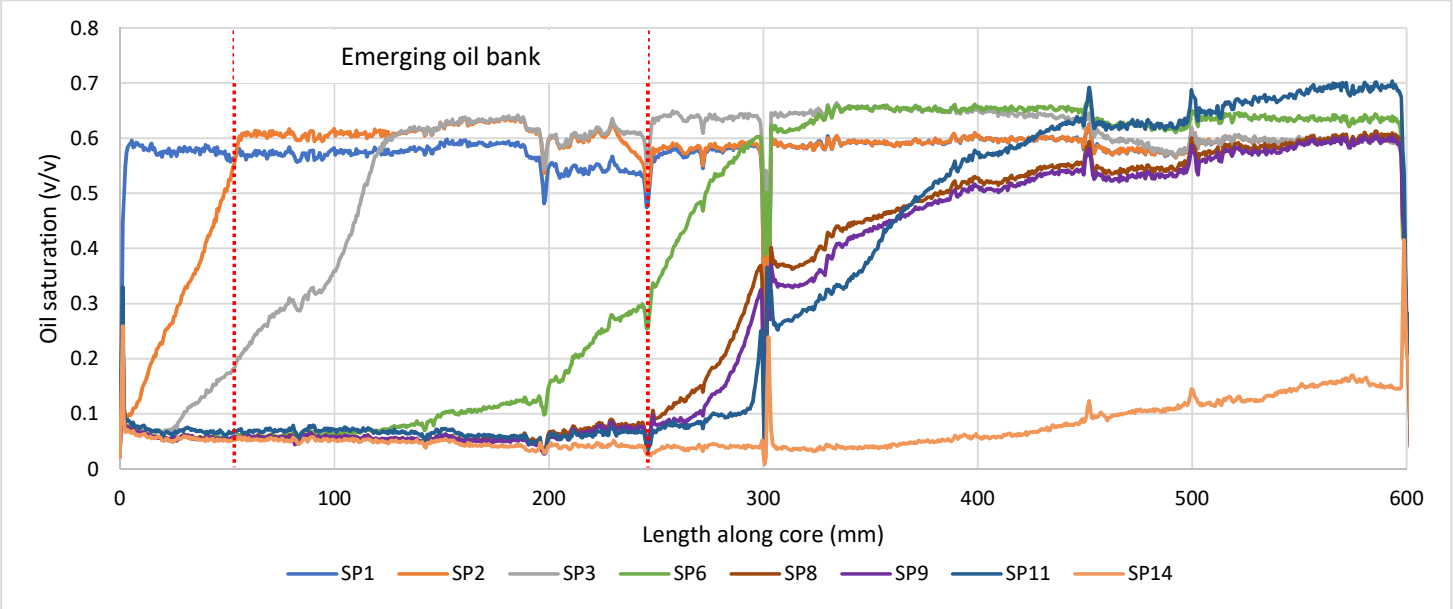

Figure 3.22: Saturation profiles per CT-scan in experiment 1 using composite core

3.4.8 Comparing iododododecane and dodecane oil experiments with a 60cm stacked core

After experiment in the CT-room repeat experiments were performed using dodecane oil. Figure 3.23 shows the comparison between experiment 2 using iododecane oil and experiment 4 using dodecane oil. In both experiments optimal surfactant with a viscosity if 45cP and polymer with viscosity of 50cP were used.

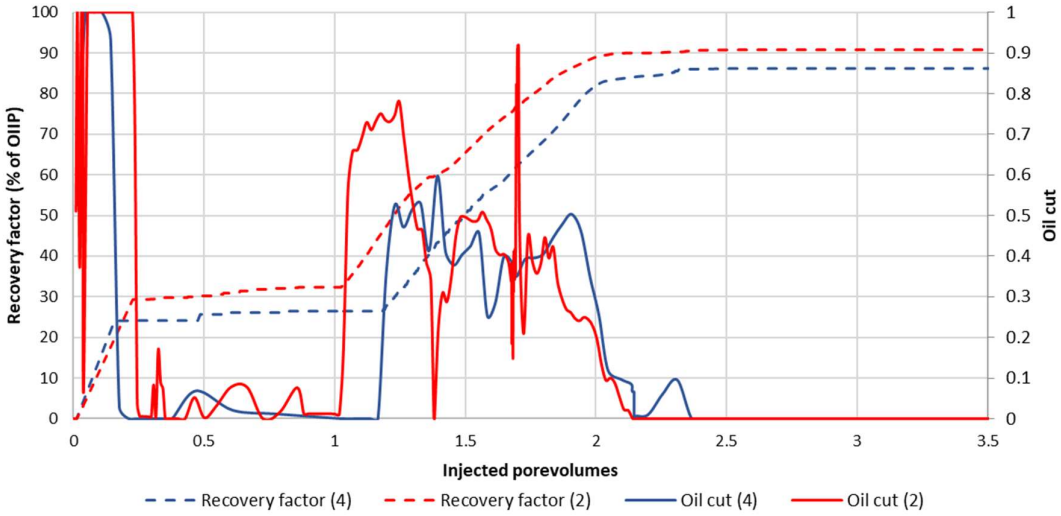

Figure 3.23: Recovery factors and oil cuts for iododododecane experiment 2 and dodecane experiment 4

Table 3.11 shows the relevant parameters for both experiments and a significant difference in initial oil saturation. Possible reason is the lower viscosity of the dodecane oil used in experiment 4, compared to iododododecane oil. The low viscosity could cause unstable displacement of brine by oil, allowing the oil front to reach the semi-permeable plate early on and trapping brine behind it.

Table 3.11: Relevant parameters for iododecane experiment 2 and dodecane repeat experiment 4		
	Experiment 2	Experiment 4
Initial oil saturation	0.72	0.58
Waterflood recovery factor (% of OIIP)	32.4	26.5
Chemical flood incremental recovery factor (% of OIIP)	58.4	59.7

The results show that there is a difference in waterflood recovery factor of 5.9% of OIIP. Since dodecane oil is the more mobile oil, one would expect a better recovery factor in the waterflood. On possible reason for this observation could be the difference in initial oil saturation. The chemical flood incremental recovery factors lie closely together with a difference of only 1.4%. However, experiment 4 does see a lower oil cut than experiment 2, contrary to the same comparison of the solid 60cm core.

3.5 Results and conclusions of 1m core experiments

Following the experiments done using the 60cm Fontainebleau cores, solid and unstacked, are a series of experiments performed on a solid 1m Bentheimer core. The major difference between the Fontainebleau and Bentheimer lies in their mineralogic composition; Fontainebleau has a quartz content of over 99%, while Bentheimer is a less clean sandstone. Bentheimer generally consists of 91.7% quartz, 4.9% feldspars and 2.7% of various clay minerals (Peksa, 2015). Other major difference between these rock types is that the Bentheimer core is much more porous and permeable.

3.5.1 Establishing heterogeneity through permeability measurements

Permeability measurements on the 1m Bentheimer core proved to be troublesome due to its high permeability. At low flow rates the pressure differences between adjacent pressure sensors is so small that a great spread in permeability was obtained. Fluctuations in flow rates by the pump and uncertainty in the pressure measurements add to this effect to the extent that permeability calculations in a single core section is unacceptably inaccurate. To still get a sense of the heterogeneity in pore geometry, permeability is evaluated in 3 core sections of equal length, seen in Figure 3.24.

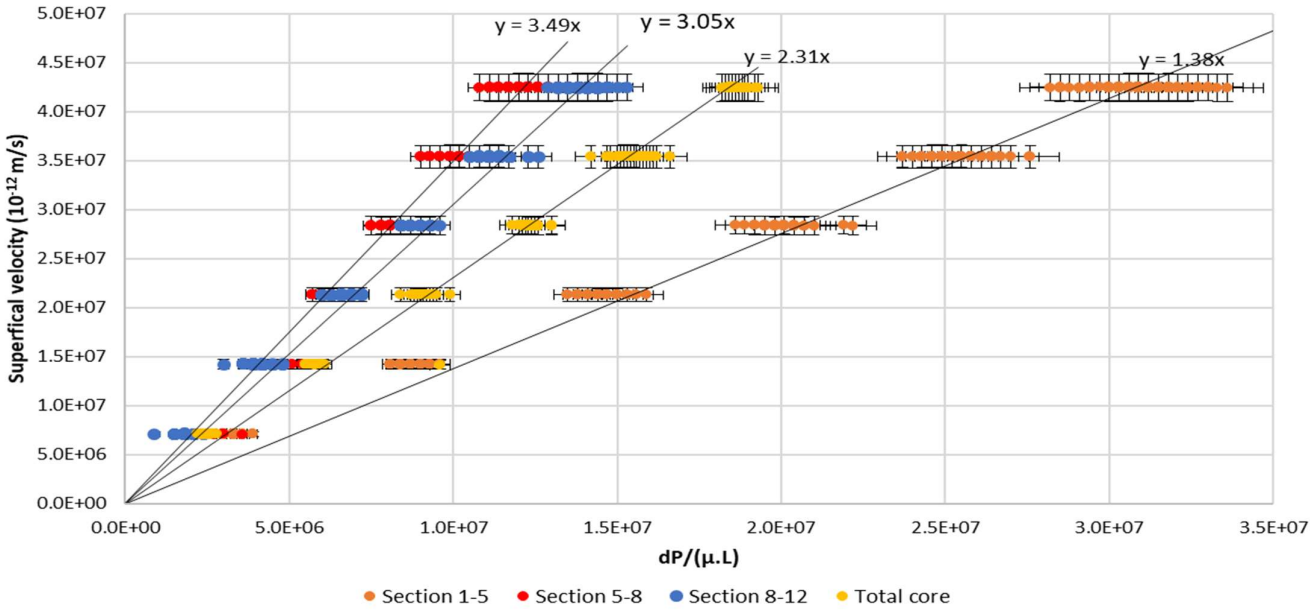

Figure 3.24: Permeability data for stacked 60cm core (Section 1-5 for example, refers to the core section between sensors 2 and 3). Trendline slopes are an estimate for average permeability in Darcy

As stated before, the data contains a spread in data, worst of which is observed in section 1-5. This section is closest to the pump and the spread is likely to be caused by fluctuations in flow rate. Even with this spread an idea of the cores heterogeneity is obtained. The data shows that section 1-5 is less permeable than sections 5-8 and 8-12, which do lie close together.

3.5.2 Oil filling of the 1m Bentheimer core

The evaluation of the heterogeneity showed a clear difference in permeability between the first and last sections of the core, a difference which is very much visible in Figure 3.25(bottom). The Figure shows a contrast in oil in place between the first and last half of the core. In general, with higher porosity comes higher permeability. The more permeable last half of the core should have greater porosity, but porosity calculations using CT-scans show that this is not the case (Appendix C). The CT-scan of a dry core seen in grey scale with enhanced contrast in Figure 3.25(top) does show some inconsistencies in the rock. It appears that the first half of the core contains some layering; flow across this layering could be the reason for the lower measured permeability.

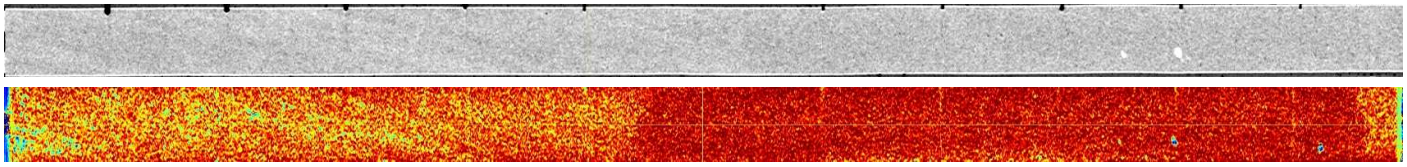

Figure 3.25: CT-scan of a dry core with enhanced contrast (top) and CT-scan of the 1m Bentheimer core after oil filling (bottom)

If a difference in porosity is not the reason for the greater oil in place in the last section, than inefficient drainage must be the reason. The likely cause for this observation could be an unstable oil front during oil filling which reached the semi-permeable plate early on. In this process the oil bypasses some water and traps it, the oil front cannot pass through the semi-permeable plate and no more oil can be injected.

3.5.3 Production data of experiment 1 using a 1m Bentheimer core

The first experiment performed using the 1m Bentheimer core was done in the CT-room, Table 3.12 shows relevant parameters for this experiment. In this experiment surfactant-polymer and polymer were used with viscosities higher than that of the microemulsions, since this setup showed much promise in identifying oil bank behaviour.

Table 3.12: Relevant parameters of experiment 1 using 1m Bentheimer core

Initial oil saturation (% of PV)	SP-salinity (%wt NaCl)	SP viscosity (cP)	SP volume (PV)	Polymer viscosity (cP)	Polymer volume (PV)	Waterflood recovery factor (% of OIIP)	Chemical flood incremental recovery factor (% of OIIP)
63%	4.5 (optimal)	45	0.5	50	1	54.3	24.9

Figure 3.26 shows the production data gathered during this experiment. The waterflood has a relatively high recovery factor of 54.3%, higher than any encountered in previous experiments. Since this is a much more permeable core than those used in previous experiments, this high recovery factor shows the influence of pore geometry on sweep efficiency. However, it does appear that water flood breakthrough occurs relatively early in the experiment at 0.25 pore volumes injected at the typical field rate. Due to time constraints the bump floods were initiated as soon as the oil cut dropped below 0.1.

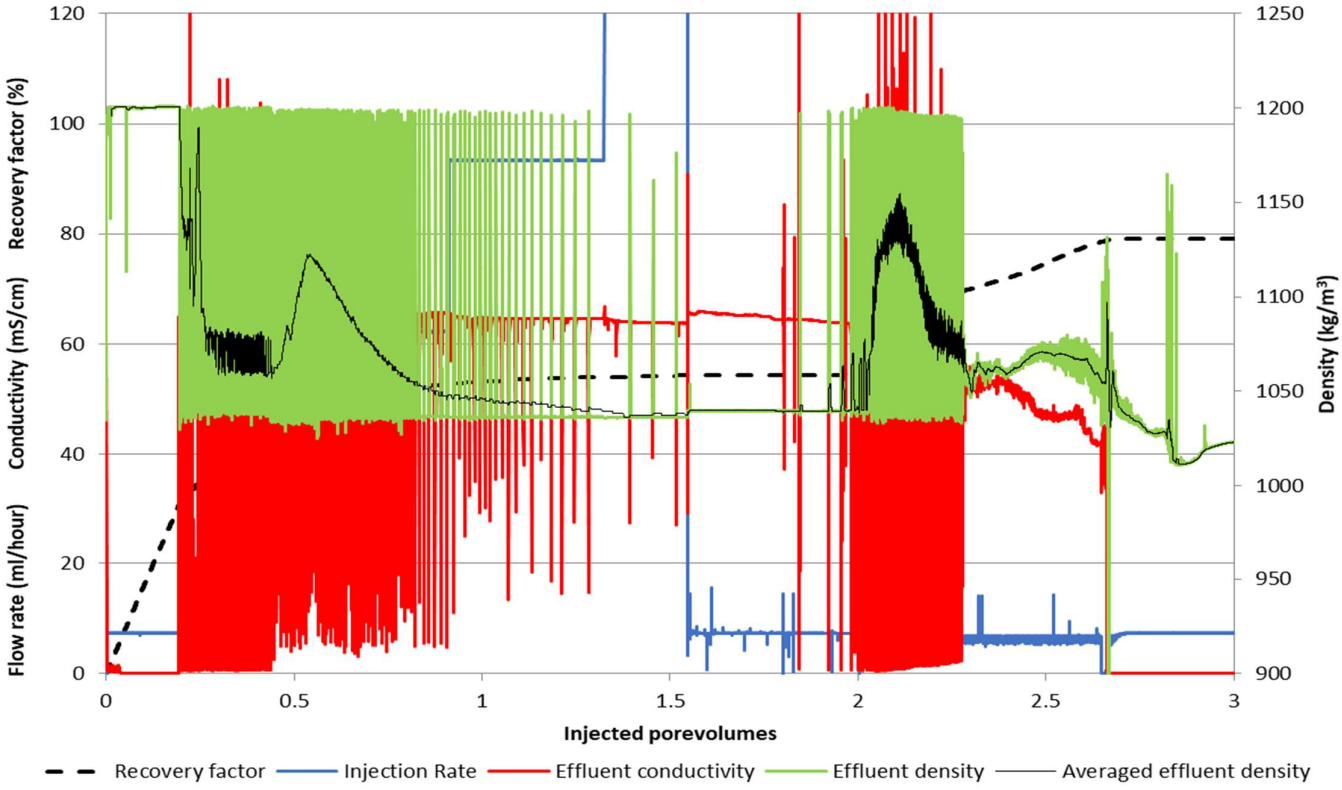

Figure 3.26: Production data for experiment 1 using a 1m Bentheimer core

The incremental recovery factor for the chemical flood of 24.9% of OIIP is not very high compared to previous experiments. Possible reason for this could be the fact that the initial oil saturation was also low compared to previous experiments. This would leave little oil to be mobilised after the waterflood. The production data does have some signs of an efficient sweep. Breakthrough of the SP-slug and microemulsion production starts after 0.5PV of SP has been injected and the average effluent density is high, suggesting a high oil cut as is confirmed in Figure 3.30.

3.5.4 CT-scans of experiment 1 using a 1m Bentheimer core

Figure 3.27 shows the CT-scans taken during this experiment. Figure 3.27(a) shows a CT-scan taken after the waterflood. This image shows a great difference in oil saturation between the first a last half of the core. The first half, which had the lowest initial oil saturation, appears to have retained the highest oil saturation after the waterflood while the last half, which had the higher initial oil saturation has a lower residual oil after waterflood. This again illustrates the effects of pore geometry on oil displacement: the more permeable section saw the most oil displaced and the less permeable section saw the least. At the very end of the core there is an area with an oil saturation higher than the surrounding core section.

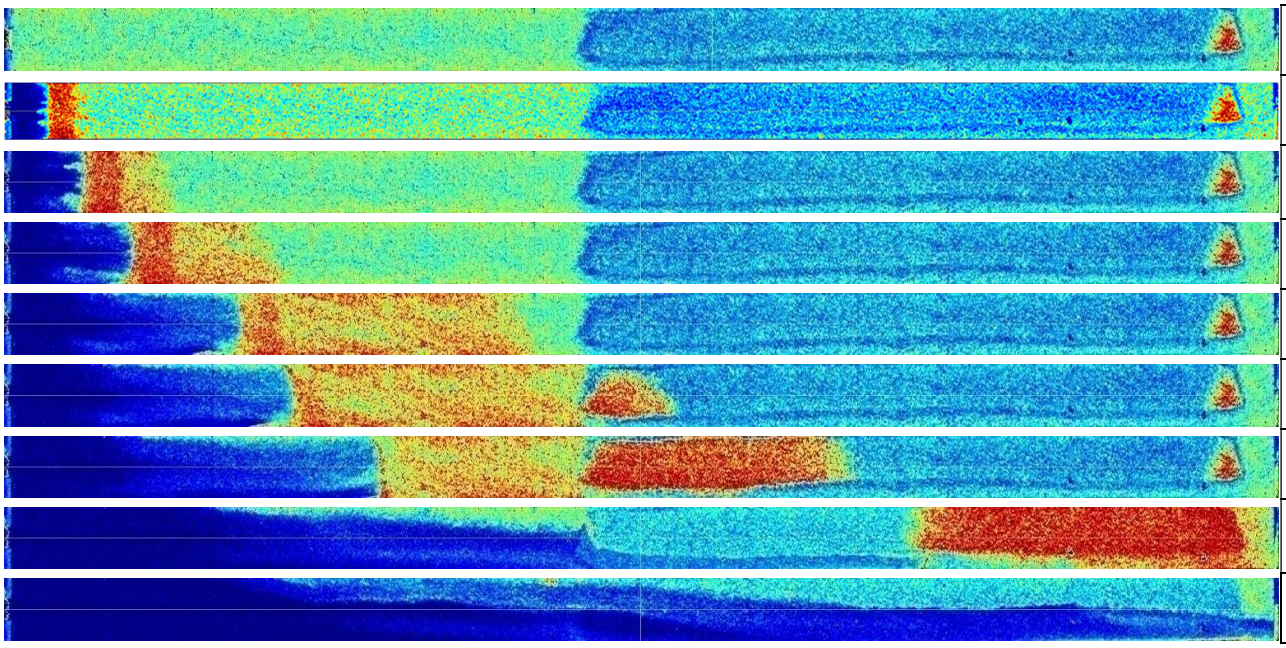

Figure 3.27: CT-scans of chemical flood of experiment 1 of 1m Bentheimer core (vertical cross-section at the core centre). Fluids are injected from the left. Blue and red colours signify low and high oil saturation, respectively. Annotations beside the scans indicate the injected volume at the time of the scan

Figure 3.27(b) shows the SP-slug entering the core. The is efficient, almost piston-like displacement and early oil bank formation. Figure 3.27(c) shows the further development of the oil bank. The higher oil saturation is found just past the SP-slug front and gradually decreases further ahead. The are some bright spots at the end of the SP-slug, caused by the mixing of surfactant and oil. Figure 3.27(e) shows the oil bank has increased in length and the difference in oil saturation between the start and end has lessened. Figure 3.27(f) shows the oil bank passing through some sort of boundary. There is a divide in the core between the two core sections of different permeabilities that allows the flow of oil through a small section of it. One possible explanation for this could be the presence of a fracture that provides a preferential path for the oil. Figure 3.27(g) shows how the oil bank, after passing through the boundary, comes together again to form an oil bank; this remerged oil bank seems to have a higher saturation than before the boundary. In Figure 3.27(h) the oil bank is being produced and the SP-slug passes through the boundary. The slug passes through it in an unstable manner wherein the bottom section core sees a better sweep and fingering occurs all the way to underneath the oil bank.

The scan in Figure 3.27(i) was done before a completed chemical flood, but it does show the breakthrough of the SP-slug. The slug seems to have fingered from the boundary to the end of the core and has swept the bottom section of the core better. After this scan was taken an additional 2% of OIIP of oil was produced, which was probably the result of the polymer slug displacing some oil unswept by the SP-slug.

3.5.5 Oil saturation from CT-scans in experiment 1 using a 1m Bentheimer core

Figure 3.28 shows the saturation profiles composed from the CT-scans. Most observations mentioned directly above can be recognised here. Scan SP1, SP2 and SP3 show that the highest oil saturation is directly ahead of the SP-slug. The rise to this peak oil saturation becomes less steep between scans SP2 and SP4, indicating the occurrence of mixing. Up to scan SP6, before the oil bank hits the capillary boundary, the peak oil saturation decreases while the oil bank length increases. The increased oil saturation after the boundary is not observed here, since the saturation profiles consist of average oil saturation per cross-sectional core slice. Figure 3.27(g) shows lower saturations at the bottom of the core, which bring down the average saturation in the profiles.

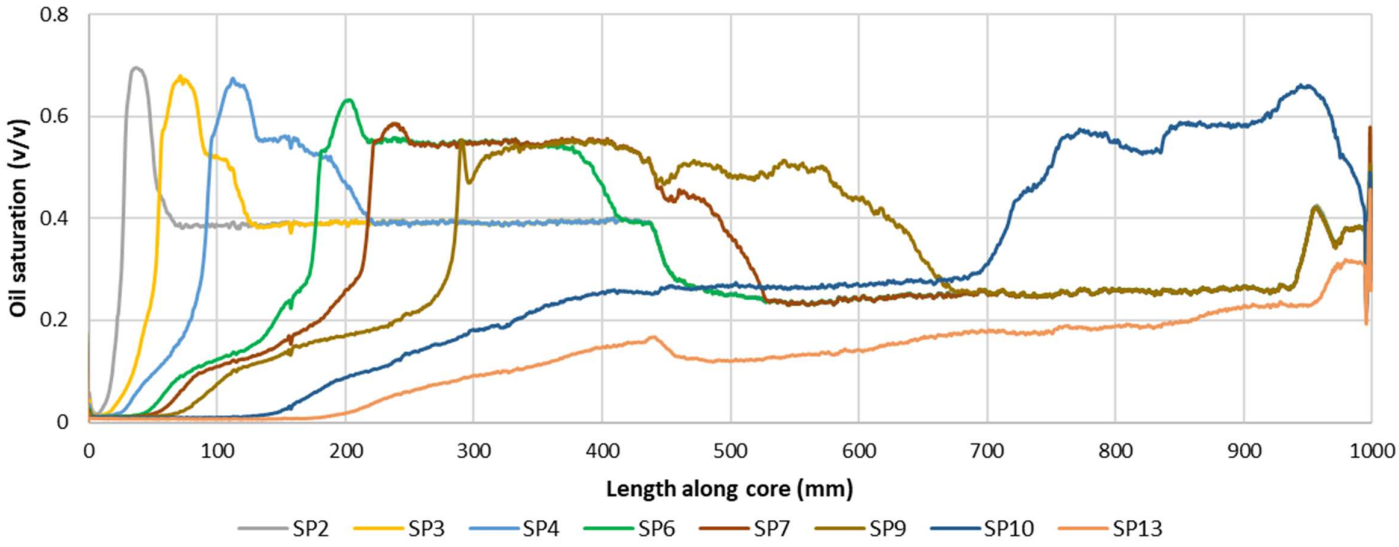

Figure 3.28: Saturation profiles per CT-scan in experiment 1 using a 1m Bentheimer core

3.5.6 Comparison with dodecane experiment

A second experiment was performed on the 1m Bentheimer core outside of the CT-room. Here the lighter dodecane oil, optimal surfactant and surfactant-polymer and polymer, with viscosities higher than that of the microemulsions were used. Table 3.28 shows the relevant experiment parameters.

Table 3.28: Relevant parameters of experiment 2 using 1m Bentheimer core

Initial oil saturation (% of PV)	SP-salinity (%wt NaCl)	SP viscosity (cP)	SP volume (PV)	Polymer viscosity (cP)	Polymer volume (PV)	Waterflood recovery factor (% of OIIP)	Chemical flood incremental recovery factor (% of OIIP)
48%	3.75 (optimal)	45	0.5	50	1	53.2	21.1

First point of note is that during this experiments oil filling a relative low oil saturation of 0.48% was obtained. Possible reason for this could be the same as what caused the difference in oil saturations between the core sections in the previous experiment; the oil front bypassed some water and by the time it reached the semi-permeable plate the water was trapped. The water flood recovery factor only shows a 1.1% of OOIP difference with experiment 1.

The chemical flood recovery factor was in experiment 2, 3.8% less than in experiment 1, which is an unexpected result since dodecane oil has lower viscosity than iododododecane oil. One possible explanation is that of the low initial oil saturation that, after a waterflood recovery approximately the same as in experiment 1, would leave less oil to be displaced during the chemical flood.

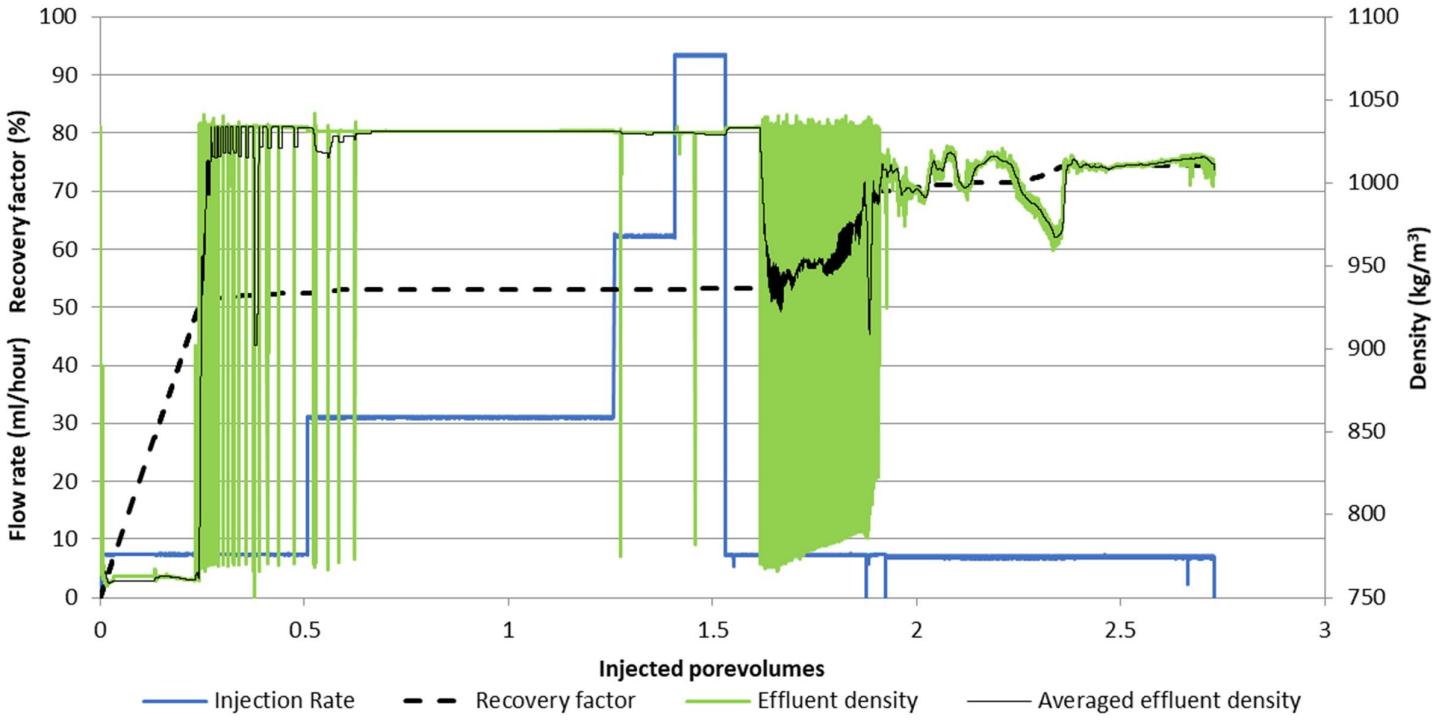

Figure 3.29: Production data of experiment 2 using a 1m Bentheimer core

The averaged effluent density in the production data also remains close to the density of brine, suggesting a lower oil as is depicted in Figure 3.30. Experiment 1 saw an oil cut up to 0.68 while the oil cut in experiment 2 does not exceed 0.36.

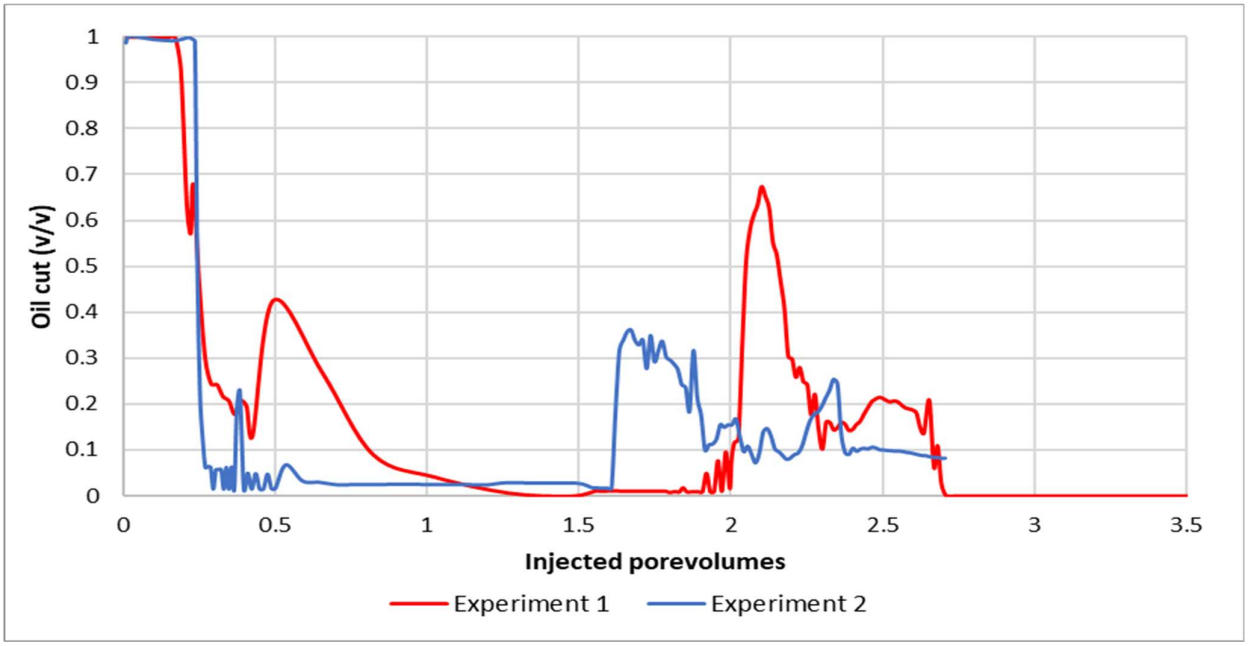

Figure 3.30: Averaged oil cuts for experiment 1 (iodododecane) and experiment 2 (dodecane)

3.6 Evaluation of oil mobility through relative permeability data

As mentioned in Sections 1.5 and 1.6, the Buckley-Leverett and JBN methods are valuable tools in identifying oil mobility using relative permeability data. These approaches are applied using production data from the experiments. The most relevant objective here in relative permeability analysis is the effect of core length on the oil mobility, but a straight forward comparison is often not easy to make. The hypothesis is such that, a greater core length should yield a greater oil mobility. The reasoning behind this is that a greater path through a porous medium gives a greater window of opportunity for dispersed oil droplets to coalesce into an oil bank. However, rock and fluid properties play a role so significant, that it is sometimes not easy to attribute differences in oil mobility to core length alone.

The water flood relative permeability is displayed using conventional relative permeability curves, the relative permeability data for the chemical flood is displayed using pseudo relative permeability curves. These curves are assigned initial saturation conditions corresponding to the final saturation conditions of the water flood. They are a useful tool in evaluating oil mobility in a heterogeneous core with a focus on the chemical flood

3.6.1 Relative permeability data: 60cm versus 100cm core.

One such ambiguous comparison is that between experiment 1 with the 60 cm Fontainebleau core and experiment 1 with the 1m Bentheimer core, discussed in Sections 3.3 and 3.5, respectively. Besides core length other significant parameters are surfactant-polymer viscosity (10cP in the 60cm core versus 40cP in the 1m core) and core permeability (a factor of 130 greater in the 1m core).

Figure 3.31 shows the relative permeability curves for experiment 1 of the 60cm Fontainebleau core. The Figure shows the BL-curves made to fit the JBN-datapoints using the Corey exponents and endpoint relative permeabilities and by matching BL production data with experimental production data. The BL-curves are treated as the final relative permeability curves.

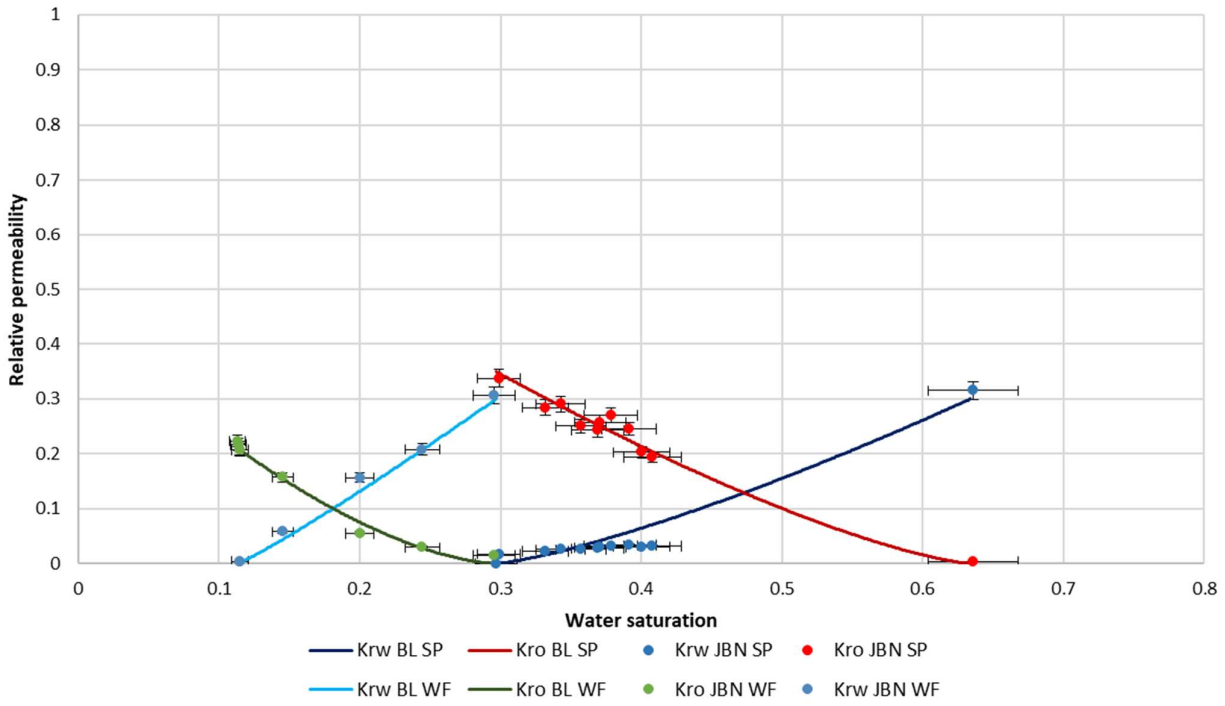

Figure 3.31: Relative permeability curves for water and chemical flood from Buckley-Leverett (BL) and JBN methods for 60cm core

Figure 3.32 shows the relative permeability curves for experiment 1 of the 1m Bentheimer core. One apparent difference between Figures 4.1 and 4.2 is the difference in presence of JBN datapoints along the range of water saturation. In the curves pertaining to the chemical flood in Figure 4.2, there are datapoints along the entire BL-curve, whereas they are more focused at initial and final saturation in Figure 3.31. Reason for this is the fact that the explicit JBN method depends greatly on measured fractional flow of oil and water. In the 60cm experiments fewer intermediate values for oil cut were registered. The Buckley-Leverett method on the other hand, is an implicit one that matches relative permeability curves to production data.

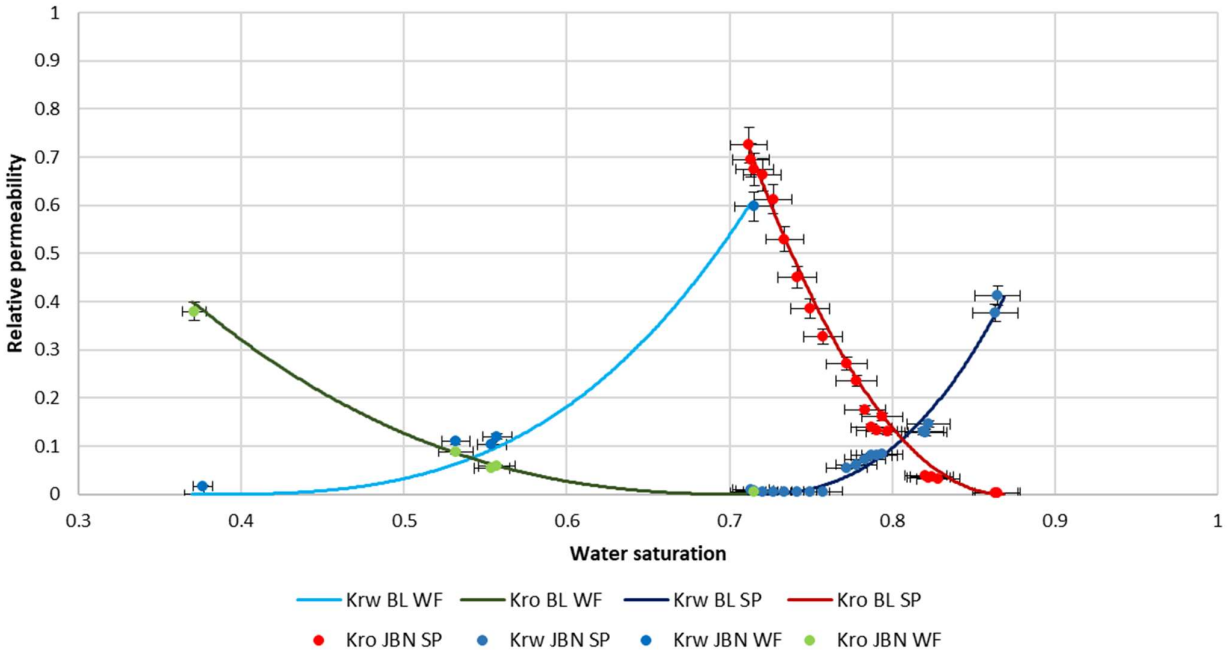

Figure 3.32: Relative permeability curves for water and chemical flood from Buckley-Leverett (BL) and JBN methods for 1m core

Figure 3.33 shows the comparison between the relative permeability curves for water and chemical flood for both the 60cm and 1m cores. The graphs in Figures 3.31 and 3.32 are difficult to compare due to their different initial and final saturations of both floods between the two experiments. By normalizing them, by assigning the relevant saturations of the 60cm experiment to the 1m experiment, a proper comparison as in Figure 3.33 can be made. Normalizing in this context means that one experiment is assigned the initial and final saturations of the experiment it is compared with.

When focusing on the oil relative permeability curves certain conclusions can be deduced. A consistent result is that in both the waterflood and chemical flood the oil is more mobile in the 1m core than in the 60 cm core. The waterflood oil relative permeability shows the increased mobility due to the core's greater length and greater permeability. The oil relative permeability in the chemical flood shows a greater difference between the two experiments, which here can be attributed to the greater core length and permeability and increased surfactant-polymer viscosity in the 1m core. Although oil mobility is better in the 1m core, the extent of the relevance of the contributing parameters is not clear.

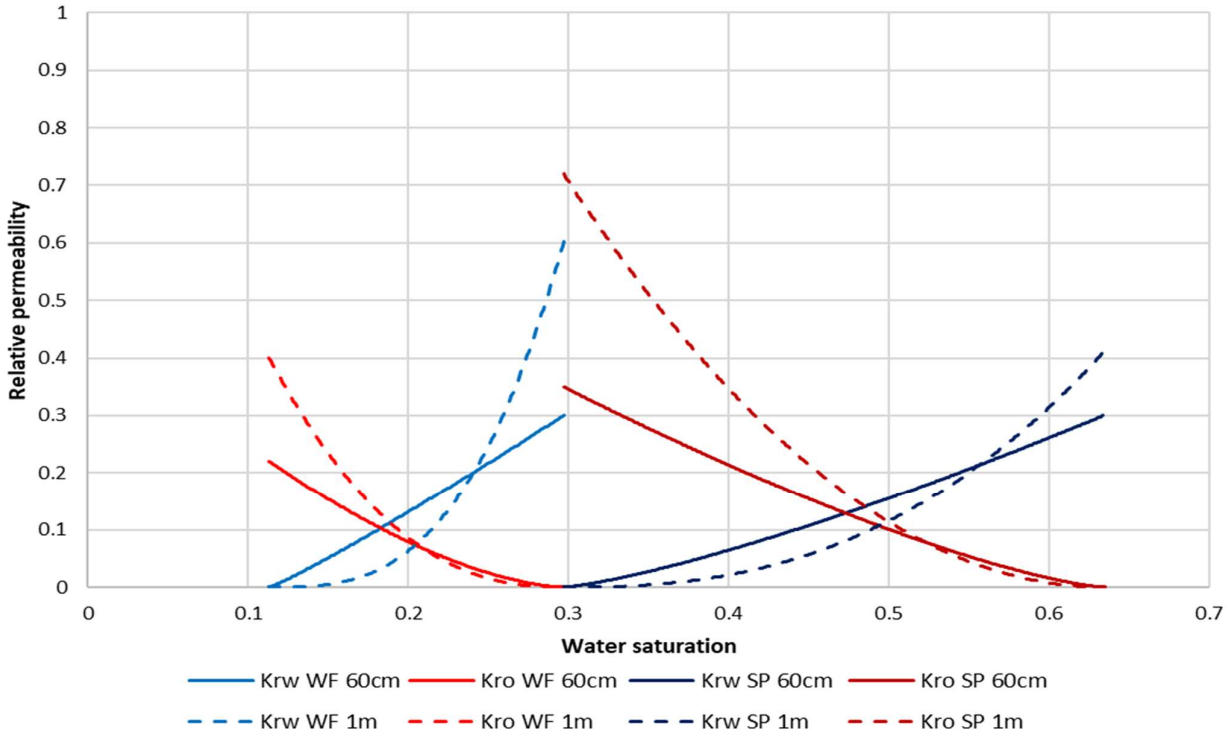

Figure 3.33: Comparison of relative permeability curves of the 60cm and 1m cores

3.6.2 Relative permeability data: low permeability versus high permeability 7.5cm cores

The comparison of the 60cm and 1m core experiments is an ambiguous one, in that more than one parameter contributes to the relative permeability data. In this section a much clearer comparison is made between experiments using two cores of equal length and identical injectants, but with different permeabilities. The experiments used are those discussed in Section 3.2.4, with high permeability (120 mD) 7.5cm and low permeability (14 mD) core. Figures 3.34 and 3.35 show the combined Buckley-Leverett and JBN relative permeability of the high permeability and low permeability experiments, respectively. Figure 3.36 shows the comparison of these two figures.

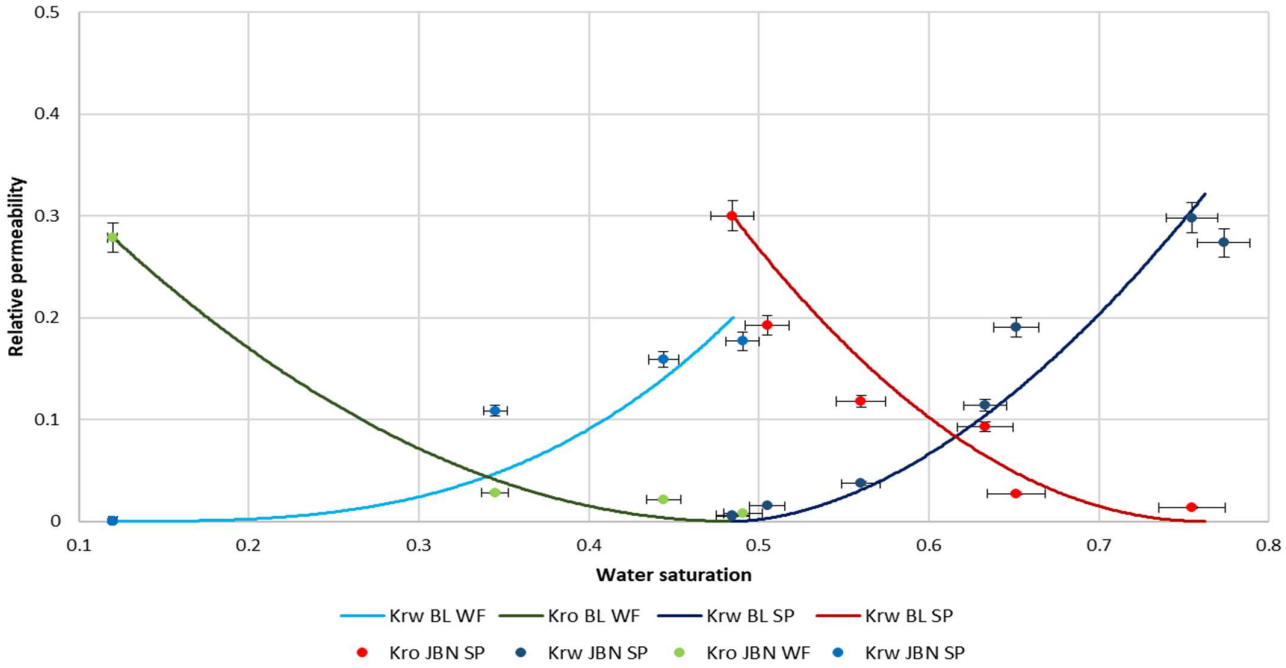

Figure 3.34: Relative permeability curves for water and chemical flood from Buckley-Leverett (BL) and JBN methods for high permeability 7.5cm core

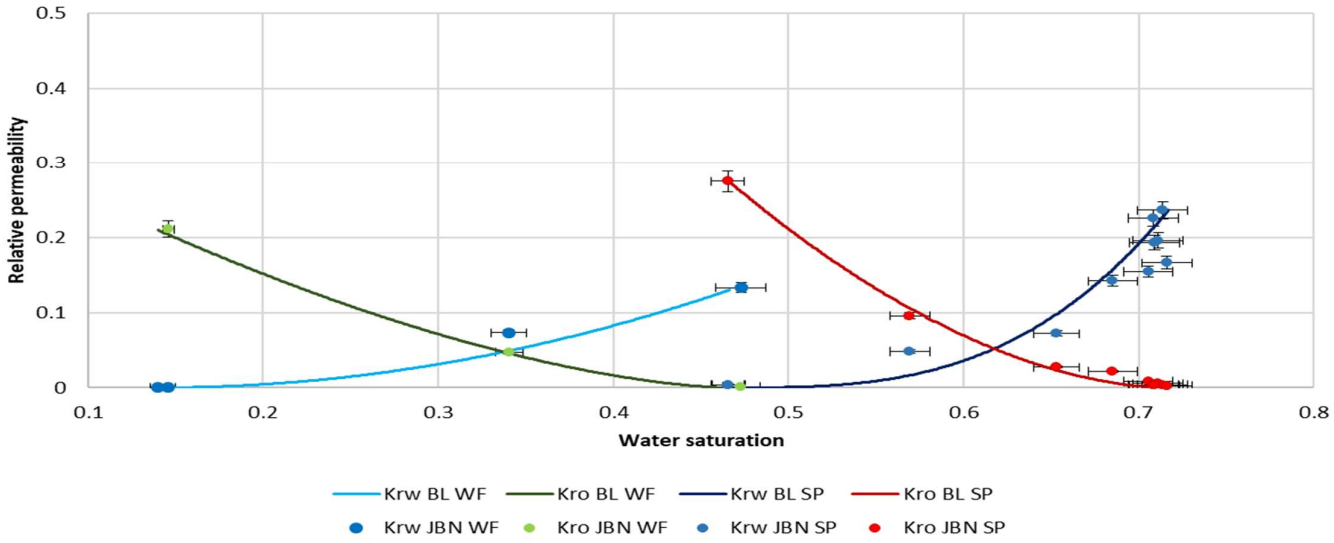

Figure 3.35: Relative permeability curves for water and chemical flood from Buckley-Leverett (BL) and JBN methods for low permeability 7.5cm core

Contrary to the comparison between the 60cm and 1m core data, here the normalization of initial and final saturations is not deemed necessary since there is not much difference between the two experiments. Figure 4.6 does tell a clear story of higher oil mobility in the high permeability core. This difference in oil relative permeability indicates the effect of pore geometry on oil mobility.

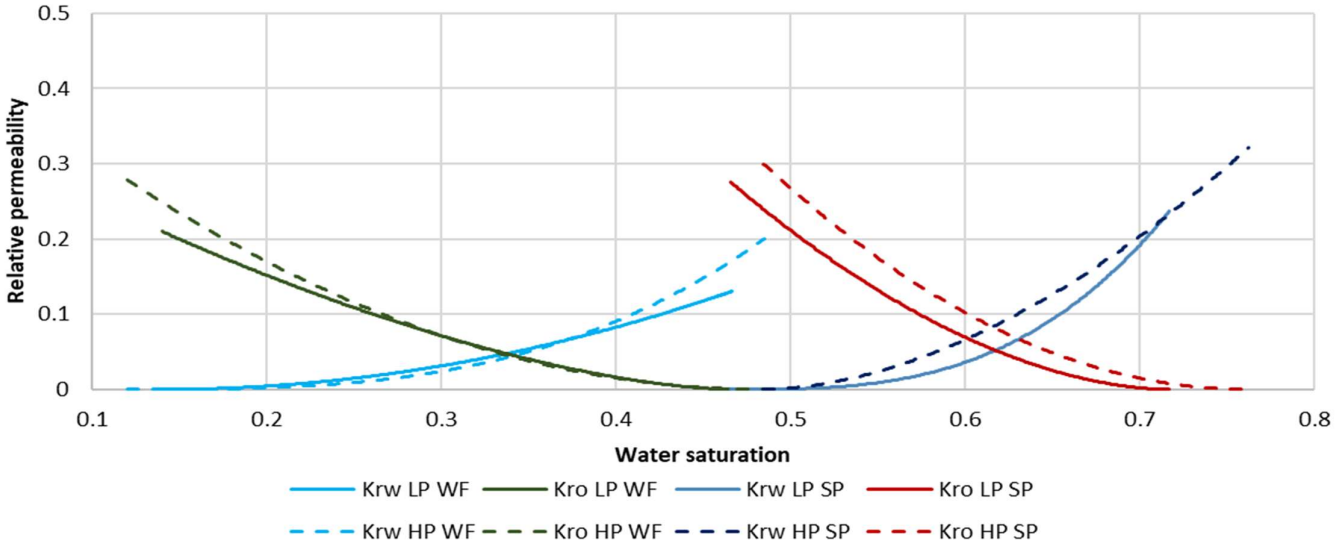

Figure 3.36: Comparison of relative permeability curves from the low permeability (LP) and high permeability (HP) 7.5cm cores

3.6.3 Relative permeability data: 7.5cm versus 60cm core

Most suitable method in evaluating the effect of core length on oil mobility, is by comparing the 7.5cm low permeability and 60cm cores. With permeabilities of 14 mD of the 7.5 cm core and 17.8 mD of the 60 cm core and identical chemical flood compositions, they are similar enough to attribute major difference in oil relative permeability to core length and to neglect the effects of pore geometry. This comparison is seen in Figure 3.37. The oil relative mobilities in the waterflood are quite similar, while there is a significant difference in the water mobility. The oil relative mobilities in the chemical flood show that the oil is more mobile in the 60 cm core than in the 7.5 cm core. This observation supports the earlier mentioned hypothesis of greater oil mobility at greater core length. In the 60 cm core there is more space for oil droplets to coalesce and more time for the oil bank to increase in size.

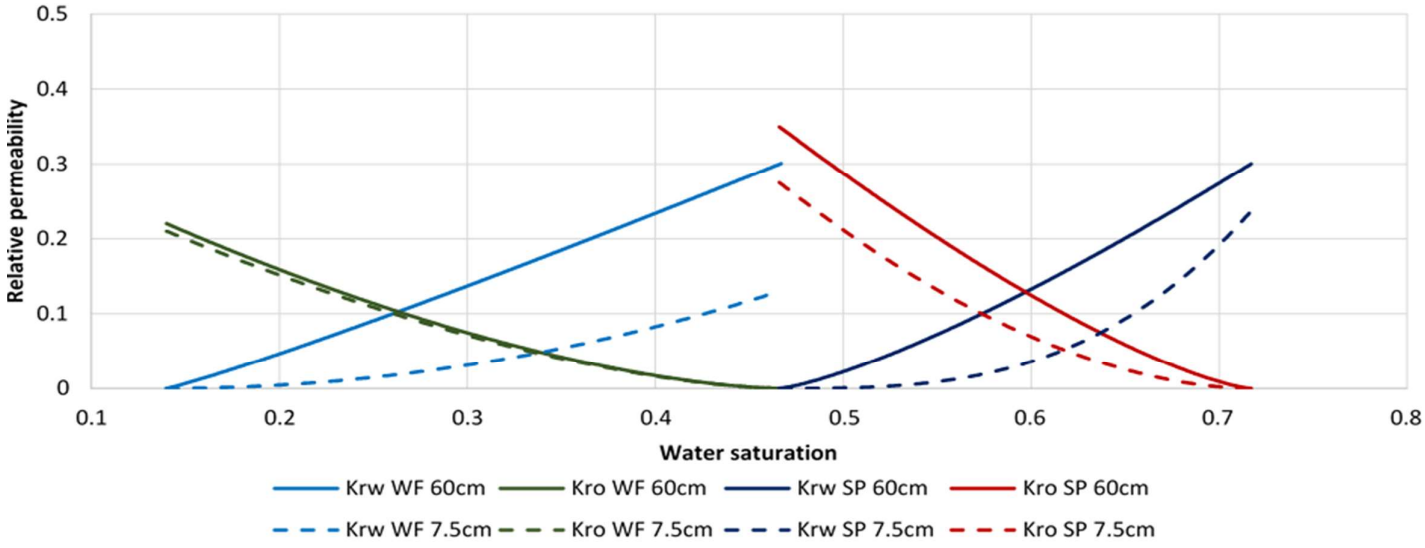

Figure 3.37: Comparison of relative permeability curves from the 7.5 cm and 60 cm cores

4 Discussion

1 Lower waterflood recovery factors in 60cm core

Comparing waterflood production data of the 7.5cm and 60cm cores, showed that in the 60cm core experiments the waterflood yielded a lower recovery factor. Waterflood sweep efficiency generally depends on two key factors: rock wettability and pore geometry. Since both cores are of the Fontainebleau sandstone, one can assume that differences in wettability are minor or non-existent at all. That leaves the reduction in waterflood efficiency to be attributed to the pore geometry. Permeability measurements showed that average permeability of 7.5 and 60cm cores differed with a factor 7. This low permeability in the longer core along with its increased capillary forces, could the major cause for the reduction is waterflood efficiency. This notion is supported by the waterflood recovery factor in the high permeability 1m Bentheimer core, which reached values greater than that of the 7.5cm core.

2 Optimal vs suboptimal SP (Section3.2.5) (7.5 % 60cm)

Comparison of production data of experiments using optimal surfactant and experiments using suboptimal surfactant showed consistent results in both the 7.5cm and 60cm cores. One relevant conclusion to be drawn from these results are that is that of lower oil recovery factors at suboptimal surfactant conditions. It appears that suboptimal surfactants, as expected, lower interfacial tension to a smaller extent and mobilise less oil. Second conclusion pertains to the effluent composition; data shows that at optimal surfactant, more microemulsions seem to be produced. This can be attributed to the fact that in a suboptimal system, micelles are drawn into the water phase and there is no distinct microemulsion phase between oil and water, as was shown in Sections 1.3 and 3.1

3 Effects of permeability (pore geometry) on incremental oil recovery

In comparing production data of experiments using cores of equal length, but ranging permeability, shows that there is a dependency of incremental oil recovery on permeability. The clean oil produced, relative to the core pore volume, seems to increase in size with increasing permeability and porosity. One explanation for this observation is the fact that in a porous medium, lower permeability comes with tighter pore network. Since capillary forces also depends on the pore geometry, capillary forces increase with decreasing permeability. The function of surfactant is lowering the interfacial tension, but at low permeability IFT is not reduced to the same extent as in a high permeability scenario.

4 Increasing SP and polymer viscosity above microemulsion viscosity drastically increases sweep efficiency.

CT-scans taken during the experiment performed on the solid 60 cm core showed that using SP and polymer viscosities of 10cP and 15cP, respectively, yielded an inefficient sweep and fingering during the chemical flood. This effect was initially attributed to heterogeneity within the core itself. The first experiment using the stacked 60cm core was performed under the impression that the higher permeability and lower sensitivity to heterogeneity would mitigate the effect of heterogeneity on the sweep. Although a capillary boundary was present at the interface of the two cores that composed the stacked core, before hitting this boundary the SP-slug showed a great deal of fingering, leading to the conclusion that not only heterogeneity effects sweep efficiency in this specific study. Following this initial experiment, were measurements of viscosity of the microemulsions formed in the type (III) optimal surfactant, which showed that microemulsion

viscosity lied well over that of the polymer and SP-solutions at 40cP. Increasing the SP-slug and polymer's viscosity above that of the microemulsions to 45 and 50cP respectively, showed an increase in sweep efficiency and oil recovery factor. Conclusion that can be drawn from this is that is that microemulsion mobility plays a big part in SP flood sweep efficiency and that increasing SP and polymer viscosity above microemulsion viscosity drastically increases sweep efficiency.

5 Effects of heterogeneous boundaries on chemical flood sweep efficiency

In Sections 3.4 and 3.5, showing results of the stacked 60 cm Fontainebleau core and 1m Bentheimer core respectively, show the effects of extreme heterogeneities on the chemical flood. Both cores contain sections that act as a preferential path for fluids, which negatively effects the displacement stability. The low viscosity chemical flood using the stacked core shows the sensitivity of the SP-slug to this thief zone, to the extent that fingering occurs even before the slug has reached this heterogenous boundary. The high viscosity chemical flood using the stacked core, shows that fingering before the SP-slug has reached the boundary is mitigated to some extent; there is piston-like displacement up until the point the slug passes through it. After the slug passes through the thief zone, fingering is initiated and there is again unstable displacement. The result of the high viscosity chemical flood does show an overall better sweep than in the low viscosity chemical flood. The same effect is observed in the 1m Bentheimer core experiment, which was only performed using a high viscosity chemical flood. Up until the discontinuity there is piston like displacement. Even after the oil bank passes through this thief zone it remerges. The SP-slug however is forced into a fingering path after having passed through the thief zone. The general conclusion here is that these extreme heterogeneities are detrimental to stable displacement and while increasing chemical flood viscosity lowers its effects somewhat, does not solve the issue completely.

6 Saturation calculation based on CT-scans and oil bank quality

Section 1.9 shows how oil saturation distribution in the core is calculated using CT-scans. Most interesting observation here is progression of the oil bank during the chemical flood in the 1m core, seen in Section 3.5.4 CT-scans of experiment 1 using a 1m Bentheimer core. The data shows a general trend where, at optimal surfactant with optimal viscosity, there is almost piston like displacement with an oil bank that gradually increases in length with highest oil saturations at the SP-slug interface. Comparing Sections 3.4.6 and 3.5.4, shows the difference in quality of an oil bank between the stacked 60 cm and 1 m cores. The quality of an oil bank is measured in terms of increased saturation of core sections when the oil bank passes through them. This increased oil saturation seems to be greater in the 1m core.

6 Relative permeability curves and oil mobility

Relative permeability curves composed by the Buckley-Leverett and JBN method based on fitted and experimental data, show the oil mobilisation during the chemical flood. Differences in oil relative permeability can be attributed to several parameters, making it hard it to narrow down the extent in which a single factor affects oil mobility. One comparison, between low permeability 7.5cm and 60cm cores, shows that a greater core length is indeed beneficial to the oil mobility. The comparison between a low permeability and a high permeability 7.5cm core shows the effects of permeability, or rather pore geometry, on oil relative permeability. Any comparison with the 1m Bentheimer core is an inconclusive one since it has much greater permeability than any core and it used in a high viscosity chemical flood, latter of which was also only performed on the stacked core, which had several complex properties.

5 Recommendations

Looking back on the experimental part of this study raises some ideas on how some experiments can be improved in future work.

One major recommendation stems from the experiments performed on the stacked 60 cm core. Initially the stacking of two high permeability cores seemed like an adequate way to obtain a longer high permeability core, but the result leaves much to be desired. The boundary between the two stacked cores shows such a degree of heterogeneity, that it is virtually impossible to compare it to the solid low permeability 60 cm core and draw conclusions on the effects of permeability in long cores, which was the major objective in stacking the cores. The recommendation here is to focus more on the boundary between the stacked cores and design to be as continuous as possible, and if possible avoid stacking cores altogether.

Second recommendation has to do with the volume of surfactant-polymer and polymer injected. These volumes were deliberately kept as predetermined values to be able to make adequate comparison with previously done work. Varying the volume of chemicals injected and evaluating the variations effects on incremental oil recovery, should give some insights into the efficiency of a surfactant in terms of injected volume of surfactant per volume of produced oil. Not only would results from this data have great research value, they could also generate results of great interest within an economic framework.

Third recommendation pertains to the difference in chemical flood viscosity of certain experiments. In Section 3.4.5 the choice for a chemical flood with viscosity greater than that of the microemulsion was explained, but the viscosities here are quite binary in the sense that they are either much lower just above the viscosity of the microemulsions. To draw an irrefutable conclusion on the effects of viscosity on displacement efficiency, one should perform chemical floods of varying viscosity. If it is indeed the effect of chemical flood viscosities exceeding that of the microemulsions that so drastically increase sweep efficiency, one should observe unstable displacement at any viscosity up until viscosity of the microemulsion, after which stable displacement should be achieved. The general idea here is the conclusion of increased sweep efficiency due to increased viscosity could be better supported if more than 2 combinations of viscosity were used.

A fourth recommendation is to design core flood experiments to simulate real scenarios as closely as possible. Several factors in this study could be approved upon to better evaluate and tackle issues and complications that would arise in a chemical flood on a real scenario. One way to do this is to use brine in a core flood as similar as possible to the brine found in the subsurface. In this study the brine composition was kept relatively simple with just one salt dissolved in it. Real reservoir brines however have more complexed make-up with several types of salts in solution, that are likely to effect optimality and viscosity of surfactant and polymer solutions. Another wat to better simulate a real chemical flood is to use a less ideal type of oil, preferably crude oil. This dodecane and iododododecane oils used in this study's experiments have much simpler composition and more important much lower viscosity than crude oil.

Appendix A: Error analysis

Measurements performed during experiments often contain a certain degree of inaccuracy due to apparatus limitations. Most relevant of these inaccuracies are discussed here.

A.1 Accuracy of produced oil volume from density and mass flow rate measurements

One relevant error stems from inaccuracies in measurements from the Coriolis mass flow meters. The parameters measured from this device, density of pure phases (ρ_{brine} and ρ_{oil}), effluent density (ρ) and mass flow rate ($\dot{m}$), are used in calculating volume of produced oil (N_p). All density measurements and mass flow rates measured by the Coriolis meters have an accuracy of 0.2% (Bronkhorst, 2018).

Another parameter is that of the time between measurements (dt). This value is a pre-set parameter for loop time. Malfunctions in the experimental apparatus stall this loop and cause a difference between loop time and real time. The magnitude of this error varies from experiment to experiment but was in an extreme case found to be a deviation of 1s per 90s, or 1.1%.

$$N_p = \frac{\dot{m}}{\rho} * dt * \frac{\rho - \rho_{oil}}{\rho_{brine} - \rho_{oil}} \qquad \text{Eq.A.1}$$

Equation A1 shows how produced oil is calculated from measured values. Using Equation A.1 and the rules of error propagation, the error in produced oil was found to be:

$$\partial N_p = \sqrt{\partial \dot{m}^2 + \partial \rho^2 + \partial (dt)^2 + (\partial \rho + \partial \rho_{oil})^2 + (\partial \rho_{brine} + \partial \rho_{oil})^2} = 1.3\%$$

The same errors have certain implications for the calculation of the oil cut. The oil cut if calculated from density alone and its error follows from:

$$\partial f_o = \sqrt{(\partial \rho + \partial \rho_{oil})^2 + (\partial \rho_{brine} + \partial \rho_{oil})^2} = 0.6\%$$

A.2 Accuracy of permeability from density and mass flow rate measurements

Permeability calculations are also affected by measurements by the experimental apparatus. Pressure data from the pressure transducers (dP), flow rates from the Coriolis meters (Q) and measurements of core dimensions are used in estimating permeability and so their inaccuracy affect that of the permeability. Permeability relates to the measured parameters as depicted in Equation A.2.

$$K = \frac{Q * \mu * L}{A * dP} = \frac{\dot{m} * \mu * L}{\rho * A * \Delta P} \qquad \text{Eq.A.2}$$

Manufacturer specifications indicate that the maximum error for pressure measurements is 0.5% (Keller, 2017). Errors in the core dimensions are caused by irregular drilling and cutting of the cores, the greatest of which was found to have a deviation of 12mm from the intended length. For the viscosity of water the general value of 0.001 Pa.s was used, but (Thorade, 2010) shows that salinity can cause an increase of up to 5 µPa.s. The rules of error progradation and Equation A.2 yield the following maximum error for permeability.

$$\partial K = \sqrt{\partial \dot{m}^2 + \partial \rho^2 + \partial \mu^2 + \partial (\Delta P)^2 + \partial A^2 + \partial L^2} = 3.24\%$$

Appendix B: Viscosity measurements

To be able to make adequate comparisons between experiments in this study and in previously done work, it is important that viscosities are kept as consistent as possible. As stated in Section 1.4, salinity and all other parameters are kept constant while HPAM-concentration is varied to obtain a required viscosity. For both the surfactant-polymer and the polymer solutions a multiple mixtures of varying HPAM-concentrations are made. Viscosity measurements with a rheometer are performed until a solution with adequate viscosity is found.

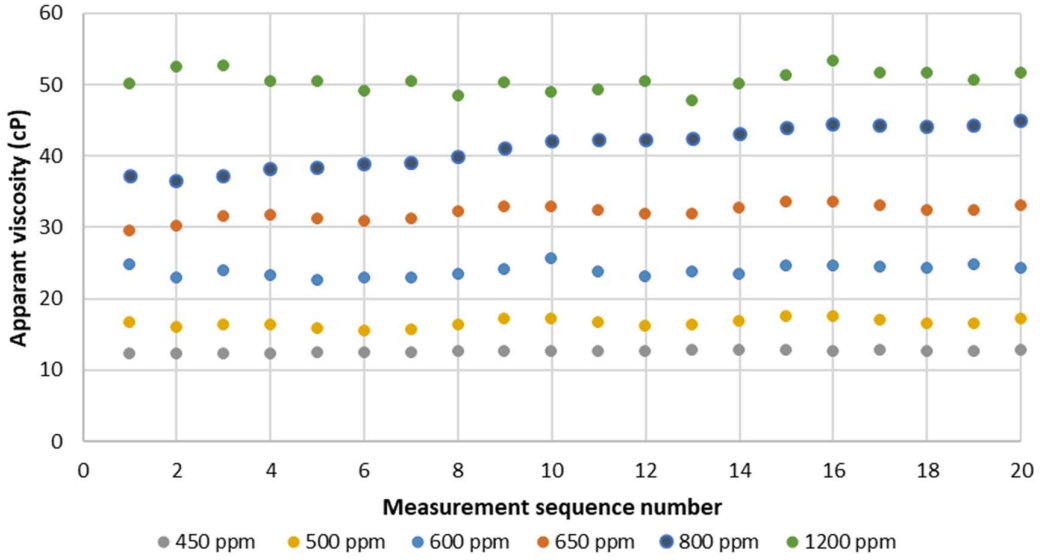

*Figure B1: Effect of HPAM-concentration in **polymer-solution** on viscosities at shear rate of 6 s^{-1}*

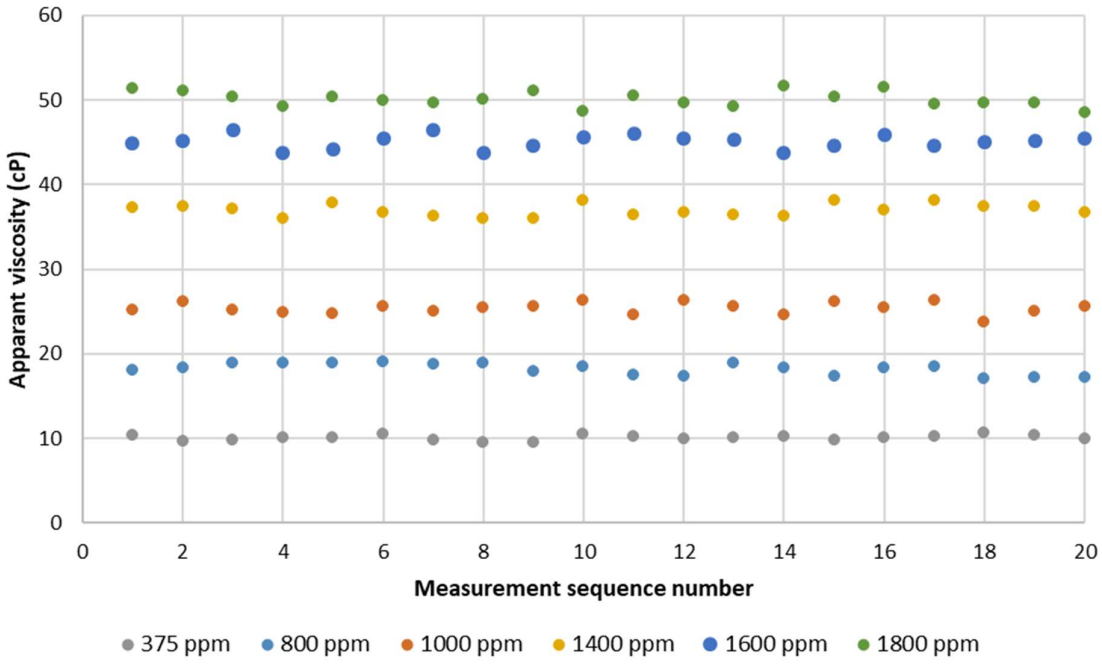

*Figure B2: Effect of HPAM-concentration in **surfactant-polymer** on viscosities at shear rate of 6 s^{-1}*

Figures B1 and B2 show the apparent viscosities at the typical shear rate for both the polymer and surfactant polymer. One clear conclusion is that in the low-salinity polymer lower concentrations of HPAM are required to obtain a specific viscosity than in the surfactant polymer. Comparing the 800 ppm HPAM concentrations of both solutions show that at this concentration the polymer reaches a viscosity of over 40cP while the surfactant-polymer does not exceed 20cP at this concentration.

From this data the required concentrations for the core flood experiments were chosen. For the low viscosity chemical flood, a polymer with HPAM-concentration of 500 ppm and surfactant polymer with HPAM-concentration of 375 ppm were chosen. For the high viscosity, chemical floods, a polymer with HPAM-concentration of 1200 ppm and surfactant-polymer with HPAM-concentration of 1600 ppm were chosen

Another interesting observation is encountered in measuring viscosity of a polymer solution before and after an experiment, the results of which are seen in Figure B3. The produced polymer was collected from the effluent in a production interval where it was clear from production and density data that polymer was being produced. Viscosity measurements on this produced polymer show that the viscosity has dropped between being injected and being produced. Most likely reason could be a change in salinity in the polymer-solution. The polymer passes through a core that has seen a surfactant-polymer and brine with 3.75% NaCl salinity, much higher than the polymers 1000 ppm NaCl salinity. It is possible that contact between polymer and brine or surfactant-polymer increases the polymers salinity, which effectively lowers its viscosity.

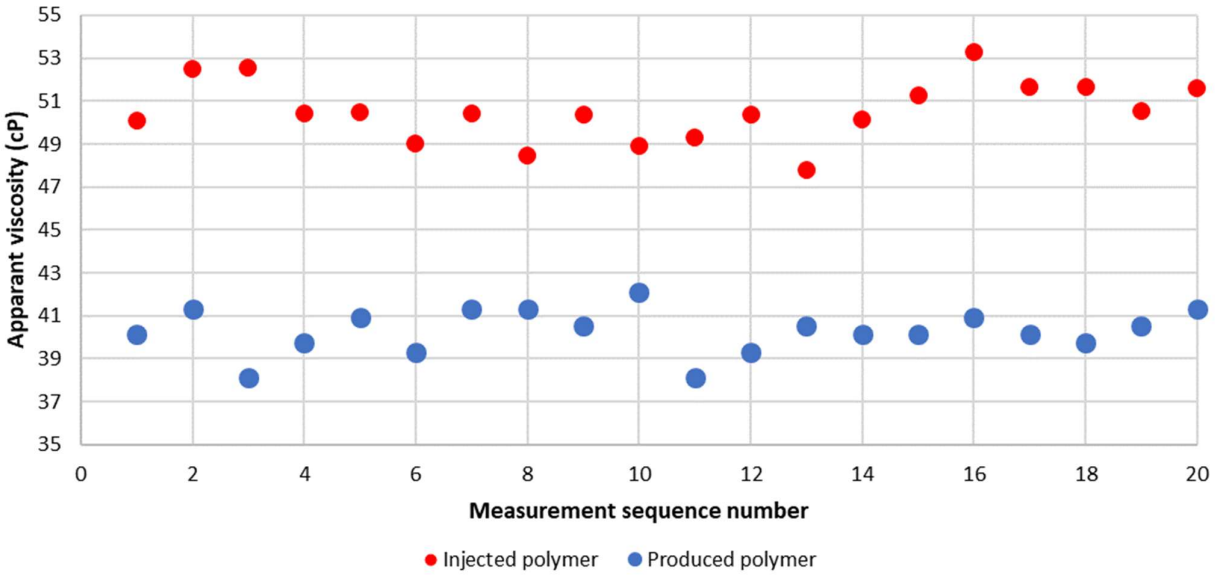

Figure B3: Viscosity measurements of polymer before and after a chemical flood

Appendix C: CT-scan saturation accuracy

Section 1.9 discusses a method to estimate saturation along the core using data from CT-scans. A major side not there, was that the method was an approximation only, which begs the question of the accuracy of this approximation.

One method to evaluate the accuracy of this approximation is to calculate the oil in place from the CT-scans, production data and effluent observations and to compare these results. By subtracting the produced oil from production data or effluent observations from the oil initially in place, an estimate of the oil in place can be made, as seen in Equation C.1. In this calculation it is also important to subtract the oil present in the dead volume after the core, a volume of oil estimated by multiplying the dead volume by the last measured oil cut.

$$OIP = OIIP - N_p - f_0 * V_{dead} \qquad \text{Eq.C.1}$$

The calculations from the CT-scans require a different approach. This data contains average oil saturation for each slice, which is located a distance (dx) from the next slice. The average saturation per slice ($S_{o,n}$) is multiplied by that slice's porosity (φ_n), the cores cross-sectional area (A) and the distance between slices to obtain a volume of oil present in a core section of length dx. The summation of oil in place per core section results in an estimate for oil in place in the entire core, as depicted in Equation C.2.

$$OIP = \sum_{n=1}^{N} S_{o.n} * \varphi_n * dx * A \qquad \text{Eq.C.2}$$

Figure C.1 shows the comparison of results from these calculations for the first experiment of the 1m Bentheimer core discussed in Section 3.5. The results show overall great consistency. At the last two scans and scan 12 the results differ somewhat. Since all data was processed in the same manner, a clear explanation of this divergence cannot be given at this time. The difference between production data and CT-data at point 12 is 12 mL and at point 16 8mL, 5.9% and 3.8% of OIIP, respectively

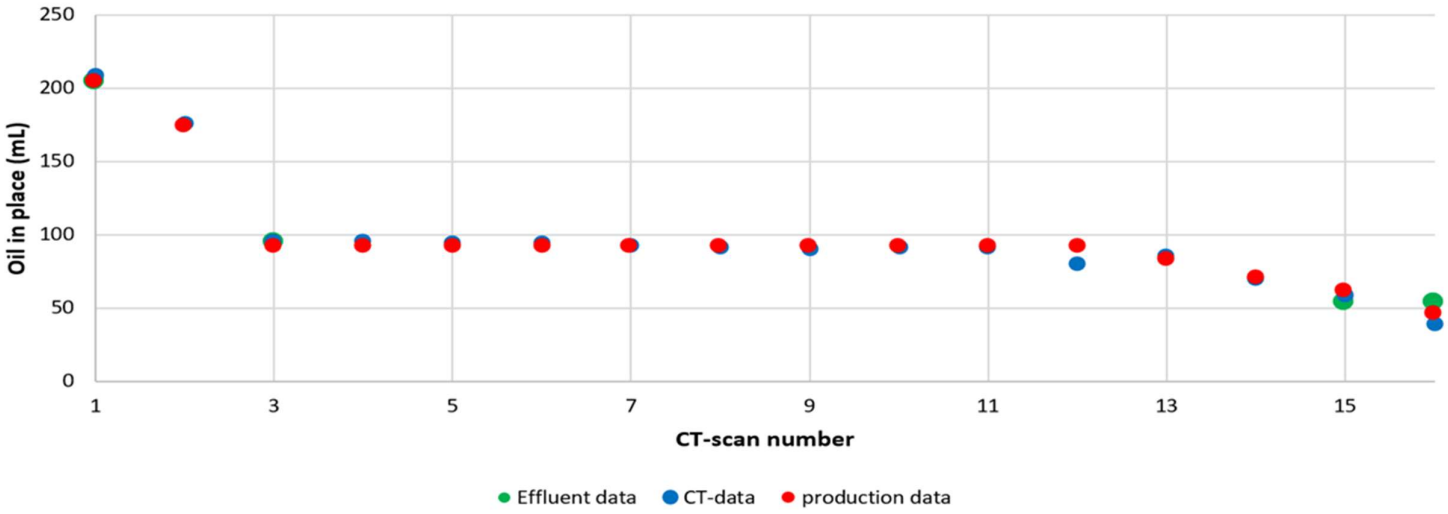

Figure C1: Oil in place from production data, effluent observations and CT-data (1m Bentheimer, experiment 1)

The results of the first experiment using the stacked 60cm Fontainebleau core the results are not as precise. The intermediate datapoints do not vary much. The data pertaining to the first, last and second-to-last CT-scans do shows significant difference with production and effluent data, 10.7 mL, 2.5 mL and 7.3 mL, respectively. The intermediate datapoints, which are most relevant in evaluating oil bank behaviour, luckily do show consistent results.

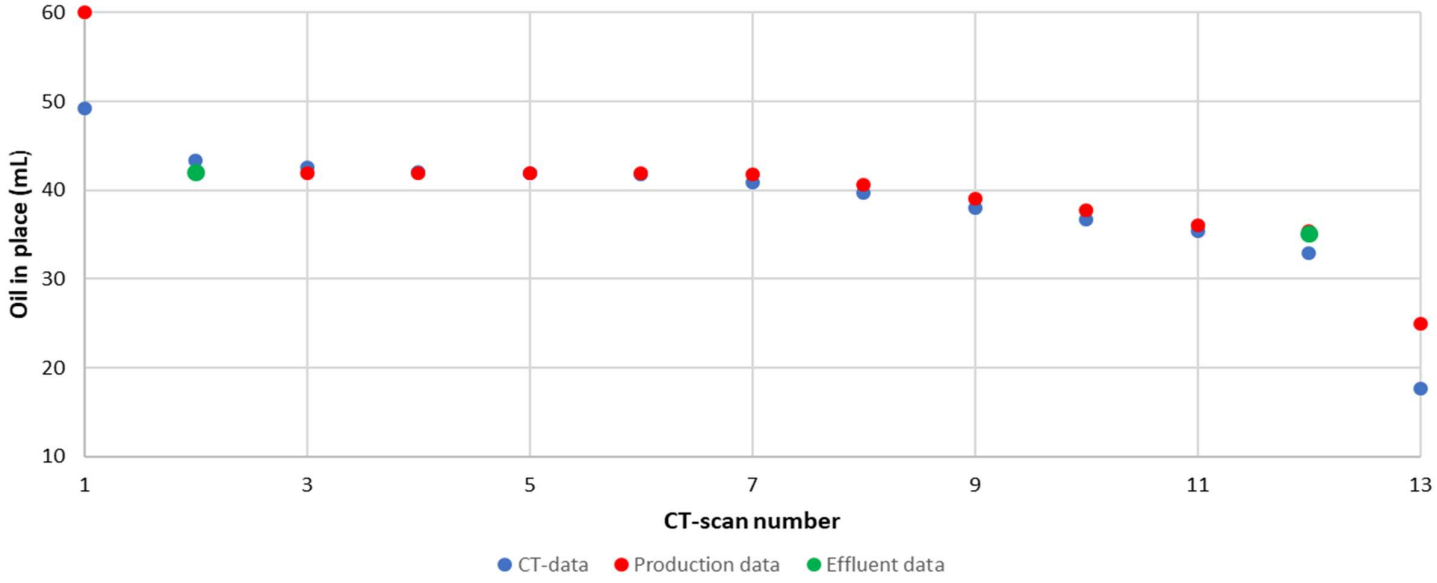

Figure 2: Oil in place from production data, effluent observations and CT-data (60cm stacked Fontaine Bleau, experiment 1)

The second experiment using the stacked core, results seen in Figure C.3, shows overall consistent values. The greatest difference is observed at scan 11, where CT-data shows 8mL more oil in place than production data.

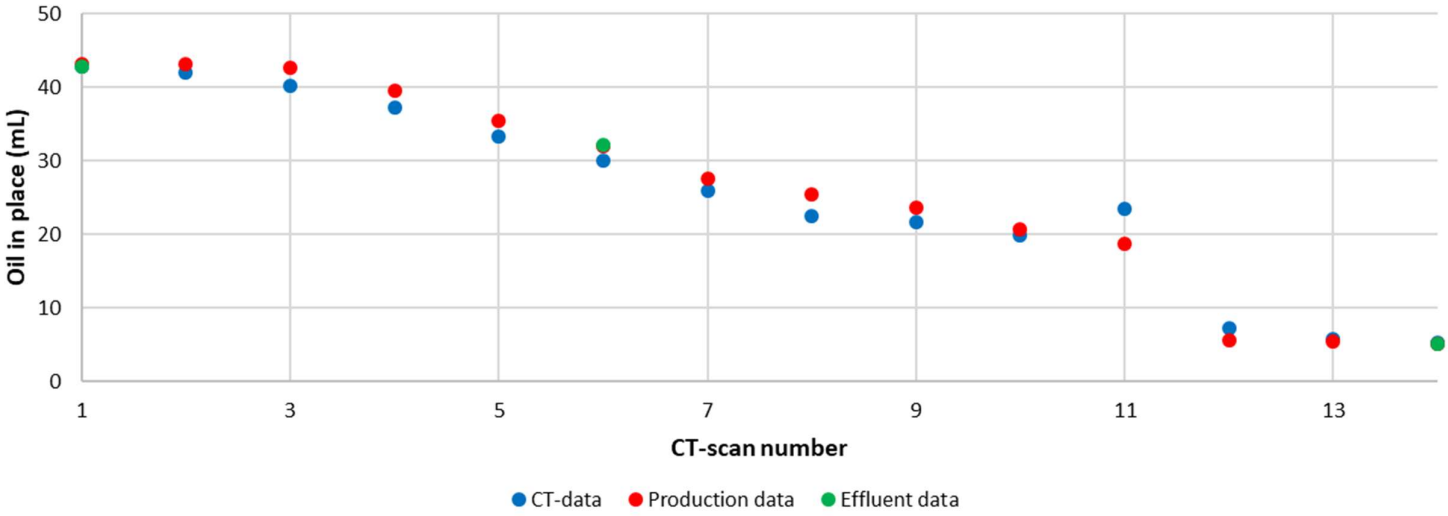

Figure 3: Oil in place from production data, effluent observations and CT-data (60cm stacked Fontaine Bleau, experiment 2)

Appendix D: Results of tracer tests

In Section 1.8 the method of using a tracer analysis to identify the accessible pore volume is discussed. The major goals of the tracer analyses are to estimate the pore volume and check if a core has returned to its initial conditions after being cleaned. By matching experimental data with model predictions, which depend on porosity, an estimation of the pore volume is obtained. Figure D.1 shows a typical best fit between the model and experimental data.

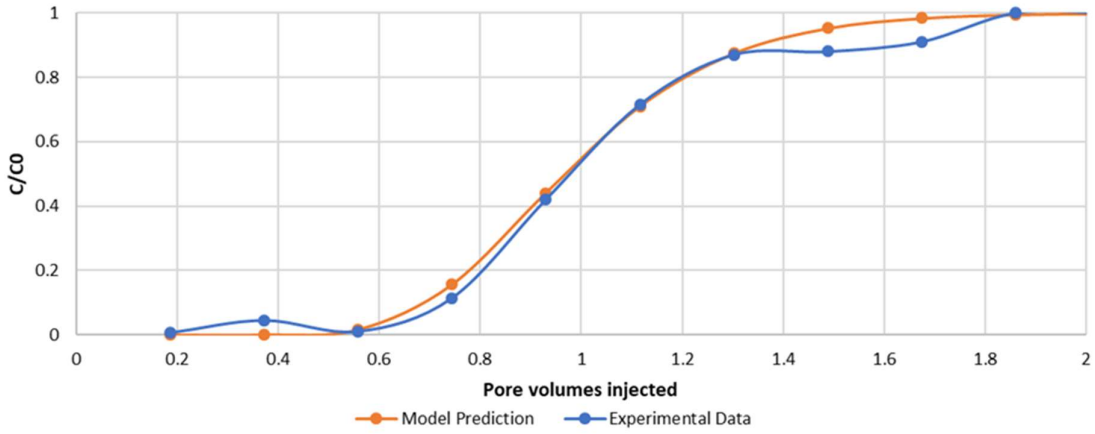

Figure D.4: Matched model prediction and experimental data of initial tracer analysis (7.5cm high perm core)

Figure D.2 shows the tracer analyses of the 7.5 cm high permeability core. This specific core has seen most core floods and tracer analyses, so it serves best in evaluating tracer results in the long run. The data contains the results of a tracer analysis before the core was used in an experiment, and following analyses performed in between experiments after the core had been flushed with IPA, all normalised to a single pore volume. One apparent observation in Figure D2 is that there is a general trend wherein the curves shifts to the left after each experiment. This leftward shift indicates an earlier increase in KI-concentration in the effluent, caused by a reduced accessible pore volume. There are several possible explanations for this reduced accessible pore volume. First of which could simply be an inadequate cleaning of the core, allowing some oil to remain the core. Second of which, could be adsorption of surfactant or polymer to the rock, as described in (Lake, 1989).

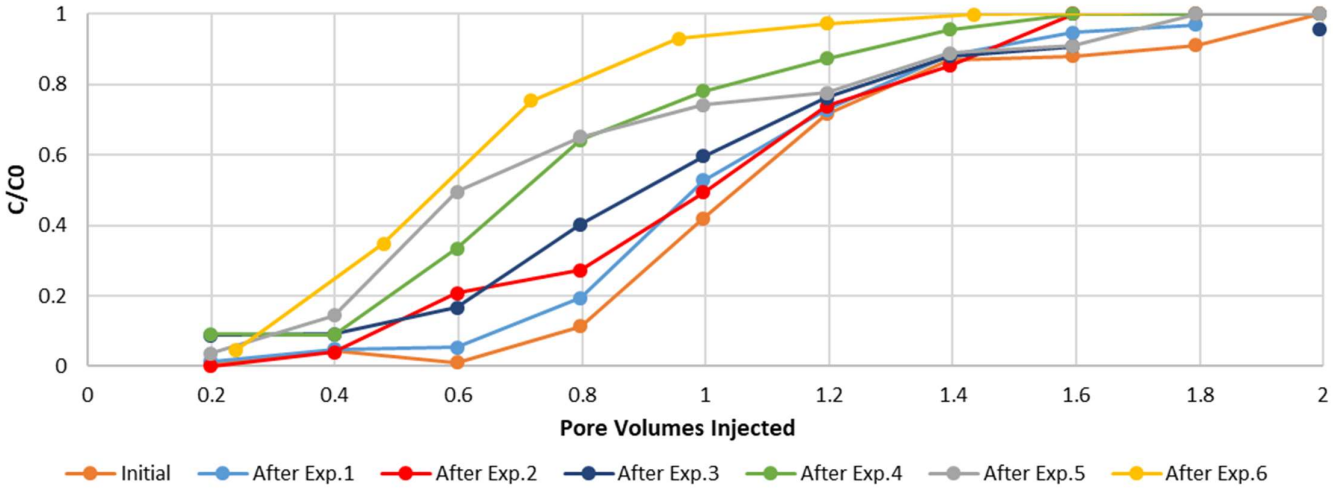

Figure 5: Compilation of tracer analysis results for a 7.5cm high perm core

Appendix E: Core stacking procedure

In Section 3.4 results from experiments using a composite 60cm core were discussed. This appendix chapter describes the steps taking in stacking two 30cm cores into a composite 60cm one.

There are several factors to be considered to ensure the transition from one core to the other is as continuous as possible. First consideration is minimising capillary forces at the boundary between the two cores. In this project this issue was tackled by filling the space between the two cores with a piece of one of the cores. The piece was ground up and the resulting sand was filtered down to the dominant grain size of the cores, a grain size determined in (Al Saadi, Ongoing).

Another potential problem is that cores had to be aligned adequately enough to minimise distortion of the flow path and to ensure that the composite core would fit in a core holder. This challenge was tackled by placing a 10cm long aluminium tube around the boundary between the two cores. The tube's inner diameter must match the outer diameter of the cores, as is depicted in Figure E.1. To keep the stacked cores aligned in the Perspex tube when they are cast in glue, a support made of dried glue is placed around the aluminium tube. Small supporting blocks made of dried glue are stuck to the aluminium tube to support it against the Perspex tube.

Figure E.6: Core to be stacked with guiding aluminium tube

In summation the stacking of two cores is done by taking the following steps

- Cut the cores to 1cm bigger the required size and save a piece of about 2cm from one of the two cores.
- Apply the thin layer of glue onto both cores.
- Cut the excess 1cm of both cores to expose the sides that'll be connected.
- On the side of the exposed core ends, mill the outer diameter of both cores down to a diameter of 4.1cm over a length of 5cm.
- Crush the saved 2cm and sieve the resulting sand to the dominant grain size
- Glue on the aluminium tube support blocks that are big enough to occupy the void between the aluminium tube and the Perspex tube and insert one core into the aluminium tube.
- Pour the sieved sand into the aluminium tube and onto the core end. Make sure that the sand is distributed evenly over the entire core end.
- Insert the second core into the aluminium tube and press and hold them closely together.
- Cast the whole in glue via the conventional core casting procedure while making sure that the cores remain as close together as possible, by placing a weight on top of the composite core for example.

Figure E.2 show the stacked cores inside the Perspex tube before they are cast in glue.

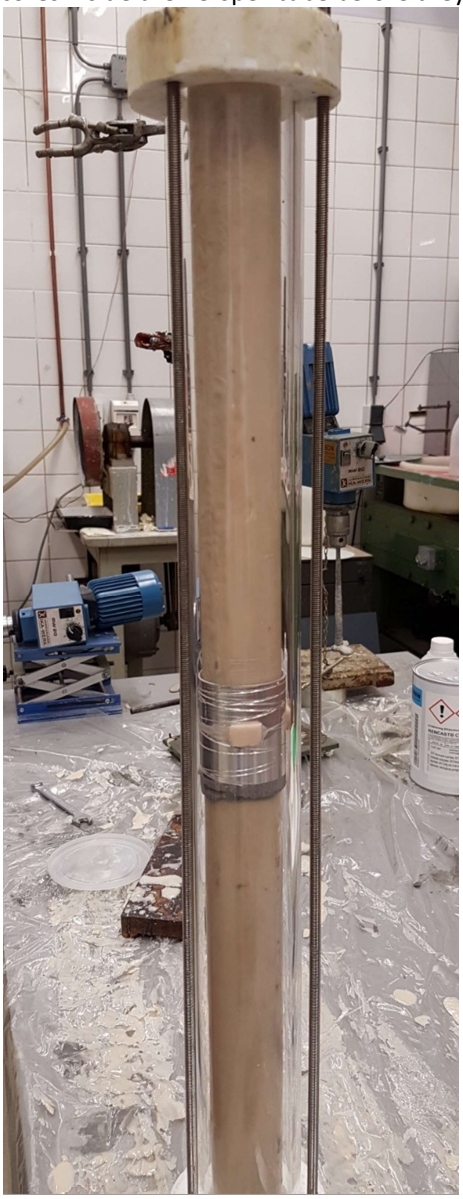

Figure E.7: Stacked cores before being cast in glue

Many steps were taken in an attempt to make sure that the boundary between the stacked cores is as continuous as possible, but the results discussed in Section 3.4 show that this was not completely achieved. The problem probably lied in the equal distribution of the crushed and sieved. Figure E.2, showing CT-scans of the boundary between the two cores, supports this notion. It appears that the bottom part of the core contains much more sand than the top part.

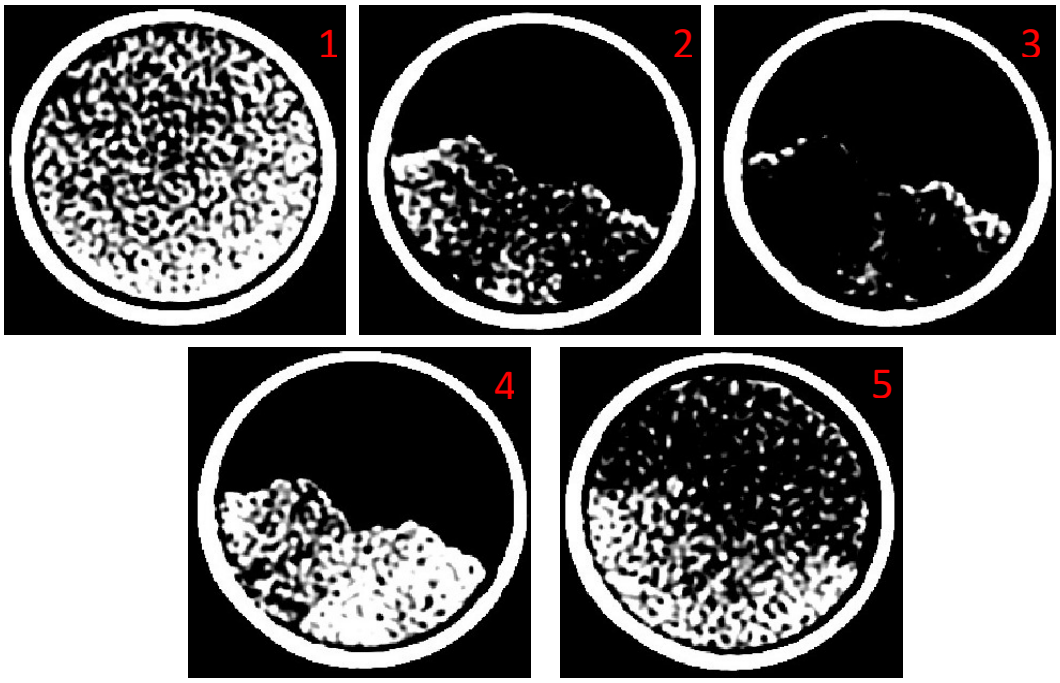

Figure E.8: CT-scans of the boundary between the stacked cores with sequence numbers in red.

Bibliography

Al Saadi, F. (Ongoing). Oil Bank Mobilization and transport.

Berg, S. (2017). Shear rate determination from pore-scale flow fields. *Springerlink*.

Bronkhorst. (2018). *mini CORI-FLOW M1x series Instruction Manual.* Bronkhorst.

Coats, K. H. (1964). Dead-end pore volume and dispersion in porous media. *Society of petroleum engineers journal* , 73-84.

Corey, R. B. (1964). HYDRAU uc properties of porous media. *Hydrology papers*, 37.

Feeman, T. G. (2010). *The mathematics of medical imaging.* Springer.

International Energy Agency. (2017). *Key world energy statistics.* Paris: International energy agency.

Johnson, E. F. (1959). Calculation of relative permeability from displacement experiments. *Transactions in AIME*, 370-372.

Keller, K. G. (2017, March). Piezoresistive Pressure Transmitters Series 23/25 Specifications. Winterthur.

Lake, L. W. (1989). *Enhanced oil recovery.* Austin: Prentice-Hall.

Leverett, S. B. (1942). Mechanism of fluid displacement in sands. *Transactions of the AIME*, 107-116.

Muggeridge A, C. A. (2014). Recovery rates, enhanced oil recovery and technological limits. . *Philosophical transactions Series A,* .

Odell, J. A. (1988). Non-Newtonian behaviour of hydrolysed polyacrylamide in strong elongational flows: a transient approach. *Polymer 29.7*, 1179-1190.

Peksa, A. E.-H. (2015). Bentheimer sandstone revisited for experimental purposes. *Marine and Petroleum Geology*, 701-719.

Rapoport, L. A. (1953). Properties if linear water floods. *Journal of Petroleum Technology*, 139-148.

Sandrea, I. (2007). GLOBAL OIL RESERVES-1: Recovery factors leave vast target for EOR technologies. *Oil & gas journal*.

Seright, R. (2005). Clean up of oil zones after gel treatment. *SPE international symposium on oilfield chemistry*.

Swej Shah, A. H.-V. (2017). *Foam-Flooding Experiment.* Delft: Geo-Engineering Lab.

Thorade, H. F. (2010). Density and viscosity of brine: An overview from a process engineers perspective. *Chemie der Erde - Geochemistry*, 23-32.

Tromp, R. H. (2006). Arrested segregative phase separation in capillary tubes. *Physical Review*, 74.

Wardlaw, N. C. (1982). The effects of geometry, wettability, viscosity, and interfacial tension on trapping in single pore-throat pairs. *Petroleum Society of Canada*.

Welge, H. J. (1952). A simplified method for computing oil recovery by gas or water drive. *Journal of Petroleum technology*, 91-98.

Wijsman, M. (2018). *Characterisation of Surfactant Polymer Oil Bank Mobilisation Through Relative Permeability Analysis.* Tudelft MSc thesis.

Winsor, P. A. (1968). Binary and multicomponent solutions of amphiphilic compounds. Solubilization and the formation, structure, and theoretical significance of liquid crystalline solutions. *Chemical reviews*, 1-40.